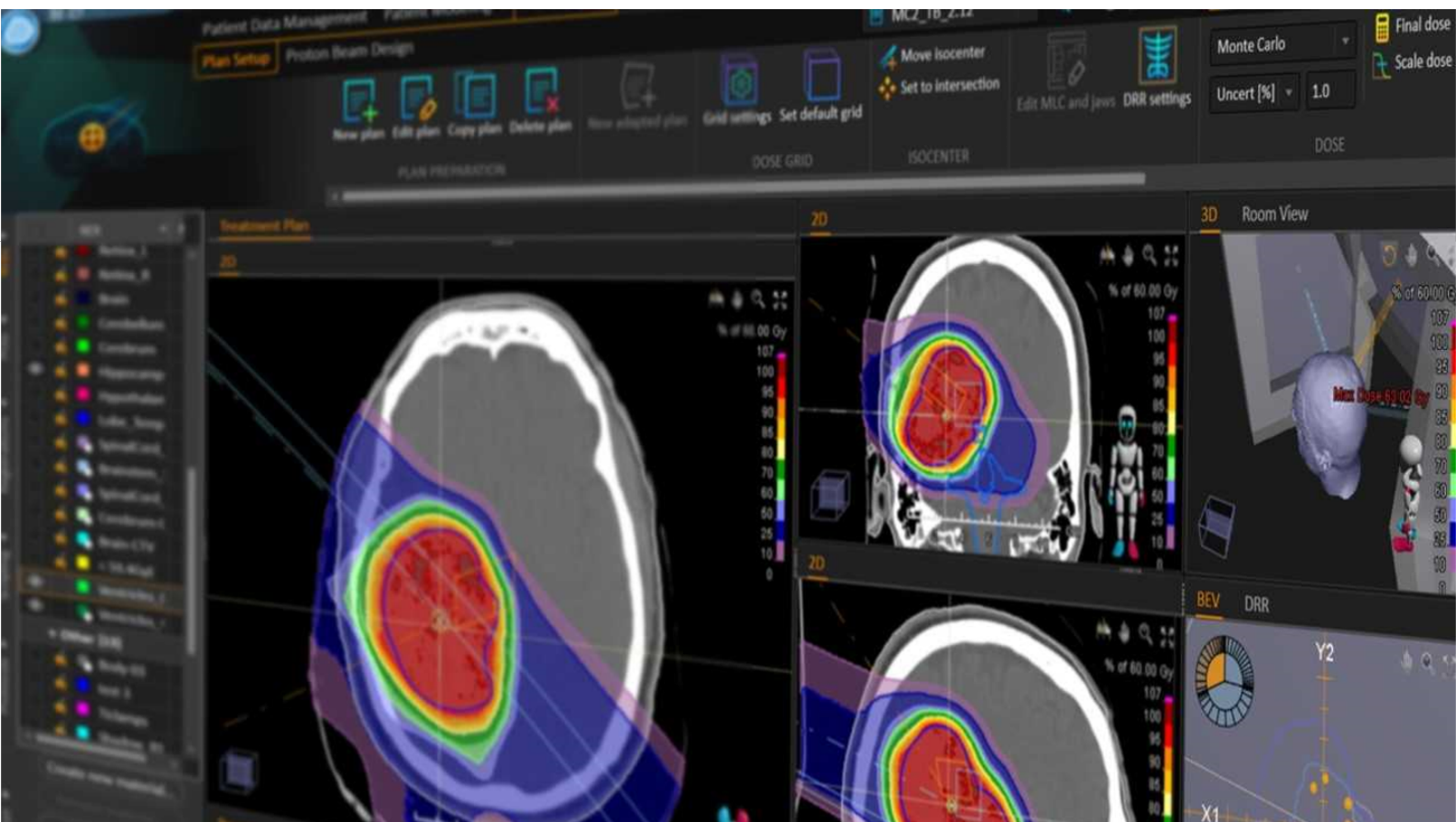


# The increased risk of post-treatment contrast-enhancing brain lesion in IMPT of glioma, and the mitigation thereof in treatment planning

Marleen van Doorn





# The increased risk of post-treatment contrast-enhancing brain lesion in IMPT of glioma, and the mitigation thereof in treatment planning

by

Marleen van Doorn

To obtain the degree of Master of Science in Biomedical Engineering  
at the Delft University of Technology,  
to be defended publicly on Wednesday December 16, 2020 at 14:00 PM.

Student number: 4359267

Committee:	Prof. Dr. Mischa Hoogeman (chair)	TU Delft/EMC/HollandPTC
	Dr. Ir. Danny Lathouwers	TU Delft
	Dr. Frans Vos	TU Delft
	Prof. Dr. Marco van Vulpen	TU Delft/HollandPTC
	Dr. Steven Habraken	EMC/HollandPTC





# Contents

<b>Abstract</b>	<b>1</b>
<b>Preface</b>	<b>3</b>
<b>1 Introduction</b>	<b>5</b>
1.1 Radiotherapy . . . . .	5
1.2 Proton Therapy . . . . .	6
1.3 Radiotherapy workflow . . . . .	7
1.3.1 Tumor targeted volumes . . . . .	7
1.3.2 Plan optimization. . . . .	7
1.3.3 Treatment modality selection . . . . .	7
1.4 Relative Biological Effectiveness. . . . .	8
1.4.1 Definition . . . . .	8
1.4.2 Linear-quadratic model-based RBE . . . . .	8
1.5 Linear Energy Transfer. . . . .	9
1.5.1 Dose- and Track-averaged LET: $LET_d$ and $LET_t$ . . . . .	10
1.6 Relation between $LET_d$ and RBE . . . . .	10
1.6.1 $LET_d$ times dose as surrogate for RBE. . . . .	10
1.6.2 An increasing biological effect with increasing $LET_d$ . . . . .	10
1.7 Increased radiobiological effectiveness . . . . .	10
1.7.1 Clinical evidence of increased brain injury and RBE . . . . .	11
1.7.2 The POLO and NTCP model . . . . .	11
1.8 MCsquare. . . . .	13
1.8.1 Dose and $LET_d$ calculation . . . . .	13
1.8.2 Validation. . . . .	13
1.9 Project outline . . . . .	13
<b>2 Materials &amp; methods</b>	<b>15</b>
2.1 Implementation of MCsquare . . . . .	15
2.1.1 Commissioning of HollandPTC Beam Data Model . . . . .	15
2.1.2 Dose and $LET_d$ distribution . . . . .	15
2.2 Implementation of POLO and NTCP . . . . .	15
2.3 Patient cohort, treatment planning data, and contouring . . . . .	16
2.4 Evaluation of RBE/LET effect . . . . .	17
2.4.1 Comparison of proton vs photon plan . . . . .	17
2.4.2 The contribution of $LET_d$ . . . . .	17
2.4.3 Individual Pencil Beam Contribution . . . . .	17
2.4.4 Strategies to mitigate the RBE/LET effect. . . . .	17
2.4.5 Combination of treatment modalities . . . . .	18
2.5 General outline . . . . .	19
<b>3 Results</b>	<b>21</b>
3.1 Implementation and verification . . . . .	21
3.2 Comparison of proton and photon treatment plans. . . . .	21
3.3 Deviations in NTCP. . . . .	23
3.3.1 Computation deviations . . . . .	23
3.3.2 Delineation deviations . . . . .	23

3.4	Individual pencil beam contribution . . . . .	24
3.5	Impact of beam settings on the NTCP . . . . .	24
3.5.1	Robustness . . . . .	24
3.5.2	Beam angle . . . . .	25
3.5.3	Beam energy . . . . .	28
3.6	Combined radiotherapy modalities - protons and photons. . . . .	31
3.6.1	Clinical proton plan with clinical VMAT plan . . . . .	31
3.6.2	Clinical proton plan with partial proton transmission plan . . . . .	31
3.6.3	Comparison of combined radiotherapy modalities . . . . .	31
3.7	Comparison of different planning strategies . . . . .	35
<b>4</b>	<b>Discussion</b>	<b>37</b>
4.1	The impact of robustness on the NTCP . . . . .	37
4.2	The impact of field angle arrangement on the NTCP . . . . .	37
4.2.1	Improvement with a 2-field arrangement . . . . .	37
4.2.2	Improvement with a 3-field arrangement . . . . .	37
4.2.3	The underlying POLO distribution to determine the NTCP . . . . .	38
4.2.4	Towards the optimum beam angle selection . . . . .	38
4.3	Impact of transmission beams on the NTCP . . . . .	38
4.4	The impact of combined treatment modalities . . . . .	39
4.4.1	The opportunity to combine different treatment modalities . . . . .	39
4.4.2	Trade-off between NTCP and brain dose . . . . .	40
4.4.3	Sequence of fractionation for a multi-modality radiation treatment. . . . .	40
4.4.4	Optimization of combined radiotherapy modalities . . . . .	40
4.5	Comparison of different planning strategies . . . . .	41
4.6	Interpretation and relevance of the NTCP model . . . . .	41
4.6.1	Inter-patient comparison . . . . .	41
4.6.2	Relation with symptomatic development . . . . .	41
4.7	Delineation uncertainties . . . . .	42
4.8	Future perspectives. . . . .	42
<b>5</b>	<b>Conclusion</b>	<b>43</b>
<b>6</b>	<b>Appendix</b>	<b>45</b>
6.1	Models for the Relative Biological Effectiveness . . . . .	46
6.2	Figures and Tables . . . . .	47
<b>7</b>	<b>Literature study</b>	<b>61</b>
7.1	Literature search . . . . .	61
7.2	Biological studies . . . . .	61
7.3	From pre-clinical to clinical . . . . .	64
7.4	Clinical data. . . . .	65
7.5	RBE models. . . . .	69
7.6	Discussion . . . . .	72
7.7	Conclusion . . . . .	74
	<b>Bibliography</b>	<b>75</b>

# Abstract

**Background/purpose:** Proton radiotherapy has a dosimetric advantage over photon therapy to spare healthy tissue closely positioned to the tumor mainly due to the absent exit dose. In The Netherlands, the Proton therapy centers currently take a relative biological effectiveness (RBE) of 1.1 compared to photons to deliver an iso-effective treatment. However, initial clinical evidence indicates a variable proton RBE in brain patients with the linear energy transfer (LET) as an important physical parameter. The LET significantly increases at the end of the radiation field, and contributes to an increased probability to develop brain lesions. With the introduction of radiation response models, the first goal this thesis is to evaluate the impact of the RBE/LET effect in intensity-modulated proton therapy (IMPT) plans. Furthermore, the main goal is to reduce the RBE/LET effect in treatment planning.

**Methods:** We incorporated the probability of lesions origin (POLO) model published in literature [1] to determine the RBE model-based normal tissue complication probability (NTCP) for three glioma patients treated with IMPT at HollandPTC, The Netherlands. The dose and LET distributions were computed using a Monte Carlo system. For the investigation of the RBE/LET effect in treatment planning, we modified several beam settings of the clinical IMPT plan, including the beam angle, beam energy, and robustness. Furthermore, we combined treatment modalities to reduce the NTCP.

**Results:** We compared the results of the clinical used IMPT plan with the results obtained by the modified IMPT plans. The local redistribution of  $LET_d$  leads to a decrease in NTCP up to the point when the  $LET_d$  becomes uniform. The robustness did not reveal deviations in terms of the NTCP. By choosing appropriate beam angles that result in a smeared-out  $LET_d$  distribution, the NTCP does not improve for small deep-located tumors, improves relatively modest by 11.6% for elongated tumors, and significantly improves by 37.0% for large, superficially-located tumors. The inclusion of partial transmission beams lowers the NTCP by 30-50% relative to the clinical IMPT plan while limiting the relative increase in mean brain dose by 5-16%. When comparing the IMPT plan with the photon plan used for plan comparison, the VMAT plan always results in the lowest NTCP and provides a relative improvement in NTCP by 60-75%. Meanwhile, the mean brain dose significantly increases by 50-80% compared to the clinical IMPT plan. Intermediate NTCP- $D_{mean}$ (brain - CTV) values are achieved when combining protons with the photons or by including proton transmission beams.

**Conclusion:** In general, we can conclude that the inclusion of partial proton transmission beams is more promising than choosing appropriate beam angles to lower the RBE/ $LET_d$  effect. However, further optimization of transmission beams is required. Moreover, an improvement in NTCP is always at the cost of the mean dose to healthy tissue. On top, our results support further investigation to combine different modalities, like protons and photon fractionation.



# Preface

This master thesis is written to finalize the MSc Biomedical Engineering - Medical Physics at the TU Delft. My master thesis project is done at the Erasmus Medical Center, Rotterdam, The Netherlands, at the department of radiotherapy, and HollandPTC, Delft, The Netherlands.

First of all, I would like to thank everyone who has been involved in this project or who has contributed in his/her own way within the last nine months. During the project, I have received support of my supervisors, Mischa Hoogeman and Steven Habraken. I would like to thank Mischa for our meetings about the progress and how you suggested to proceed with the project. Thank you for sharing your ideas, and for providing valuable feedback. I want to thank my supervisors, Steven Habraken, in particular. You have been deeply involved in this project. I am very grateful for the time to learn me new things in the field of radiotherapy. Thank you for guiding me throughout the master project, providing support during the writing process, and for the encouraging words. Furthermore, I also enjoyed the personal conversations.

Furthermore, I also want to thank Alejandra Mendez Romero for your involvement. Thank you for looking at this project from a clinical perspective and for sharing your view and ideas.

Also, I would like to thank Kevin Souris and Marie Cohilis for helping me to make MCsquare work. I appreciate your willingness to help me with the technical problems by sharing your ideas how to approach a task and by answering all my questions.

To all my fellow students at the EMC and HollandPTC, to the PhD students at the EMC, the EMC radiotherapy department and everyone at HollandPTC, thank you for the great time together, for sharing your experience and providing advice when needed.

To you all, thank you very much!

*Marleen van Doorn*  
*Delft, December 2020*



# Introduction

In the fight against cancer, often a combination of different treatment modalities is applied. The three primary modalities are surgery for local treatment, chemotherapy mainly for systemic control, and radiation therapy for local-regional treatment. Other and newer approaches for systemic control are hormone-, targeted-, or immunotherapy. In this work, we focus on radiation treatment for brain tumors. Radiation therapy is applied when the tumor cannot (fully) be removed by surgery, i.e. if the tumor is in the area of the brain that is difficult to operate on, or due to the microscopic spread.

This first chapter will provide background on radiotherapy, especially on proton therapy. Before addressing the aim of this study, first the radiobiological effectiveness, the radiation response model and the dose engine used during the project will be introduced.

## 1.1. Radiotherapy

The goal of radiotherapy is to deliver high doses of ionizing radiation to the tumor while sparing as much as possible of the surrounding healthy tissue. This approach provides the highest chance to kill the cancer cells or to shrink the tumor. Unfortunately, radiation treatment inevitably involves the exposure of healthy tissue. Consequently, patients may experience associated symptoms. To reduce the risk of side effects, it is important to ensure that both the right dose and radiation treatment plan are delivered.

In terms of response time, the effect of radiation can appear after a few weeks, months, or years after radiotherapy. Biologically, there are two types of effects: deterministic and stochastic. The former occurs if the radiation dose exceeds a defined threshold for a given organ. The severity of side effects increases with increasing dose. Most of the late effects and all early effects are deterministic [2]. Examples of clinical symptoms after brain irradiation are problems in neurocognitive functioning, e.g. clear thinking, difficulties with managing daily tasks, and memory loss. These symptoms are a result of changes in vasculature or due to radiation necrosis [3]. In contrast, the severity of stochastic effects does not depend on the amount of absorbed dose. Neither is their occurrence associated with a threshold. Instead, the probability of toxicity increases with the amount of dose.

Over the past decades, extensive experience in radiation treatment with photons has been gained. As a result, photon treatment has become the conventional radiation treatment modality. Modern treatment techniques such as intensity-modulated radiation therapy (IMRT) delivers radiation using several fixed beam angles, while volumetric modulated arc therapy (VMAT) continuously reshapes and changes the intensity of the beam as it rotates around the patient. However, even with the most advanced planning techniques and the highest accuracy of delivering photon radiation, side effects are not always avoidable. The exposure of healthy tissue is inevitable due to unavoidable entrance dose and exit dose, and the infiltration of tumor cells in healthy tissue.

In recent years, proton therapy has been introduced as a promising radiation modality in treating cancer. Thereby, it has become the standard of care for specific groups of patients. The next section elaborates on the concept of proton therapy.

## 1.2. Proton Therapy

Over the past 60 years, especially the past 10-15 years, proton beam radiation therapy has been used on a larger scale. The clinical interest in using proton beams is motivated by their superior physical properties. Protons lose their energy mainly by undergoing Coulomb interactions with atomic electrons and to a lesser extent by nuclear interactions. With the release of energy, protons slow down, and eventually stop. Near the end of the penetration range, the energy loss increases rapidly till its maximum, causing the Bragg peak, after which the dose rapidly fall-off (figure 1.1, blue). Thereby, protons eliminating the exit dose.

Because the depth of the Bragg peak is directly related to the initial proton energy, proton beams of different energies and intensities can be superimposed to generate a spread-out Bragg peak (SOBP) (red). Complete irradiation is achieved with the desired dose over the tumor volume (delimited by the gray dot-dashed vertical lines).

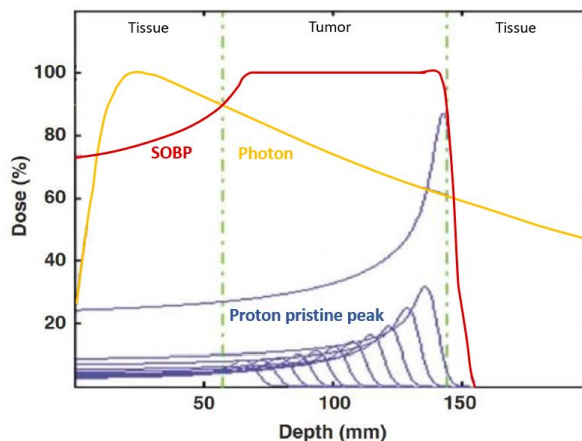


Figure 1.1: Comparison of the proton and photon depth-dose distribution. Depth-dose distributions for a photon (yellow line) and the spread-out Bragg peak (SOBP) (red line) generalized by modulated proton pristine peaks (blue lines) are shown. The tumor region (delineated by the dashed green lines) is covered by the plateau of the SOBP getting 100% of the prescribed dose. The figure is taken from [4] and edited.

In comparison, the dose-depth curve of a photon rises sharply to its maximum intensity within the first few centimeters, after which the intensity gradually decreases (yellow). By the reduction in entrance dose, but mainly by the absence of exit dose, protons allow a more conform dose of the lower and intermediate dose volumes. As a result, proton radiation lowers the integral dose. This significant dosimetric benefit of proton therapy over conventional photon therapy leads to better healthy tissue sparing [5].

In proton therapy, there are two main delivery modalities. In passive scattering, a broad uniform proton field is created by scattering the narrow beam over a larger area using a scattering foil. Next, a contoured scatterer provides beam and range uniformity. By the use of range modulators, the dose area adequately covers the tumor volume. In pencil beam scanning, energy modulation is used to modulate the depth of the protons while magnets are used to direct individual Bragg peaks to scan the target volume. If multiple scanning beam fields are used, it is called intensity-modulated proton therapy (IMPT). IMPT has a dosimetric benefit over passive scattering because it provides an improved conformality to irregular targets. IMPT also delivers less dose to healthy tissue [6].

## 1.3. Radiotherapy workflow

The radiotherapy workflow starts with the acquisition of a CT scan of a patient for a given region of interest. A team of radiation oncologists and treatment planners identifies and delineates the structures of interest, including the target volume(s), and structures to spare, i.e., organs at risk (OAR). The latter may also be delineated by an automatic contouring technique. Since an MRI scan is optimal for imaging soft tissue, like tumors or brain tissue, the MRI scan is used during the contouring phase. Thereafter, a registration of the CT scans on the MRI images is applied. The deformation is propagated to the contours to match the delineations with the CT image.

As the following steps of planning and dose delivery are based on the definition of the target volume, the delineation is a crucial step in the radiotherapy chain. Inadequate delineation of the target introduces systematic geographic misses that could lead to a reduction of the planned dose to the actual tumor [7]. To ensure that the tumor is completely covered with the prescribed absorbed dose, different target volumes are defined.

### 1.3.1. Tumor targeted volumes

The macroscopic visual tumor on medical imaging is known as the Gross Tumor Volume (GTV). The GTV is expanded to account for microscopic tumor cells spread around the GTV, which is not visible on the images. To this end, margins are used to define the Clinical Target Volume (CTV). If the patient moves or if internal organs change in size or reshape during fractionation or between fractions, then the CTV may also move.

In conventional photon therapy, the CTV is extended to account for the anatomical variations, and to allow for uncertainties in treatment delivery as well as for uncertainties in planning, like setup errors. The enlarged target volume is called the Planning Target Volume (PTV). The PTV is used to select appropriate beam sizes and beam arrangements to ensure that the CTV receives at least 95% of the actual prescribed dose to at least 95% of the CTV.

In proton therapy, the dose distribution is not conserved after anatomical changes. As the depth of a Bragg peak depends on the initial energy of the proton beam and the tissues' electron density, then changes in density along the pencil-beam path can alter the depth of an individual Bragg peak. Set-up errors do not simply result in a shift of dose, as for photons, but actually leads to a change in the overall shape of dose distribution, and therefore to dose degradation [8]. Besides, inaccuracies in the conversion of CT Hounsfield units to stopping power may also introduce uncertainties in the exact positioning of the Bragg peak. Therefore, multiple possible error scenarios of the CTV in IMPT are accounted for during robust optimization in the treatment planning system (TPS).

### 1.3.2. Plan optimization

Besides the unavoidable entry dose and the inclusion of healthy tissues within the CTV, it is inevitable to irradiate healthy tissue due to the use of robustness margins. To spare much of the healthy tissue, treatment planning settings play an important role.

After the contouring phase, a radiotherapy technician selects the desired beam angles, the total desired amount of dose in Gy (Gray), and the fractionation scheme, i.e., the number of fractions to deliver the total prescribed dose. These settings are given as input for the TPS. Then, an optimization algorithm generates a treatment plan considering the robustness margins while taking care of OAR sparing. The optimization algorithm uses a list of objectives to optimize physical goals and determine the optimal beam settings (beam energies and beam weight) for treatment delivery. Finally, the TPS calculates the total dose distribution. Afterwards, the radiation oncologist can manually modify the treatment plan to implement additional preferences, like filtering of individual pencil beams.

### 1.3.3. Treatment modality selection

In The Netherlands, the indication for proton therapy is distinguished from standard care (e.g. eye and chordoma) and model-based (e.g. brain, KNO, and breast). When considering brain cases, the decision whether the patient will undergo photon or proton treatment is firstly based on medical indication. For example, only patients with a relatively favorable prognosis, i.e., having a ten-year survival rate of at least 50%, are eligible for plan comparison. If not, patients undergo photon treatment.

A plan comparison is accomplished to decide which technique is most advantageous for the patient. For both treatment modalities, a treatment plan is designed and optimized to make an appropriate comparison. The photon plan is designed using the CT scan made at the Medical Center, while the

proton plan is generated using the CT scan from the referring centrum. If the criteria for proton treatment described in the *Landelijke Indicatie Protocol Protontherapie* (NIPP) is met, then the patient is qualified for proton therapy [9]<sup>1</sup>. The occupational group defined the dosimetric benefit of protons over photons if the average dose is reduced by at least 5% within the hippocampus and the brain outside the target volume. This criteria should be met to get insurance for proton therapy. Nevertheless, the dose reduction will always be realized. Therefore, the qualification for proton therapy is mainly based on the medical indication and technical aspects, like surgery or implant materials. The latter act as counter-indication for proton treatment. At last, the advantages and risks of both modalities are discussed with the patient to determine which treatment the patient will receive.

## 1.4. Relative Biological Effectiveness

### 1.4.1. Definition

Different radiotherapy modalities could lead to a different biological outcome even as an equivalent dose is delivered. In general, protons cause a larger biological effect than photons. To deliver an iso-effective treatment plan, less dose should be given with protons as with photons. The ratio of absorbed doses between photons and protons producing an equivalent biological effect is called the relative biological effectiveness (RBE):

$$RBE = \frac{Dose_{reference}(Endpoint_x)}{Dose_{protons}(Endpoint_x)} \quad (1.1)$$

In the early days of proton therapy, cell survival studies derived an average RBE of 1.1 relative to <sup>60</sup>Co photon radiation using a dose of 2 Gy<sub>RBE</sub> (e.g., [10, 11]). The RBE of 1.1 has been adopted and generally applied in proton planning. In practical terms: if the desired equivalent photon dose is 2 Gy, then the prescribed proton dose is denoted as 2 Gy<sub>RBE</sub>, which corresponds to a physical dose of 1.8 Gy.

### 1.4.2. Linear-quadratic model-based RBE

Within the field of radiobiology, the linear-quadratic (LQ) model is widely used to describe the biological response in terms of the cell survival probability,  $S$ , which is given as a function of radiation fraction dose,  $D$ , and the parameters  $\alpha$  and  $\beta$  that describe the radiosensitivity of the tissue:

$$S = \frac{N}{N_0} = e^{\alpha \cdot D + \beta \cdot D^2} \quad (1.2)$$

The  $\alpha$  term reflects the local damage to both sides of the DNA strand by a single charged-particle that results in a double-strand break. In other words, this event leads directly to irreparable cell damage, and thus to cell death [12]. The  $\alpha$  term is proportional to the dose. Lethal damage caused by at least two local independent ionization radiations is presented by the  $\beta$  term. By this, the  $\beta$  is proportional to the dose-squared. As the cell has the capability to repair the sub-lethal damage in-between two events, the cell is able to survive. By this, the  $\beta$  term also characterizes the cells the repair mechanisms that require at least 6 hours for a complete repair.

Figure 1.2 (left) shows the cell response as a combination of the linear  $\alpha$  term (striped gray region) and the additional contribution of the  $\beta$  term that increases with cumulative damage (uniform gray region). The ratio of  $\alpha/\beta$  reflects the tissues radiosensitivity, i.e., the  $\alpha/\beta$  is the dose at which the  $\alpha$  and  $\beta$  has an equal contribution to the overall biological outcome. Tissue with a low  $\alpha/\beta$  has a dominant  $\beta$  term, and, therefore, has a high capacity to repair DNA damage. This type of tissue is identified as late responding tissue. In general, healthy tissue belongs to this category. For example, the tissue in the central nervous system (CNS) has a  $\alpha/\beta$  value  $< 3$  Gy [13, 14]. In contrast, most CNS tumors have a higher  $\alpha/\beta$  value, e.g., the brain tumor radiosensitivity ranges between 10-28 Gy [13, 15]. Therefore, their biological outcome is mainly affected by the  $\alpha$  term and is hardly fractionation-sensitive. Tissue with a high  $\alpha/\beta$  is defined as acute responding tissue.

The most commonly used RBE model is derived from the LQ model by assuming the same level of survival fraction after photon and proton therapy (figure 1.2(right)). In this approach, a relationship is established between parameters describing the cell response for photons,  $\alpha_x$  and  $\beta_x$ , and for protons,  $\alpha$

<sup>1</sup>The Standpunt Protontherapie bij neuro-oncologische tumoren is based on the Landelijke Indicatie Protocol Protontherapie

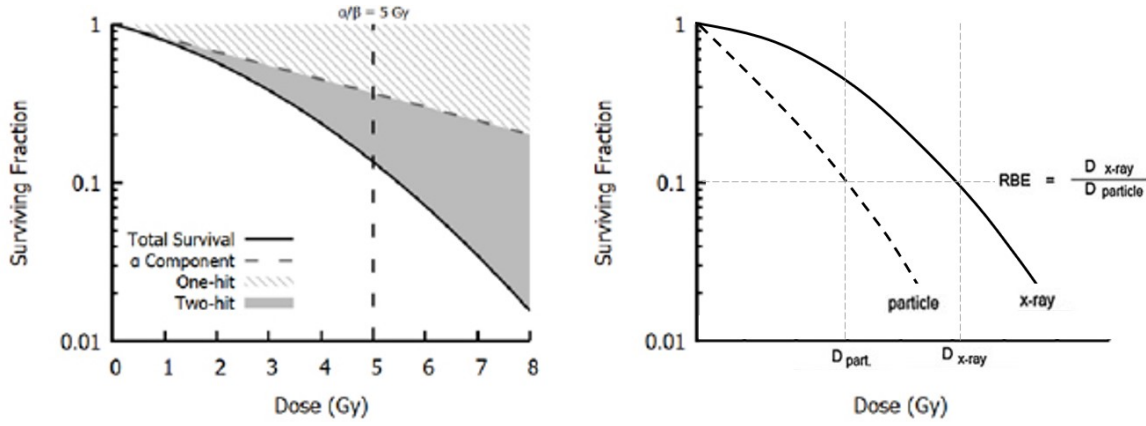


Figure 1.2: Response for cell lines using the linear-quadratic model to define the RBE. Left: The linear-quadratic model separated into a single ionization that causes lethal damage (stripped gray area) and multiple ionization hits that lead to cell death (uniform gray area). Both terms have the same contribution when the dose matches the  $\alpha/\beta$  ratio of the cell, which is 5 Gy in this example. Right: The dose-response relationship is given for a photon (solid) and a particle (dashed) using the LQ model. The left figure is taken from [12]. The right figure is taken from [16] and edited.

and  $\beta$ . Under the LQ formulation, a photon absorbed dose,  $D_x$ , and a proton dose,  $D$ , are iso-effective for a single fraction if:

$$\alpha D + \beta D^2 = \alpha_x D_x + \beta_x D_x^2 \quad (1.3)$$

By rewriting equation 1.3 in the form of equation 1.1, the RBE is defined as:

$$RBE(D_p, \left[ \frac{\alpha}{\beta} \right]_x) = \frac{1}{D_p} \left( \sqrt{\frac{1}{4} \left[ \frac{\alpha}{\beta} \right]_x^2 + \left[ \frac{\alpha}{\beta} \right]_x} \cdot RBE_{max} \cdot D_p + RBE_{min}^2 \cdot D_p^2 - \frac{1}{2} \left[ \frac{\alpha}{\beta} \right]_x \right) \quad (1.4)$$

with  $RBE_{max} \equiv \frac{\alpha}{\alpha_x}$  and  $RBE_{min} \equiv \sqrt{\frac{\beta}{\beta_x}}$ .

From equation 1.4, it can be derived that the RBE depends on the dose per fraction and tissue type. Further, the extensive cell survival study found that the RBE increases with increasing dose per fraction [17]. Besides, an increase in RBE is especially significant for tissue with a low  $\alpha/\beta$  (appendix 7.2).

Based on this general RBE model (equation 1.4), different approaches have been derived. In general, it is assumed that the  $RBE_{max}$  and  $RBE_{min}$  depend on the ionization density. Based on different assumptions of how the  $\alpha$  and  $\beta$  parameters alter with the contribution of ionization density, different models have been derived (appendix 6.1). Particles with a higher ionization density (figure 1.3, right) cause clusters of strand breaks that are more concentrated in space [18]. This type of damage is associated with a higher chance of causing direct lethal damage, and thus is more efficient in killing cells. Therefore, an increased ionization density affects mainly the  $\alpha$  term, and thus the  $RBE_{max}$  [12]. The physical parameter for the ionization density is called the linear energy transfer, which is discussed in the next section.

## 1.5. Linear Energy Transfer

The physical quantity underlying differences in radiobiological effectiveness is the linear transfer effect (LET). The LET describes the mean rate of energy release of the primary particle due to electromagnetic interactions per unit length [keV/ $\mu$ m]. Secondary particles then transfer the proton energy loss into the tissue locally. In other words, the LET describes the quality of radiation and not the quantity.

When the energy loss of all energetic secondary particles is considered, the LET is the sum of the electronic stopping power and the nuclear stopping power [20]. The latter refers to the interactions with the nuclei. The former refers to the slowing down of a particle due to the inelastic collisions with bound electrons in the medium, and dominates the energy transfer effect.

In contrast, LET is not well-defined for photons. Photons remain almost all their initial energy when traveling through tissue, or they may be absorbed within the tissue and impart dose to the surrounding primarily by its produced secondary electrons. So, the LET of photons is (mostly) that of secondary electrons.

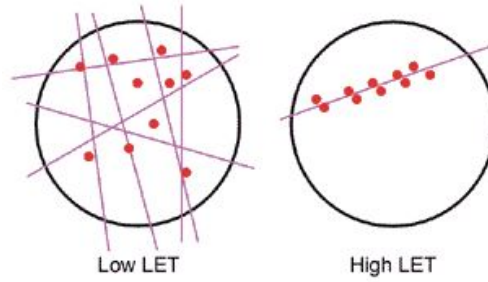


Figure 1.3: Particle tracks for different linear energy transfer distributions. Left: Several tracks passing through the given volume produce a sparse number of ionizations (low LET), which are nearly homogeneously distributed. Right: A single-track generates densely packed ionizations (high LET) within the given volume resulting in a heterogeneous distribution. Both volumes receive the same amount of ionization. The figure is taken from [19].

### 1.5.1. Dose- and Track-averaged LET: $LET_d$ and $LET_t$

Although LET is well-defined for charged particles along the track of a single particle with fixed energies, in proton treatment, we generally deal with a radiation field generated by proton beams of various energies. Therefore, the LET contributions of different proton energies must be averaged at each point in a radiation field. In general, two different concepts of LET are derived. The  $LET_t$  is defined as the energy deposition weighted by the particle fluence [20], while the  $LET_d$  is defined as the energy deposition of an individual particle weighted by the local deposited dose. Biological studies use commonly the  $LET_d$  because dose has biologically more significance than fluence.

## 1.6. Relation between $LET_d$ and RBE

### 1.6.1. $LET_d$ times dose as surrogate for RBE

However, the LET causes no effect by itself. Therefore, LET should be given in combination with a quantitative parameter. To describe the additional biological effect as result of an increasing  $LET_d$ , various studies have made assumptions of how the  $LET_d$  affects the tissues radiosensitivity parameters (appendix 6.1), and therefore the cell survival. For example, the Wedenberg et al. model [21] neglects the  $\beta$  term. Furthermore, they assume that the  $\alpha$  relates linearly with the  $LET_d$ . Then, the former exponential term of the cell survival,

$$S = e^{-(\alpha+k \cdot LET)d} = e^{-\alpha \cdot d} \cdot e^{-k \cdot LET \cdot d}$$

represents the contribution of the physical dose to the biological impact, while the latter term represents the additional biological effect. Therefore, biological studies commonly take the  $dose \times LET_d$  as a surrogate for the RBE. This simplified approach has the advantage of reducing uncertainties in the RBE that are related to the dependence of the  $\beta/\beta_x$  ratio [21]. However, this approach lacks the fractionation effect.

### 1.6.2. An increasing biological effect with increasing $LET_d$

Because protons decelerate with penetration depth, the number of secondary particles increases locally. In other words, the energy deposition becomes more efficient near the end of the proton range. Consequently, the  $LET_d$  increases towards the distal, especially at the Bragg peak. The maximum is reached just after the Bragg peak. A similar pattern is observed for a modulated beam (figure 7.1). Although the relative dose in the entrance region is higher for the modulated beam (dashed line) than using a single beam, the  $LET_d$  (thin solid line) remains unchanged. Subsequently, the cellular response in terms of cell death increases along the proton beam. This observation implies an enhanced RBE [22], especially for tissue with a low  $\alpha/\beta$  [17].

## 1.7. Increased radiobiological effectiveness

The effective proton range may be extended by a few millimeters ( $dose \times RBE$ ). Consequently, normal tissue might be effectively overdosed, leading to unforeseen toxicities [23]. The question arises whether the current clinical used RBE of 1.1 is sufficiently accurate to predict the clinical outcome, or whether the

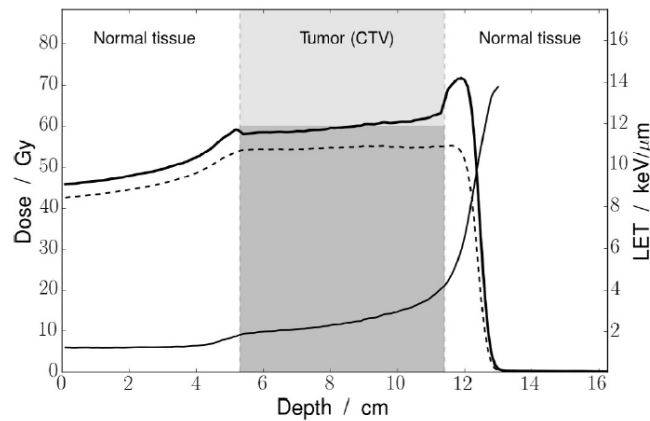


Figure 1.4: The depth-dose and depth-LET distribution for a modulated proton beam. The physical dose distribution for a modulated beam (dashed line) and the respective dose-averaged linear energy transfer ( $LET_d$ ) (solid line) are shown. The Spread-Out Bragg Peak covers the tumor region (vertical gray area). The product of physical dose times the RBE gives the effective biological dose (bold line). The figure is taken from [23].

RBE should be a variable [23]. Biological studies and clinical cohort studies have shown their interest in identifying potential RBE variations. They evaluated the consistency of the constant proton RBE of 1.1 with the outcome. My literature study (appendix 7) provides a more detailed overview of the biological studies and retrospective clinical cohort studies that relate the RBE to the increased biological effect.

### 1.7.1. Clinical evidence of increased brain injury and RBE

The awareness of the potential significant deviation in RBE that leads to unforeseen clinically symptomatic toxicity, is getting more attention because evidence is growing. In 2016, the first retrospective clinical study was initiated to identify the voxel-wise spatial variations in RBE [24], followed by others [1, 25–27]. Clinical evidence of a significant increased RBE for brain patients was found by correlating sites of contrast-enhanced brain injury observed on MRI with dose, LET, and the radiosensitive area around the ventricular system. Thereby, they emphasize the importance of LET to determine the outcome.

### 1.7.2. The POLO and NTCP model

Recently, a predictive model to calculate the probability of post-treatment changes on MRI has been established by Bahn, et al. [1] based on 110 glioma patients (grade I and II) irradiated by 3-dimensional spot scanning or IMPT. To be more specific, the model evaluates for each voxel the probability of whether a contrast-enhancing brain lesion (CEBL) will originate, called the probability of lesion origin (POLO).

#### Voxel-level statistical analysis: POLO model

The POLO model is based on the physical parameters dose and dose- $LET_d$ , as well as the radio-sensitive cell region around the ventricular system, called the periventricular region (PVR). Since brain lesions are frequently observed within the PVR, they have incorporated the PVR into their model to evaluate their healthy tissue response. Because a correlation of the dose-response in tissue of the CNS was found in the 4 mm area around the ventricular system, the distance of a 4 mm extension of the ventricular system was adopted. The inner liquid cavities are excluded from analysis as no image changes related to radio-necrosis were expected in these regions. As the goal was to predict if and where a brain lesion will originate, certain assumptions were made. It was hypothesized that CEBLs originate from a single spot of tissue breakdown from where it isotropically expands. However, once a CEBL increases in size, the information about the point of origin is lost. Therefore, only the contours at the earliest available MRI for the 30% smallest CEBL were used during analysis. The voxels inside a CEBL were statistically weighted by its position from the center and the CEBL volume. Further, only voxels inside the brain which received at least  $2 Gy_{RBE}$  were included during analysis.

The probability for a brain lesion to originate is given by the following logistic model:

$$\log\left(\frac{POLO}{1-POLO}\right) = b_0 + b_1 \cdot dose + b_2 \cdot dose \cdot LET_d + b_3 \cdot PVR \quad (1.5)$$

with the PVR as a binary risk factor. The weighting factors,  $\bar{b}_n$ , for each of the model predictors were adjusted by multivariable logistic regression. By fitting the model to the experimental data, Bahn et al. [1] found an  $b_{0-3}$  of -26.3, 0.19, 0.018, and 1.19, respectively.

To validate the model and to test its robustness, they performed five times a 5-fold cross-validation, including patients without CEBLs. As only the smallest 30% of the lesions observed were included during analysis, an extended validation was performed on the remaining 70%. For the evaluation of the model's accuracy, they calculated the area under the curve (AUC). The POLO model had a response rate of 0.94.

Figure 7.5 shows an example. A high POLO (c) was particularly found at the edge of the CTV (yellow line) with high physical dose (a) and a high  $LET_d$  (b), which correlates to the area of the observed CEBL (white line) within the PVR (delineated by light and dark blue line). Voxels encountered as CEBLs in-

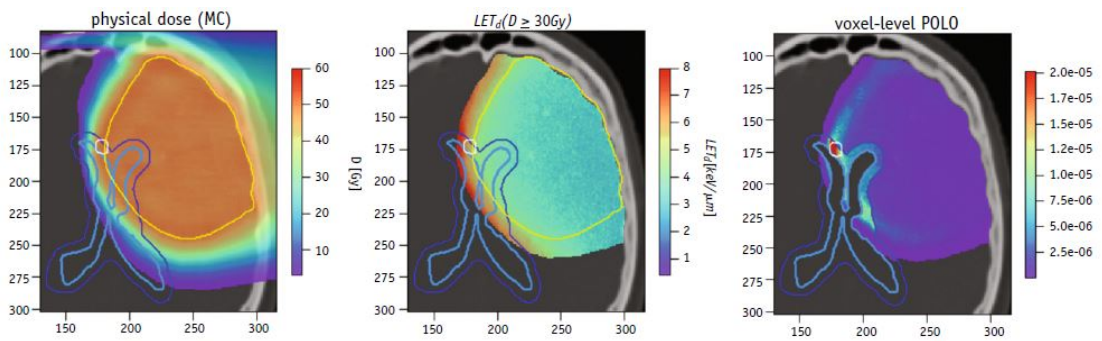


Figure 1.5: Voxel-wise prediction model-based on dose and  $LET_d$ . (a) Physical dose ( $RBE = 1.1$ ). (b) The dose-averaged LET ( $LET_d$ ) distribution is only shown in combination with doses above 30 Gy ( $RBE = 1.1$ ). (c) The predicted voxel-level probability of lesion origin (POLO) distribution. The light and dark blue lines depict the ventricular system and the 4-mm region around, respectively. The PTV is depicted by the yellow line, whereas the observed CEBLs contour is presented in white. The figure is taken from [1].

deed predicted high POLO, in regions of high dose (mean: 53.5  $Gy_{RBE=1.1}$  (median), max. 55.4  $Gy_{RBE=1.1}$  and high  $LET_d$  (range: 3.56 to 8.18 keV/um). Most CEBLs were located close to the ventricular system: 79% of the CEBLs were situated within 4 mm distance, and 92% within 10mm distance from the ventricular system. Further, 90% of the CEBLs were found at the distal edge of at least 1 beam. Altogether, the model predicted a 3-fold increased risk in the 4 mm region around the ventricular system. As similar observations were made in studies with glioma and glioblastoma patients treated with photons, Bahn et al. [1] believed that this behavior is independent of the radiation modality.

#### Patient-level risk prediction: $NTCP_{CEBL}$

Based on the POLO distribution, the normal tissue complication probability ( $NTCP_{CEBL}$ ) for the development of 1 or more CEBLs was derived to test the feasibility of predicting the patient-level risk. Other studies (e.g. [28]) assume a serial tissue organisation to describe the tissue reactions within the central nervous system. Bahn et al. [1] adapted this assumption of a serial architecture by applying a multiplication of each POLO voxel,  $i$ , to come up with  $NTCP_{CEBL}$  model,

$$NTCP_{CEBL} = 1 - \prod_{i=1}^n (1 - POLO_i), \quad (1.6)$$

where the  $n$  is the total number of voxels. The  $NTCP_{CEBL}$  had a good characterization ability (AUC = 0.78). In general, the model assumes that a lower  $NTCP$  is achieved when considering a lower dose, a lower dose $\times$ LET, by avoiding sensitive tissue like the region around the ventricular system, or by reducing the number of involved voxels.

## 1.8. MCsquare

For this work, we used an open-source Monte-Carlo (MC) proton dose engine, called MCsquare [29], to simulate proton dose and the  $LET_d$ . MCsquare was developed to improve the MC simulations within accuracy limits and with calculation speed required in the clinic. Although the generally used MC codes, e.g., Geant4 [30], FLUKA [31], and TOPASS [32], are very accurate, they are also impaired with relatively long computation times and are therefore unattractive for routine clinical use. In general, the advantage of MC simulations compared to analytical models is the improved accuracy in dose calculation, especially when considering range uncertainties due to inhomogeneous tissue.

### 1.8.1. Dose and $LET_d$ calculation

During penetration through matter, the proton loses energy mainly due to multiple electromagnetic and inelastic interactions. To determine the correct energy loss, the stopping power and cross-section are required for each voxel. Therefore, in MCsquare, each voxel of the medical image is labeled with the appropriate material according to its density. Based on the density, the corresponding stopping power and cross-section is computed from a database of multiple materials. Since only the elements H, C, N, O, P, and Ca have a concentration of  $>1\%$  within human tissue, the material is defined as a mixture of those elements. As there could be deviations between proton beams of different machines, the physical information (like spot size and energy spread) are stored in a database that is calibrated with measured data of the used equipment. Altogether, the cross-section and stopping power are derived from a database, instead of applying a correction to water data.

Once the stopping power and cross-section are determined, the proton dose can be simulated by evaluating the proton energy loss per voxel as well as the energy deposition of secondary particles. To limit computation time, EM interactions (secondary electrons), are simulated in a condensed way. Their energy is absorbed locally. In contrast, collisions with orbital electrons, with an energy loss above certain energy threshold, are simulated individually. Also the track of nuclear interactions that produce secondary protons, deuterons, and alphas are determined individually. The kinetic energy transferred to heavier recoil nuclei is locally absorbed. Further, prompt gammas are produced, but not considered. Although neutrons are also generally produced in nuclear inelastic events, MCsquare neglects their contribution to the local dose as it is less than  $0.5\%$ . Once the proton enters the next voxel, its remaining range is scaled. Finally, if the kinetic energy of the proton reaches the cut off energy, all remaining energy is locally deposited and absorbed. In the  $LET_d$  calculations, the same secondary particles are taken into account as for the dose distribution, except for the recoil particles.

### 1.8.2. Validation

The performance of dose calculation in MCsquare has been benchmarked with Geant4 for a homogeneous water phantom and a heterogeneous phantom consisting of water, bone, and lung tissue [29]. The MCsquare dosimetric results were in good agreement with Geant4. The dose has also been evaluated by using an inhomogeneous phantom consisting of water, bone tissue, and PMMA [33].

The MCsquare based computed  $LET_d$  has been validated [34] by comparing the results with the microdosimetry measurements and with the  $LET_d$  calculated by a clinical treatment planning system (RayStation, v6R). Both dose and  $LET_d$  had a good agreement in terms 3%/3mm gamma passing rate ( $>90\%$ ) [33, 34], and their uncertainties were within the clinically acceptable level of  $7\%$  ( $\pm 2\%$  and  $6\%$ , respectively).

For this project, we used a graphical interface, called openREGGUI, which has a plugin to launch the MCsquare dose and  $LET_d$  simulation and to visualize those distributions.

## 1.9. Project outline

Current treatment planning of intensity-modulated proton therapy (IMPT) of neurological tumors is solely based on dose. However, numerous biological studies showed that the radiobiological effect of protons varies with depth. As it is unavoidable to use beams that stop in front of critical organs with current planning strategies, these organs potentially receive additional dose. Furthermore, clinical evidence is growing which states that RBE/LET effect plays a role in an increased risk to develop toxicities [1, 24–27].

The concern about the potential impact of increased RBE/LET at the distal edge is also growing at the proton therapy centers in The Netherlands, and hence, also at HollandPTC in Delft. These proton centers aim to get a better understanding of the RBE/LET effect in proton therapy. Besides, they want to reach an agreement of how to deal with a varying RBE/LET in clinical practice. A first step is to identify the current impact of the RBE/LET effect in clinical IMPT plans. With the introduction of the predictive POLO model that translates the RBE/LET effect into a clinical endpoint, the first goal of this thesis is to evaluate the RBE/LET effect in clinical IMPT plans created at HollandPTC. Because the POLO model relates the effect of RBE to the toxicities of glioma patients, we also focus on glioma patients.

Furthermore, different strategies have already been identified how to migrate the RBE/LET effect during treatment planning (appendix 7.5). Those studies mainly focused on  $LET_d$  optimization while maintaining the dose distribution (e.g. [35–37]). Other studies investigated how one can prevent  $LET_d$  hot-spots within the brainstem by manually editing beam setting (e.g. [38–40]). However, none of these strategies have been evaluated in terms of a clinical endpoint. Therefore, the second and main goal of this thesis is to identify strategies how to reduce the RBE/LET effect in treatment planning.

# 2

## Materials & methods

### 2.1. Implementation of MCsquare

In this thesis, we used the open-source Monte Carlo dose engine, MCsquare [29], as it facilitates the calculation of both the dose and the dose-weighted linear energy transfer ( $LET_d$ ).

#### 2.1.1. Commissioning of HollandPTC Beam Data Model

To reproduce a dose that matches the dose calculated by the treatment planning system (RayStation, v7), we needed an accurate beam model in MCsquare. We did a full commissioning to model the beam of the HollandPTC proton treatment machine to generate the beam data library (BDL) that contains the parameters that characterize the proton beam for various energies such as (i) the beam shape in air (spot size and divergence), (ii) the proton energy spectrum considered as a Gaussian (mean and standard deviation), and (iii) the calibrated number of protons per MU to compute the absolute dose. In addition, the BDL contains parameters to account for the range shifter. During CT calibration, the CT numbers (HU) were converted into a material with given properties, such as density and elemental composition, in order to determine the stopping power.

#### 2.1.2. Dose and $LET_d$ distribution

Radiation treatment plans were generated by the treatment planning system (RayStation TPS, v7). The dose was re-calculated by MCsquare on computed tomography (CT) images (original CT resolution:  $1.0 \times 1.0 \times 1.0 \text{ mm}^3$ , MCsquare CT resolution:  $0.684 \times 0.684 \times 1.0 \text{ mm}^3$ ) used for clinical treatment planning. The same data was used to perform the  $LET_d$  calculations in MCsquare.

The implementation in terms of dose was validated by comparing the calculated dose profile to that of the clinical dose plan. The performance of the  $LET_d$  calculation has been approved by Wagenaar et al. [34] (section 1.8.2). Both dose and  $LET_d$  distributions were simulated using  $2 \cdot 10^7$  number of protons with a resulting statistical uncertainty of 1% or 2%.

### 2.2. Implementation of POLO and NTCP

To evaluate the potential clinical impact of  $LET_d$ , we implemented the recently published model by Bahn et al [1] - the probability of lesion origin (POLO) and the patient-risk calculation in terms of  $NTCP_{CEBL}$  (section 1.7.2) - in Matlab (R2017a). In the following, the  $NTCP_{CEBL}$  will be denoted as  $NTCP_{all}$  (see below).

The POLO model is based on the physical dose ( $59.4 \text{ Gy}_{RBE}/1.1 = 54 \text{ Gy}$ ), the  $LET_d$ , and the PVR. The  $LET_d$  calculated by MCsquare could directly be imported into the POLO model. Voxels inside the PVR were classified as a binary risk factor. As no tissue is located within the ventricular system, all voxels within the ventricular system were eliminated. Further, all voxels outside the brain were set to zero.

The POLO model is based on a grid dimension of the planning CT with a resolution of  $0.6 \times 0.6 \times 3 \text{ mm}^3$ . However, the scored distributions in MCsquare have a different resolution of  $0.684 \times 0.684 \times 1.0 \text{ mm}^3$ . Therefore, we had to correct for the difference in voxel volume to calculate the  $NTCP_{all}$ . The

POLO distribution was interpolated and resampled to the appropriate grid size by using the Matlab function `griddedInterpolant({sx, sy, sz}, POLO)`, with  $s_{x,y,z}$  as the new voxel grid. To validate this approach, the POLO distribution was also corrected by the volume ratio, according to:  $POLO_{\text{resampled}} = POLO_{\text{original}} \cdot \frac{V_{\text{original}}}{V_{\text{resampled}}}$ .

We implemented three different NTCP models (figure 2.1). First, the NTCP as described by Bahn et al. [1] is used (left) (NTCP<sub>all</sub>). All voxels inside the body were taken into account, except the voxels from the ventricles' inner liquid cavities. However, as the NTCP refers to the complication probability of the healthy tissue, we decided to define an NTCP that neglects the CTV voxels in the NTCP calculation (right) (NTCP<sub>CTV</sub>). We also made a distinction between the voxels inside the PVR, which are infiltrated by the tumor cells, and the voxels in the PVR, which are located outside the CTV (middle) (NTCP<sub>CTV,+PVR</sub>).

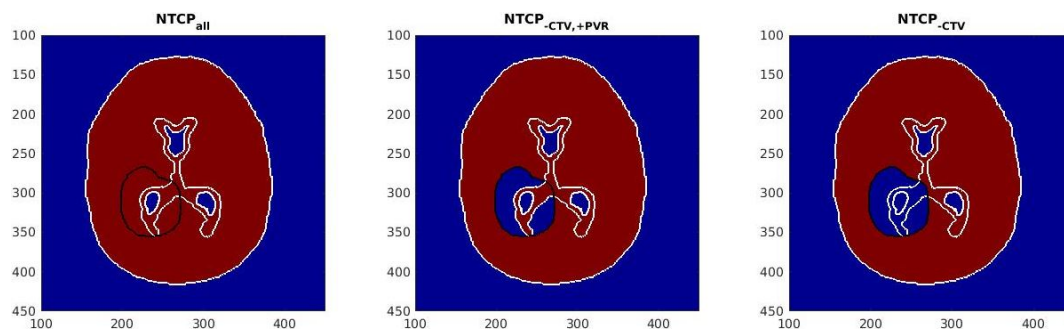


Figure 2.1: Representation of three NTCP definitions. Left: All voxels inside the body are included (NTCP<sub>all</sub>). Middle: The voxels inside the CTV, excluding the voxels of the PVR, are removed from the NTCP<sub>all</sub> (NTCP<sub>CTV,+PVR</sub>). Right: All voxels inside the CTV are excluded from the NTCP<sub>all</sub> (NTCP<sub>CTV</sub>). In all three NTCP definitions, the ventricles' inner liquid cavities were excluded from the analysis. Red: Voxels included during analysis. Blue: Voxels excluded from the analysis. For reference, the ventricles (delineated by the inner white lines), CTV (black), and the body (outer white boundary) are presented.

### 2.3. Patient cohort, treatment planning data, and contouring

We used the treatment planning data, including the CT, structure delineation, and clinical IMPT plan, from 3 patients referred from Erasmus Medical Center to HollandPTC for treatment of neurological tumors of 59.4 Gy<sub>RBE</sub> in 33 fractions. Treatment was based on a three-field irradiation. Clinical characteristics are listed in table 2.1. For comparison, the clinical VMAT treatment plan prepared for the plan comparison were analyzed. The same beam settings and objectives were used to re-optimize the VMAT plan on the planning-CT from HollandPTC, resulting in an almost equal treatment plan to an absorbed dose of 59.4 Gy in 33 fractions.

Table 2.1: Clinical characteristics

Patient	$V_{\text{CTV}}$ [cm <sup>3</sup> ] <sup>1</sup>	CTV shape <sup>2</sup>	CTV location	Symptoms
No. 1	266.5	Spherical	Deep, right-lateral to the brainstem	yes
No. 2	620.8	Elongated	Mostly deep, the lateral side of the CTV is superficial	no
No. 3	889.6	Elongated	Superficial, left lateral-anterior	no

<sup>1</sup> The clinical target volume is calculated by multiplying the tumor voxels times the size of a single voxel ( $0.6 \times 0.6 \times 3.0 \text{ mm}^3$ ).

<sup>2</sup> Simplified description of the target shape.

The ventricular system was identified and contoured by a clinician or by me. The contours were verified by a clinician. The 4 mm extension around the ventricular system was obtained by applying an expansion function. However, the delineation of structures may vary between clinicians or potential deviations may be introduced due to the image quality. Therefore, we tested the robustness of the NTCP<sub>all</sub> outcome on the periventricular definition by isotropically expanding the range of 1 to 6 mm.

## 2.4. Evaluation of RBE/LET effect

### 2.4.1. Comparison of proton vs photon plan

To assess the risk of the proton treatment plans in terms of NTCP, the clinical used IMPT plans were analyzed. In case of photons, the  $LET_d$  is (mostly) that of secondary electrons. Models assumed that photons generated by a 6 MV linac or  $^{60}\text{Co}$  source has a uniform  $LET_d$  of 0.3 keV/ $\mu\text{m}$  (e.g. [41]). For  $^{137}\text{Cs}$  photon radiation a  $LET_d$  of 1.0 keV/ $\mu\text{m}$  is assumed (e.g. [42]). We adopted these  $LET_d$  values to evaluate the VMAT plans.

### 2.4.2. The contribution of $LET_d$

To separately analyze the contribution of the  $LET_d$  and dose, we made a theoretical comparison by applying a uniform proton  $LET_d$ , in the same way as was done for photons. Since the POLO is based on the physical dose, a higher  $NTCP_{\text{all}}$  is expected when using photons compared with using protons for a given uniform  $LET_d$ . The analysis may provide an indication (i) to what extent we have to reduce the proton  $LET_d$  in order to achieve a similar  $NTCP_{\text{all}}$  as with photons, and (ii) of what  $NTCP_{\text{all}}$  value we can achieve with protons when assuming an average LET of 2-3 keV/ $\mu\text{m}$  [17].

### 2.4.3. Individual Pencil Beam Contribution

To get a better understanding of the impact of an individual pencil beam on the  $NTCP_{\text{all}}$ , we re-calculated the  $NTCP_{\text{all}}$  after filtering one pencil beam from the total treatment plan. The contribution of the individual filtered pencil beam is defined as the decrease in  $NTCP_{\text{all}}$ . The dose of the individual pencil beam,  $d$ , was subtracted voxelwise from the total treatment plan,  $D_{\text{total}}$ , by which we obtained the re-calculated dose,

$$D_{\text{min}j,i} = D_{\text{total}i} - d_{j,i}, \quad (2.1)$$

with the filtered pencil beam,  $j$ , and voxel  $i$ . In contrast,  $LET_d$  is weighted to the total physical dose. Therefore, the re-calculated  $LET_d$ ,

$$LET_{\text{min}j,i} = \frac{l_{\text{total}i} \cdot D_{\text{total}i} - l_{j,i} \cdot d_{j,i}}{D_{\text{min}j,i}}, \quad (2.2)$$

is corrected for both the dose and  $LET_d$  of the filtered pencil beam, with  $l$  as the  $LET_d$  of the filtered pencil beam and  $l_{\text{total}}$  as the original  $LET_d$  distribution.

### 2.4.4. Strategies to mitigate the RBE/LET effect

RBE mitigating strategies, which mainly focus on  $LET_d$ , have been investigated by many others optimization (see appendix 7.5 for more detail). The selection of the robustness, beam angle, and beam energy have the potential to reduce the biological variability without explicitly using optimization algorithms besides dose optimization. Therefore, these beam parameters are of interest for this work.

We used RayStation to manually edit the beam parameters of the clinically approved plan. Thereby, the aim is to investigate (i) the impact of planning parameters on the NTCP and (ii) the level of NTCP which can be achieved when using protons.

#### Robustness

To investigate the impact of robustness on the RBE/LET effect, we re-optimized the clinical treatment plan with different robustness margins. The beam weights were re-optimized using the same objectives as for the clinically used plan resulting. No manual edits were applied as was done in the clinical approved IMPT plan. Besides, the cost functions were edited to limit computation time. Due to these deviations compared to the clinical IMPT plan, the  $NTCP_{\text{all}}$  may deviate.

#### Beam-angle

By re-arranging the proton beams, the  $LET_d$  can be redistributed. To investigate the influence of different beam angle configurations on the NTCP, we created a 2-field, with one beam that is fixed and a second beam that changes in direction. In addition, we generated various treatment plans consisting of three beams, as commonly applied in IMPT plans at HollandPTC. The goal is to investigate the impact on NTCP while considering the observations when using a 2-field set-up. We allowed beam angles to pass through a large proportion of the brain tissue. For each arrangement, RayStation performed an

optimization to determine the beam settings. For optimization, we used the same objectives as for the clinically used plan (appendix 6.1, table 6.1) to obtain a comparable plan.

### Proton energy

As the Bragg peak has the greatest contribution to the  $LET_d$ , another way to reduce  $LET_d$  values is to eliminate the Bragg peak. By increasing the number of shoot-through (pencil) beams, also called transmission beams, the dose in the brain will increase. At the same time, the  $LET_d$  decreases. Therefore, an optimum in NTCP is expected.

Ideally, individual pencil beams with the greatest contribution to the  $NTCP_{all}$  should be extended. However, the identification of these spots is hard without computing the pencil beams individually. Together with the re-optimization, it requires too computation-intensive procedures. Therefore, we choose to use transmission layer. In our first approach, we investigated the impact of a single layer. We started with the layer that has the highest energy and increased its energy up to the maximum of 244 MeV. Then, we increased the energy of the layer with the second highest energy. This procedure was repeated until all layers of a single beam were turned into transmission layers. Furthermore, different combinations of transmission beams can be made. In our second approach, we increased the energy of multiple layers for at least two beams.

However, by increasing the proton energy, the Bragg peak is replaced by the entrance dose of the proton beam. For full CTV coverage, the beam weights were re-optimized at each step. During the optimization step, a minimum objective list was used, including only the external dose fall-off, minimum and maximum dose description for the CTV, and maximum dose objective for outside the target volume (appendix table 6.3-6.5). No robust optimization is applied, as RayStation failed when applying a robust optimization with (partial) transmission beam. For comparison, we also re-optimized the clinical IMPT plan with a minimal objective list.

In general, the clinical IMPT plan was used as starting point to generate an IMPT plan including transmission layers. However, if a beam was directed towards the thorax or shoulder and turns into a transmission beam, then the Bragg peaks were still present within the body. Nevertheless, we used the original setting for these patients in order to identify the effect of transmission beams compared to the clinical planning strategies.

The generated plans were exported from RayStation via dicomRT files to MCsquare. After calculating the MCsquare dose and  $LET_d$ , the NTCP was determined in Matlab (R2017a).

### 2.4.5. Combination of treatment modalities

Up to now, we have studied the LET/RBE effect for protons and photons separately. However, both proton treatment and photon treatment have their advantages and disadvantages. It is of interest to identify the relationship in  $NTCP_d$  for a combination of two treatment modalities. Therefore, we incorporate (i) photon treatment fractions along with proton delivery (IMPT-VMAT) or we modified a number of fractions of the clinical IMPT by (ii) turning beams into transmission beams (IMPT-TB). If not all beam layers have been extended, then we denote this as an partial transmission beam plan (IMPT-pTB).

#### Proton plan including photon fractions: IMPT-VMAT plan

As the contribution of the proton and photon fractions to the POLO are dependent on each other, the POLO cannot easily be added.

With  $LET_d$  as intrinsic quantity, a single proton can deliver the same  $LET_d$  as with thousands of protons. When the patient receives the same treatment at each fraction, the  $LET_d$  remains unaffected when changing the number of fractions,  $f$ , for a certain modality. By contrast, the total dose equals a summation of all doses per fraction,  $d$ . Then the POLO model reads

$$\log\left(\frac{POLO}{1-POLO}\right) = b_0 + b_1 \cdot \sum_1^f d + b_2 \cdot \sum_1^f (d \cdot LET_d) + b_3 \cdot PVR, \quad (2.3)$$

where the  $b_{0-3}$  are the model weighting factors.

Second, the contribution of the proton fractions,  $f_p$ , and photon fractions,  $f_\gamma$  can be separated. Then the linear combination of the POLO is given as,

$$C = b_0 + b_1 \cdot \left( \sum_1^{f_p} d_p + \sum_{1+f_p}^{f_p+f_\gamma} d_\gamma \right) + b_2 \cdot \left( \sum_1^{f_p} (d_p \cdot LET_{d,p}) + \sum_{1+f_p}^{f_p+f_\gamma} (d_\gamma \cdot LET_{d,\gamma}) \right) + b_3 \cdot PVR, \quad (2.4)$$

where the  $d_p$  and  $LET_{d,p}$  are the proton dose and  $LET_d$  per fraction, respectively, and the  $d_\gamma$  and  $LET_{d,\gamma}$  are the photon dose and  $LET_{d,p}$  per fraction, respectively.

Instead of the dose per fraction, we used the total physical dose. As each fraction delivers the same dose, we weighted total physical dose distributions,  $D_p$  and  $D_\gamma$ , by the ratio of the wanted number of fractions to the total number of clinically used fractions. The final equation,

$$C = b_0 + b_1 \cdot \left( \left( \frac{33 - f_\gamma}{33} \right) D_p + \left( \frac{f_\gamma}{33} \right) D_\gamma \right) + b_2 \cdot \left( \left( \frac{33 - f_\gamma}{33} \right) D_p \cdot LET_{d,p} + \left( \frac{f_\gamma}{33} \right) D_\gamma \cdot LET_{d,\gamma} \right) + b_3 \cdot PVR, \quad (2.5)$$

is used to investigate the impact of a combined treatment plan on the NTCP for different fraction combinations. We increased the number of proton fractions substituted by photon fractions from zero to the total of 33 fractions.

### Proton plan including transmission beams: IMPT-(p)TB plan

Moreover, proton transmission beams that lack the Bragg peak inside the patient can be compared to photon irradiation. For further analysis of the effect of transmission beams on the NTCP, we replaced the photon fractions in equation (2.5) by fractions with transmission proton plans as described in section 2.4.4. If the clinical plan consists of beams directed to the thorax or shoulder, then the Bragg peak will be still present within the patient when turning these beams into transmission beams. If this is the case, we modified the beam direction of that specific beam, e.g., by placing the beam within the transversal plane. In this way, more realistic combined treatment plans are generated.

## 2.5. General outline

During analysis, we used first the data from a single patient to explore the impact of different planning strategies on the NTCP. In general, the complication rate depends on the dose as indicated by the NIPP [9]. The NIPP describes that proton therapy has a dosimetric benefit over photons as the mean dose outside the target volume is reduced by >5%. As the mean brain dose is considered as an appropriate guiding parameter for the clinical outcome, we evaluated the trade-off in mean brain dose due to an improvement in NTCP, and whether the clinical goals are reached. Last, the findings were applied on two new glioma patients for comparison to identify similarities and potential differences.



# 3

## Results

### 3.1. Implementation and verification

The open source Monte Carlo dose engine, MCsquare, is successfully implemented to simulate the dose and  $LET_d$  distribution using the HollandPTC beam model. The MCsquare absorbed dose distribution is identical to the absorbed dose and range in the clinical treatment planning system (RayStation TPS, v7).

The results of the implemented POLO model in Matlab (2017a) matches that of Bahn et al. [1] as the POLO values are in the same range. Furthermore, the interpolation and resampling approaches, which correct for the voxel-volume, give an identical  $NTCP_{all}$ .

### 3.2. Comparison of proton and photon treatment plans

Table 3.1 lists the  $NTCP$  values we found for the IMPT plan and VMAT plan. It also specifies the statistical uncertainty used to compute the clinical IMPT dose distribution and  $LET_d$  distribution by MCsquare and the robustness used for optimization in RayStation. In all cases, the VMAT plan has a significantly lower  $NTCP$  compared to the IMPT plan.

Table 3.1:  $NTCP$  results of the clinically used IMPT plans and VMAT plans used for plan comparison

Patient	Plan characteristics		Patient-level risk			Stat.un. <sup>2</sup>	Robustness
	Modality	LET [keV/ $\mu$ m] <sup>1</sup>	$NTCP_{all}$	$NTCP_{CTV, +PVR}$	$NTCP_{CTV}$		
No. 1	Proton		36.0%	25.6%	16.4%	1%	3%/3mm
	Photon	0.3	9.5%	6.0%	3.5%		
	Photon	1.0	18.0%	12.1%	7.0%		
No. 2	Proton		43.2%	22.1%	16.1%	2%	3%/3mm
	Photon	0.3	16.0%	5.9%	3.7%		
	Photon	1.0	30.9%	11.9%	7.3%		
No. 3	Proton		63.0%	38.3%	24.7%	2%	3%/3mm
	Photon	0.3	25.5%	13.7%	10.2%		
	Photon	1.0	46.2%	26.5%	19.9%		

<sup>1</sup> No  $LET_d$  is provided for protons as protons have a non-uniform  $LET_d$  distribution.

<sup>2</sup> We choose a statistical uncertainty of 1% or 2% for the computation of the MCsquare dose and  $LET_d$ .

For visualization, figure 6.1 (top row) shows the physical dose and  $LET_d$  distribution of the clinically used proton plan calculated in MCsquare, and the corresponding POLO distribution using the data of patient 1. The bottom row represents the physical dose distribution for the VMAT plan, the uniform  $LET_d$  distribution of 0.3 keV/ $\mu$ m, and its corresponding POLO distribution. For reference, the delineation of the ventricles and the 4 mm margin around them are displayed in white (inner structures),

the body in white (outer boundary), and the CTV in black. The  $LET_d$  distribution only shows the  $LET_d$  for doses above 0.2 Gy. Similar distributions can be found in appendix 6, figure 6.1, for patient 2 and patient 3. The increased  $LET_d$  values are mainly found within the region where the distal ends of the proton beams overlap. Within the CTV, the  $LET_d$  ranges from 2 to 4 keV/ $\mu$ m. Behind the target volume, the  $LET_d$  increases up to 4.8 keV/ $\mu$ m (dose >30 Gy) and 9.3 keV/ $\mu$ m (dose >10 Gy). The highest POLO is observed at the edge of the radiation field with a dose of 54 Gy and a LET of 4.4 keV/ $\mu$ m.

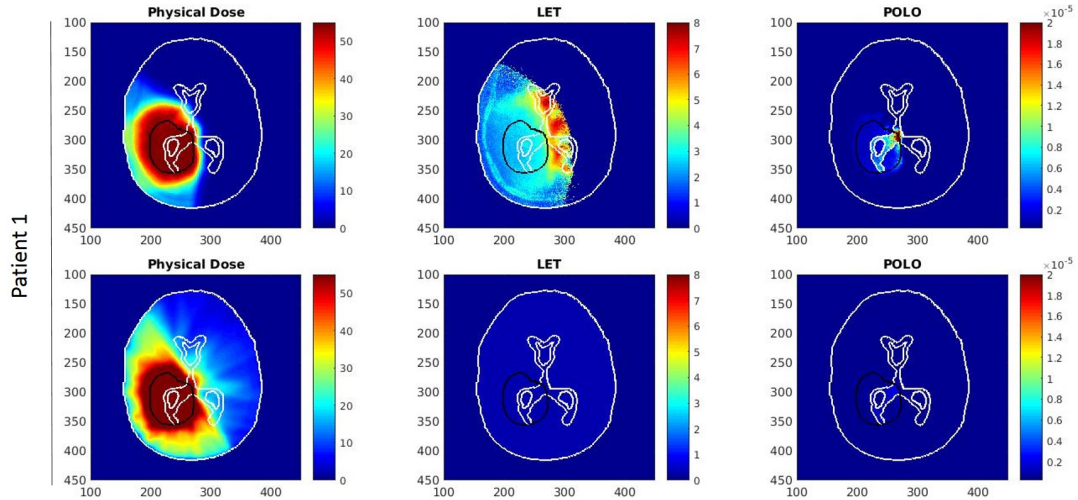


Figure 3.1: Dose, LET, and POLO for the clinical IMPT and VMAT treatment plans. Left column: The physical dose is weighted in the IMPT plan (top row) by the biological effectiveness (RBE) of 1.1. No weighting is applied for the VMAT plan (bottom row). Middle column: The dose-averaged linear energy transfer ( $LET_d$ ) is only shown for doses above 0.2 Gy. A uniform  $LET_d$  of 0.3 keV/ $\mu$ m is assumed for the VMAT plan. Right column: The per voxel probability of lesion origin (POLO). The area between the inner white structures represents the periventricular region (PVR), the outer white boundary shows the body surface, and the black structure depicts the CTV.

For a theoretical comparison, figure 3.2 shows the progression in  $NTCP_{all}$  for patient 1 when using a uniform  $LET_d$  for protons (red). With  $photons_{LET=0.3}$  keV/ $\mu$ m and  $photons_{LET=1.0}$  keV/ $\mu$ m, we found an  $NTCP_{all}$  of 9.5% and 18.0%, respectively. Similar results can be achieved using protons that have a uniform  $LET_d$  of 1.5 keV/ $\mu$ m or 2.2 keV/ $\mu$ m, respectively. However, protons have an average  $LET_d$  of 2-3 keV/ $\mu$ m [17], which corresponds to an  $NTCP_{all}$  of 16-38%. This  $NTCP_{all}$  level is the lowest we expect to achieve with protons using data from patient 1.

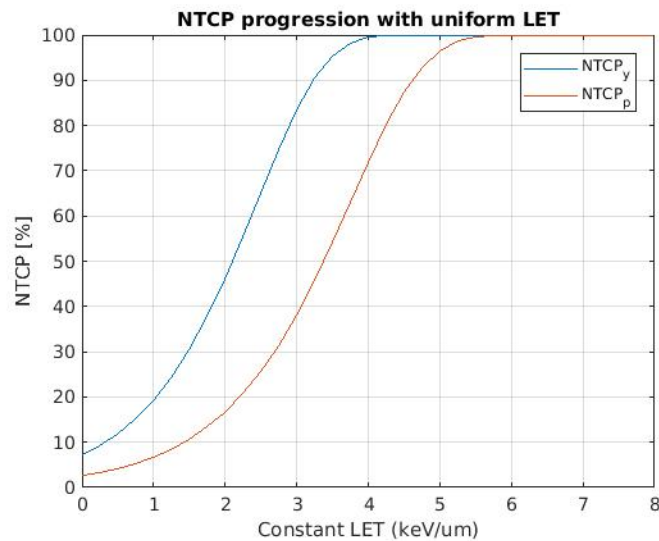


Figure 3.2: The progression in  $NTCP_{all}$  when considering a uniform  $LET_d$ . The progression of the  $NTCP_{all}$  is given for protons (red) and photons (blue) when a uniform  $LET_d$  is applied.

### 3.3. Deviations in NTCP

#### 3.3.1. Computation deviations

To identify deviations in  $NTCP_{all}$  due to the noise of the MCsquare calculation, we repeated the dose and  $LET_d$  calculation of the clinical IMPT plan used to treat patient 1 (table 3.2). We found that the  $NTCP_{all}$  has a standard deviation of 0.4%.

Table 3.2: NTCP for repeated computations.

	Simulation				Mean	Std.	Stat.un.
	Run 1	Run 2	Run 3	Run 4			
$NTCP_{all}$	36.0 %	35.0 %	35.6%	35.6%	35.0%	0.4%	1.0%

To identify the accuracy of the MCsquare calculation affecting the  $NTCP_{all}$ , we computed the dose and  $LET_d$  with a statistical uncertainty of 0.5%, 1.0% and 2.0%. In general, the  $NTCP_{all}$  increases with increasing uncertainty (table 3.3).

Table 3.3: NTCP for different statistical uncertainties.

Statistical uncertainty	$NTCP_{all}$			Time
	No. 1	No. 2	No. 3	
0.5%	35.8 %	-	-	4h
1.0%	36.0 %	42.6 %	-	<6h
2.0%	37.2%	43.2%	63.0%	<3h

Increasing the statistical uncertainty by a factor 2 means also doubling the computation time. The computation of the IMPT plan for patient 1 took two hours when applying a statistical uncertainty of 1.0%. Though a longer computation time is necessary for plans with a larger radiation field to reach the desired accuracy. Circa six hours were needed to generate the data for patient 2 with an statistical uncertainty of 1.0%. Furthermore, MCsquare had difficulties to reach the desired accuracy 0.5% for patient 2 and 1.0% for patient 3. The optimal result was not found in a reasonable time span (<36h). Therefore, we left out these  $NTCP_{all}$  levels.

#### 3.3.2. Delineation deviations

Other sources of variation in NTCP are the deviations in the PVR definition. Table 3.4 gives an overview of the  $NTCP_{all}$  for different extension distances to define the PVR. Our results shows that the  $NTCP_{all}$  deviates by 2% for the IMPT plan when varying the threshold distance of the PVR by 1 mm. A smaller increase in  $NTCP_{all}$  is found when using photons with a  $LET_d$  of 0.3 keV/ $\mu$ m or 1.0 keV/ $\mu$ m. With each mm, the  $NTCP_{all}$  increases by 0.6% or 1.0%, respectively.

Table 3.4: NTCP for the clinical IMPT and VMAT plans used for plan comparison

Expansion	$NTCP_{all}$		
	Proton	Photon $_{LET=0.3 \text{ keV}/\mu\text{m}}$	Photon $_{LET=1,0 \text{ keV}/\mu\text{m}}$
1 mm	30.1%	7.8%	15.7%
2 mm	32.0%	8.3%	17.0%
3 mm	34.1%	8.9%	17.7%
4 mm	36.0%	9.5%	18.8%
5 mm	38.4%	10.2%	20.2%
6 mm	40.6%	10.9%	21.5%

### 3.4. Individual pencil beam contribution

The contribution of each individual pencil beam to the  $NTCP_{all}$  of the clinical IMPT plan of patient 1 is visualized in a figure 3.3 (left). The contribution to the  $NTCP_{all}$  ranges between 0% to 0.06%, with a mean of 0.0046%. Figure 3.3 (right) shows the  $NTCP_{all}$  contribution against the initial energy of the pencil beam. In general, the contribution to the  $NTCP_{all}$  increases with increasing beam energy.

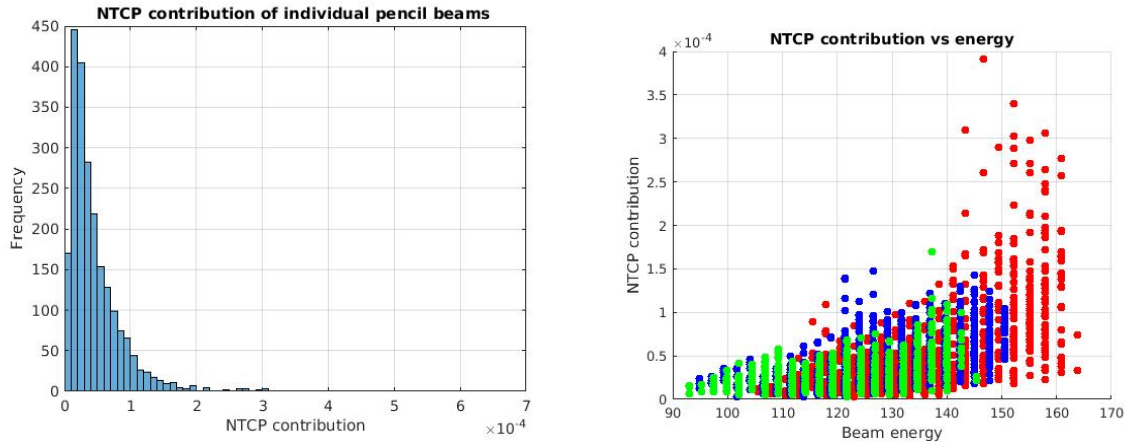


Figure 3.3: Contribution to the NTCP of individual pencil beams. Left: the individual pencil beam contribution to the NTCP. Right: the individual pencil beam contribution to the NTCP against the initial pencil beam energy. The data is subdivided for the three beams: beam 1 (red), beam 2 (blue), and beam 3 (green).

### 3.5. Impact of beam settings on the NTCP

In the pages that follow, the impact of varying the beam settings - the robustness, beam angle, and beam energy - on the NTCP are presented.

#### 3.5.1. Robustness

The first set of analyses identifies the impact of the robustness on the NTCP. Table 3.5 summarizes the obtained  $NTCP_{all}$  for different robust settings. The scored  $NTCP_{all}$  values deviate by a maximum of 0.8%. Compared to the robustness setting used for the clinical treatment plan of 3mm/3%, no improvement in terms of the NTCP was observed.

Table 3.5: NTCP for different robustness settings.

	Robustness				Stat.un
	0mm/0%	2mm/3%	3%/2mm	3%/3mm	
$NTCP_{all}$	39.4 %	40.0 %	40.2%	40.0%	1%

### 3.5.2. Beam angle

#### Two-field arrangement

Variations in NTCP were found when changing the treatment beam angles (figure 3.4, right column). Comparable field arrangements were generated with one similar beam (fixed beam), while the second beam varies (moving beam). The analysis with a 2-field were only performed with the data from patient 1. We made seven beam angle configurations in which the moving beam is spaced by 45-50° in transferal plane when fixing beam 2 (first row), fixing beam 1 (second row). These field configurations are shown figure 3.5. The dose, LET<sub>d</sub>, and POLO distribution for each arrangement are visualized in figure 6.3 and figure 6.4 (appendix 6.2). In addition, we tilted the moving beam by 45° (figure 3.4, bottom row).

Considering all field arrangements, the NTCP<sub>all</sub> ranges from a minimum of 29.7% to a maximum of 40.1%. Compared to the clinically used plan with an NTCP<sub>all</sub> of 36.0%, the NTCP<sub>all</sub> improved by a maximum of 6.3%. (19.4%). Note, relative change in NTCP is given in brackets. Besides, the NTCP<sub>CTV,+PVR</sub> (dashed line), and NTCP<sub>CTV</sub> (dotted line) decreased with a maximum of 8.2%. (32.0%) and 9.1%. (53.8%), respectively.

A change in the field arrangement results in the migrating of LET<sub>d</sub> (figure 3.4, left column, dashed lines) and in a redistribution of the dose (solid lines). The NTCP<sub>all</sub> changes proportionally with the mean LET<sub>d</sub> in the PVR (orange), and inversely with the mean dose. Additionally, the NTCP<sub>CTV,+PVR</sub>, and the NTCP<sub>CTV</sub> follow a similar tendency.

In general, the NTCP<sub>all</sub> becomes smaller when the angle between the beams becomes larger. Opposing beams result in the smallest NTCP<sub>all</sub> as the end of the beams are less overlapping (e.g. figure 6.3, 4<sup>th</sup> row). Additionally, the NTCP increases when the beams point towards the PVR (e.g. figure 6.4, 5<sup>th</sup> row).

#### Three-field rearrangement

Based on the observations using two beams, we generated various plans with three beams. Figure 3.6 shows the 3-field rearrangements with their corresponding dose distribution and LET distribution. The beams that remain unchanged with respect to the clinical plan are presented by the yellow arrow. Modified beams are given in white. We applied a larger angle between the beams by placing one beam opposite to another beam (option 1, 4 and 5), by using one oblique angle (option 2 and 5) or two oblique angles (option 3 and 6) passing the brainstem laterally. Consequently, the LET<sub>d</sub> spreads out around the target volume. The scored NTCP<sub>all</sub> ranges between 36.3% and 41.7%. Since the clinical IMPT plan has an NTCP<sub>all</sub> of 36.6%, no (significant) improvement has been achieved compared to the clinical IMPT plan. Nevertheless, all beam angle rearrangements improved the NTCP<sub>CTV</sub>, with a maximum of 5.5%. (27.4%).

A similar approach has been applied to patient 2 and patient 3 (appendix, figure 6.2). As the tumor of patient 2 is elongated in anterior-posterior direction, we directed one or two beams along this axis in combination with one oblique angle. The tumor of patient 3 is located in the superior-lateral part of the brain and is closely positioned to the skull. The clinical IMPT plan consists of one lateral beam and two beams pointing towards the ventricles and brainstem. To limit the stopping of the beams in the PVR, we let the lateral beam unchanged and diminished the angle of the other beams with respect to the transferal plane. Altogether, the NTCP<sub>all</sub> improved with a maximum of 5.2%. (11.6%) for patient 2. We reduced the NTCP<sub>all</sub> by 16.9%. (37.0%) for patient 3. Furthermore, the NTCP<sub>CTV</sub> improved by 4.6%. (27.7%) and 13.3%. (53.8%), respectively.

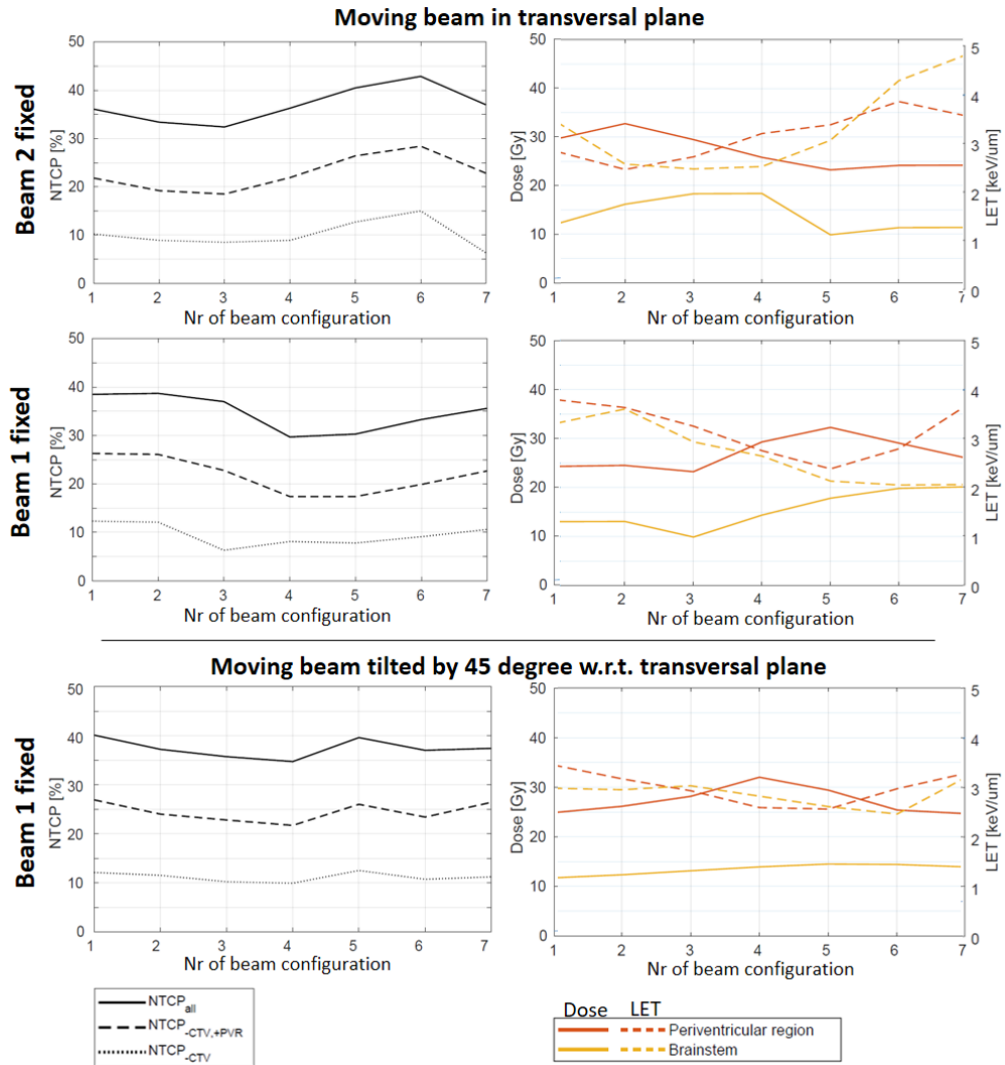


Figure 3.4: The  $NTCP_{all}$ , dose and  $LET_d$  for different beam angle configurations. While one beam is fixed, a second beam rotates clockwise in transversal plane (first and second row) or tilted by  $45^\circ$  with respect to the transversal plane (bottom row). Left: the different field arrangements impact the NTCP, where a distinction is made between  $NTCP_{all}$  (solid blue),  $NTCP_{-CTV,+PVR}$  (dashed blue), and  $NTCP_{-CTV}$  (dotted blue). Right: the change in mean dose (solid lines) and mean LET (dashed lines) are given for the periventricular region (orange) and brainstem (yellow). Note: the configurations of the presented numbers are visualized in figure 3.5.

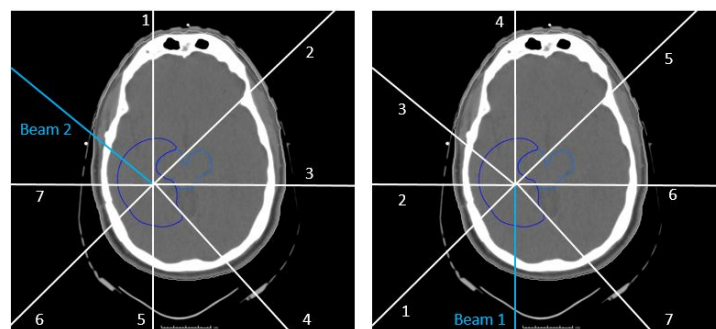


Figure 3.5: Representation of the used 2-field configurations. The CT scan is given in the inferior-superior direction. The blue line represents the fixed beam, while the white line represents the beam which changes its direction. Left: beam 2 is fixed and beam 1 changes in clockwise direction. Right: beam 1 is fixed, while beam 2 changes in clockwise direction.

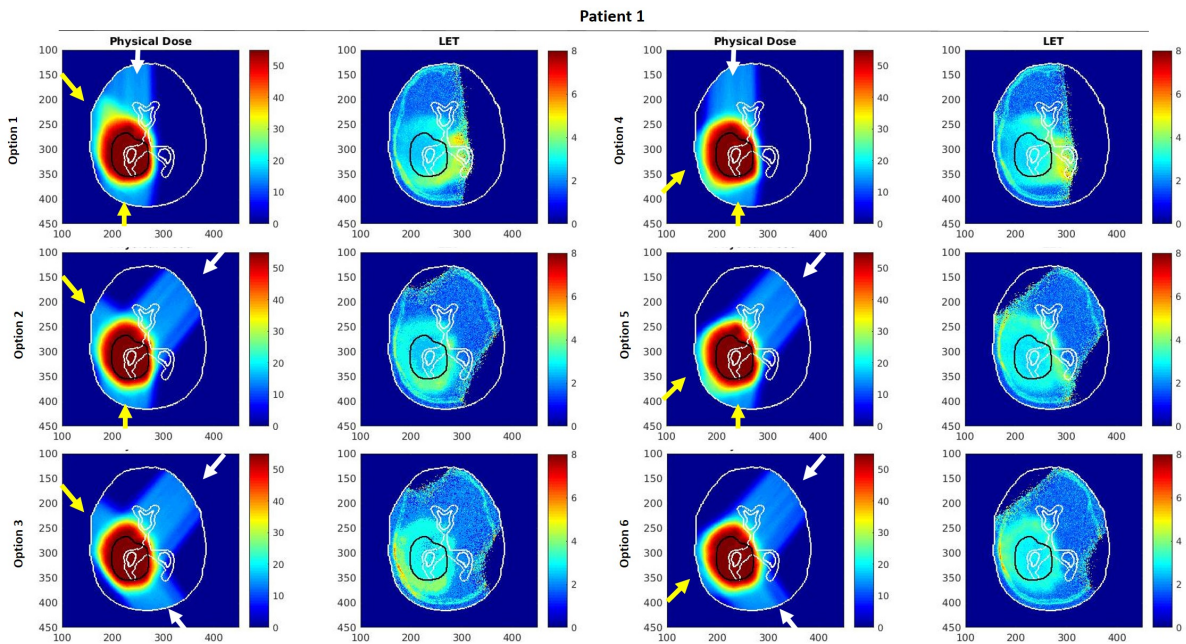


Figure 3.6: Dose and LET distribution for various beam angle configurations for patient 1. Various options of beam angle configurations are applied. For each arrangement, the physical dose (right figure). The corresponding  $LET_d$  is only shown for doses above 0.2 Gy. The arrows represent the direction of a beam. A yellow arrow represents a treatment beam used in the clinical treatment plan. A white arrow represents a beam that has been modified. For reference, the area between the inner white structures represents the periventricular region (PVR), the outer white boundary shows the body surface, and the black structure depicts the CTV.

### 3.5.3. Beam energy

To investigate the impact of the proton energy on the NTCP, we started by increasing the number of energy layers. This analysis is only performed with the data of patient 1. We observed a maximum decrease in the  $NTCP_{all}$ ,  $NTCP_{-CTV,+PVR}$ , and  $NTCP_{-CTV}$  of 7.5%, 4.9%, 2.9%, respectively (figure 3.7, left column). All beams reached its minimum in  $NTCP_{all}$  when two-third of the beam layers were shoot-through. After that, the  $NTCP_{all}$  remains unchanged. Though, before decreasing in  $NTCP_{all}$  occurs in case of beam 1 (top row) and beam 3 (bottom row), the  $NTCP_{all}$  increases when turning the first 4 layers into transmission layers. Besides, the  $NTCP_{-CTV,+PVR}$  follows the same tendency as  $NTCP_{all}$ . In contrast, the  $NTCP_{-CTV}$  decreases to a minimum when almost half of the beam layers are turned into transmission layers and subsequently increases.

In general, the mean dose (solid lines) in the PVR (orange) and brainstem (yellow) increases with increasing the number of transmission layers, while the  $LET_d$  (dashed lines) in those organs decreases (left column).

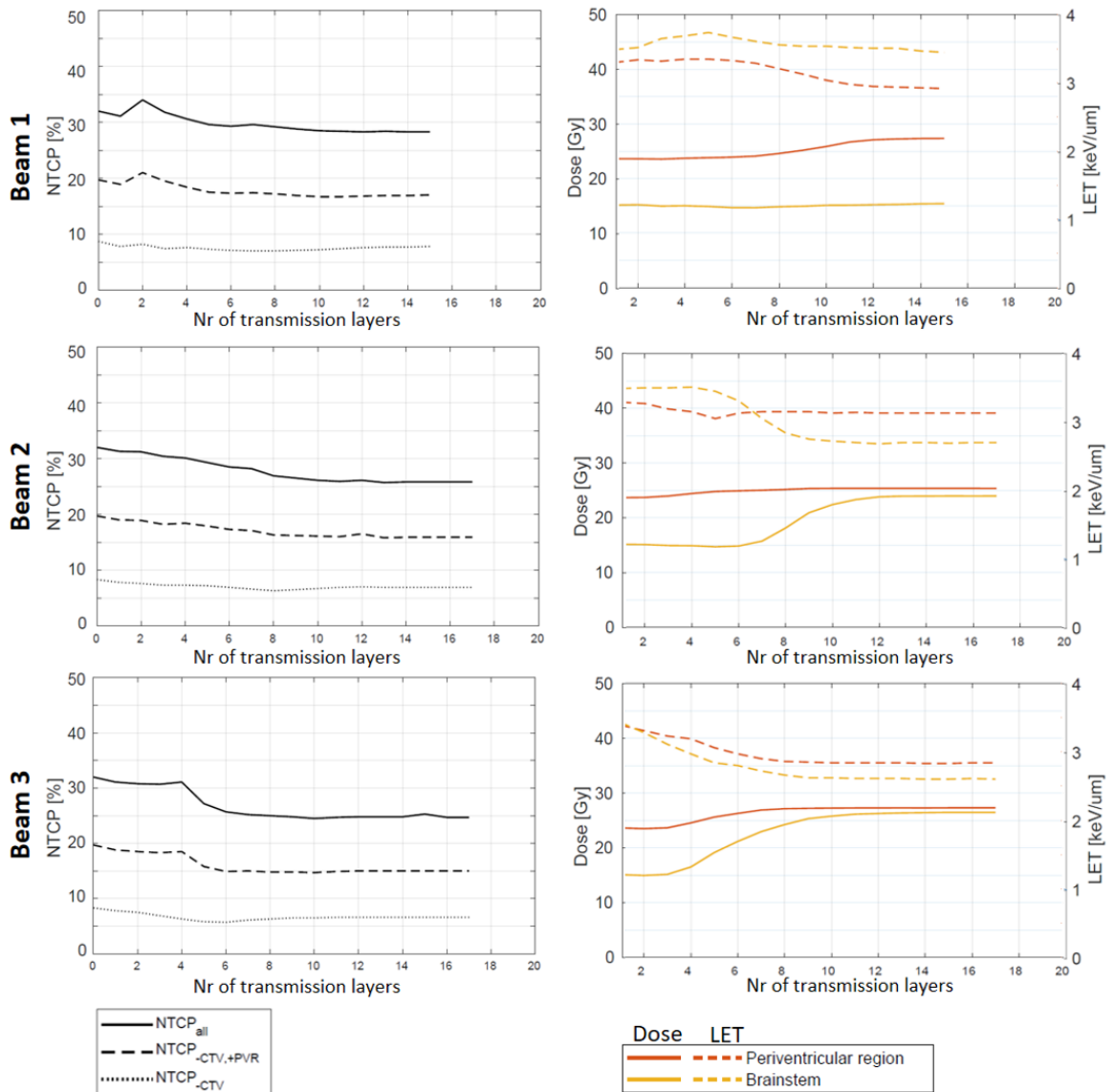


Figure 3.7: NTCP, dose, and  $LET_d$  progression by extending individual beam layers. The energy of the beam layers are increased to their maximum of 244 MeV for beam 1 (first column), beam 2 (second column), and beam 3 (third column). Left: the extension of the beam layer impacts the  $NTCP_{all}$  (solid),  $NTCP_{-CTV,+PVR}$  (dashed), and  $NTCP_{-CTV}$  (dotted). Right: the physical dose (solid lines) and  $LET_d$  (dashed lines) distribution are given for the periventricular region (orange), brainstem (yellow).

A combination of two or three transmission beams further reduces the  $NTCP_{all}$  (figure 3.8). A minimum in  $NTCP_{all}$  (red) of 17.6% is found when all the three beams are shoot-through. However, the  $NTCP_{all}$  progressively decreases to the point where half of the beam layers are shoot-through. This is called the tipping-fraction. After this point, the  $NTCP_{all}$  (left) gradually decreases or remains constant. Conversely, the  $NTCP_{CTV,+PVR}$  (middle) slowly increases with increasing number of transmission layers. This progression is even more pronounced for the  $NTCP_{CTV}$  (right). Similar patterns in NTCP are observed by including only two partial transmission beams (magenta, green, and yellow).

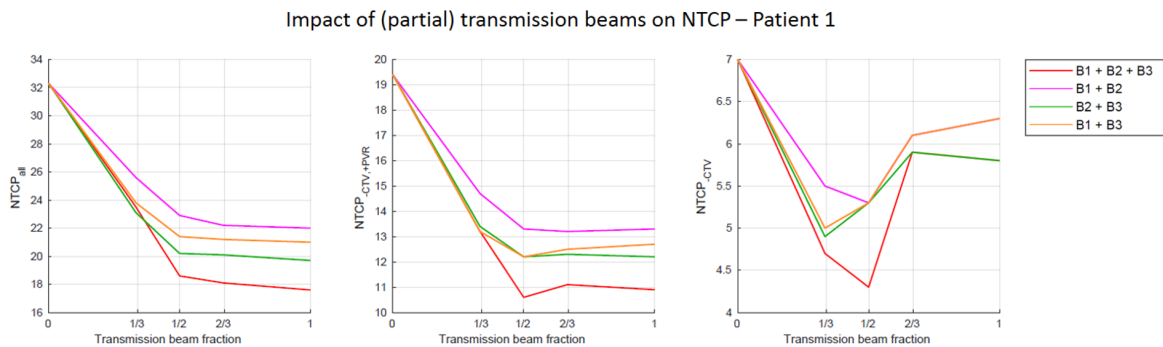


Figure 3.8: NTCP progression by extending beam layers of multiple beams using data from patient 1. A fraction of beam layers is increased for all beams together (blue line) or in dual (red, yellow, and purple line), which impacts the  $NTCP_{all}$  (left),  $NTCP_{CTV,+PVR}$  (middle),  $NTCP_{CTV}$  (right).

Meanwhile, the mean dose (solid lines) delivered to the brain increases rapidly to the point where half the number of layers are shoot-through (figure 3.9, top left). Beyond that point, the increase in dose slows down with increasing numbers of transmission beam layers. The change in mean physical dose within the PVR (bottom center) and brainstem (top right) follows a same pattern as in the brain. An opposite behaviour is seen for the mean  $LET_d$  (dashed lines). However, the  $LET_d$  remains almost constant after the tipping-fraction. Consequently, the radiation effectiveness in the PVR (bottom right) and brainstem (top right) decreases with decreasing mean  $LET_d$ , but increases once the  $LET_d$  stabilizes (figure 3.10). Further, the dose to the CTV (figure 3.9, top center) remains almost constant, while the  $LET_d$  diminishes till a value of 2.0-2.5 keV/ $\mu$ m. Thereby, the radiation effectiveness also reduces within the target volume (figure 3.10, top center).

Similar results in the mean physical dose and mean  $LET_d$  are observed for patient 2 (appendix, figure 6.10 (top) and 6.11) and patient 3 (figure 6.10 (bottom) and 6.13). It should be mentioned that two of the three beams used for patient 3 are pointing in the direction of the neck and chest.

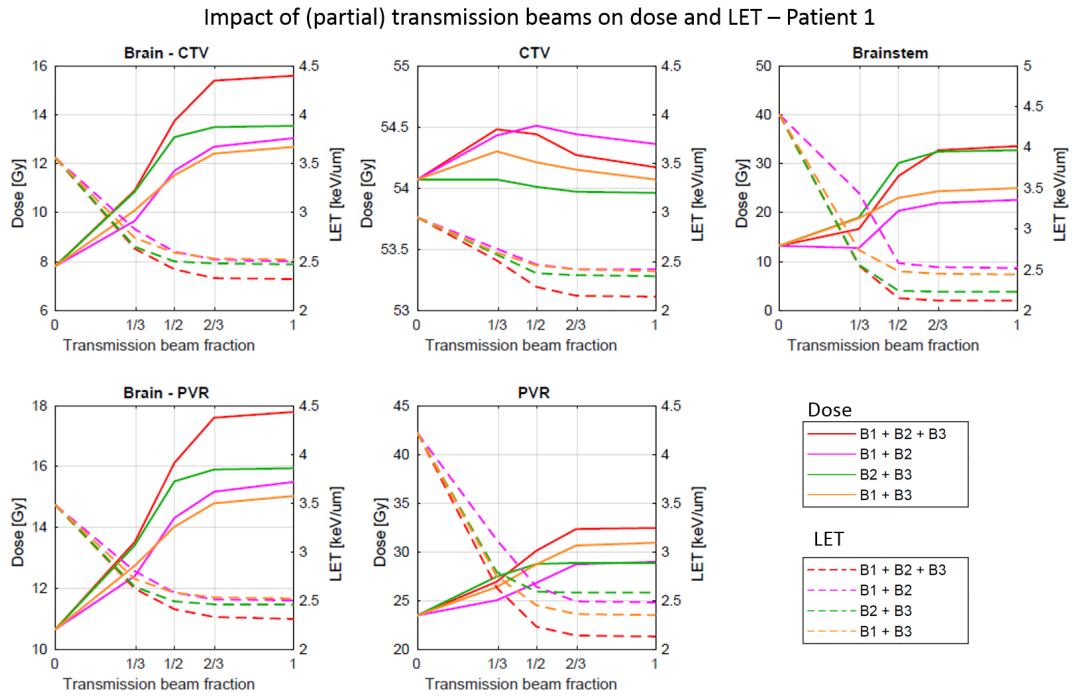


Figure 3.9: Dose and  $LET_d$  progression by extending beam layers of multiple beams using data of patient 1. A fraction of beam layers is increased for all beams together (blue line) or in dual (red, yellow, and purple line), which affects the mean physical dose (solid line) and mean  $LET_d$  (dashed lines) in the brain minus CTV (top left), CTV (top center), brainstem (top, right), brain minus periventricular region (bottom left), and periventricular region (bottom center).

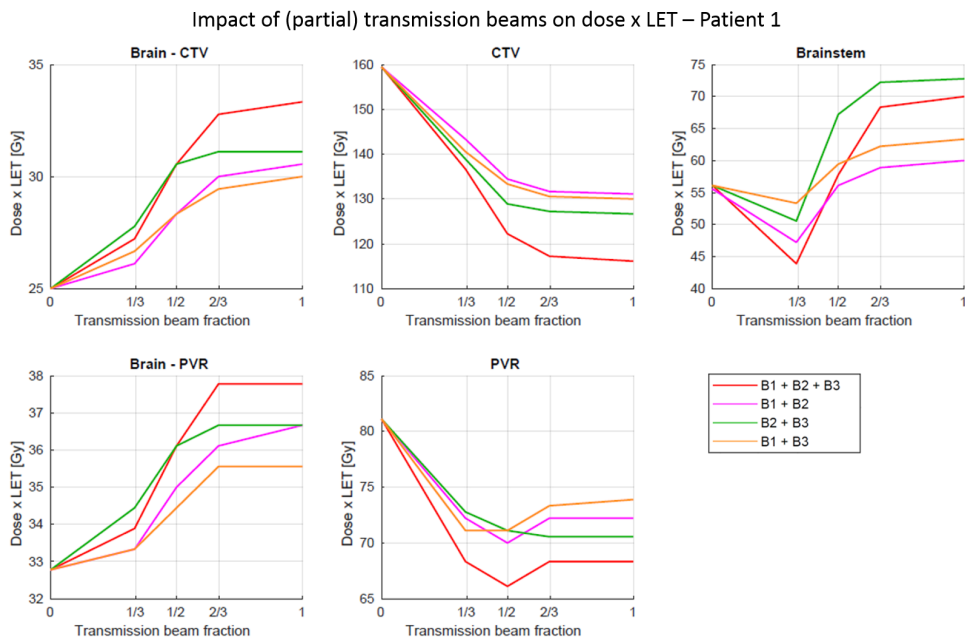


Figure 3.10: Radiation effectiveness progression by extending beam layers of multiple beams using data of patient 1. A fraction of beam layers is increased for all beams together (blue line) or in dual (yellow, and purple line), which affects the mean radiation effectiveness in the brain minus CTV (top left), CTV (top center), brainstem (top, right), brain minus periventricular region (bottom left), and periventricular region (bottom center).

### 3.6. Combined radiotherapy modalities - protons and photons

Finally, we looked at the impact of combining the clinically used proton plan with the photon plan used for plan comparison on the NTCP, called the IMPT-VMAT plan, or with partial proton transmission beams, called IMPT-pTB<sub>n</sub> plans.

#### 3.6.1. Clinical proton plan with clinical VMAT plan

The  $NTCP_{all}$  decreases non-linearly with increasing number of proton fractions substituted by photon fractions (figure 3.12, left). The contribution of photon fractions is largest for the first few involved photon fractions. Furthermore, the decrease in  $NTCP_{all}$  is steeper for photons with a  $LET_d$  of 0.3 keV/ $\mu$ m (blue) than photons with a  $LET_d$  of 1.0 keV/ $\mu$ m (cyan).

#### 3.6.2. Clinical proton plan with partial proton transmission plan

The IMPT-pTB plans showed a comparable result with the IMPT-VMAT plan if a  $LET_d$  of 1.0 keV/ $\mu$ m is assumed (figure 3.12, right). Once all proton fractions are substituted by fractions of proton partial transmission beams, then the  $NTCP_{all}$  has reached its lowest value of 18.6% (red). Instead, a similar  $NTCP_{all}$  can be realized when including 16 fractions of photon <sub>$LET_d = 0.3$  keV/ $\mu$ m</sub>. Similar results are observed using data of patient 2 and patient 3 (appendix figure 6.10). However, the clinical plan designed for patient 3 consists of two beams that are directed towards the thorax. Therefore, we choose beam angle arrangement option 3 and modified the beam energies. This adapted plan is used in combination with the clinical IMPT plan.

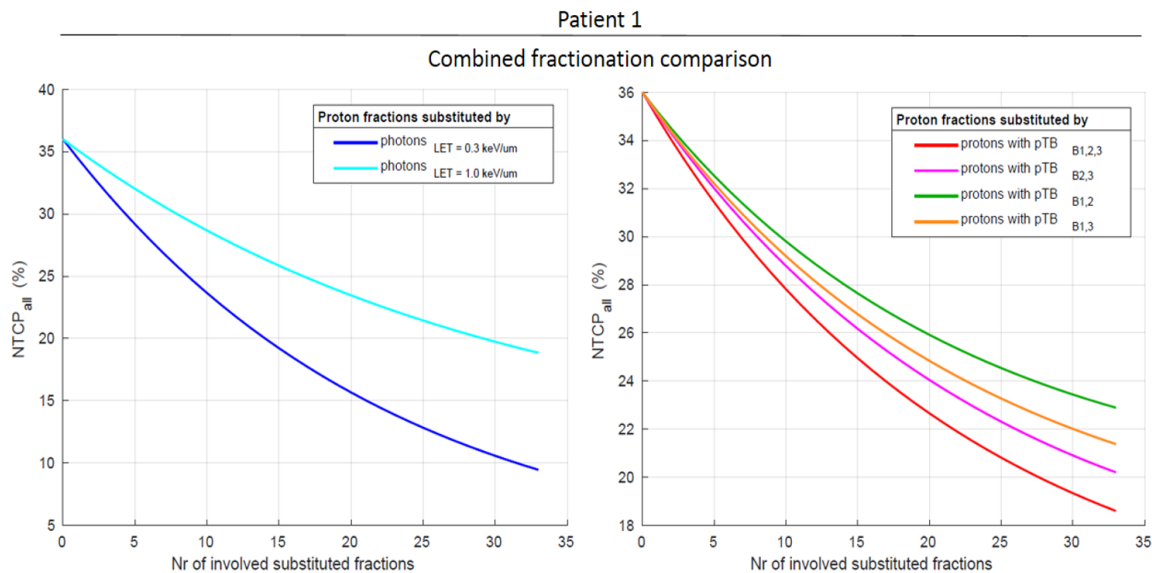


Figure 3.11: The impact of combining different treatment plans on the NTCP using data from patient 1. Left: The progression in  $NTCP_{all}$  when substituting fractions of the clinical proton plan by photons with a  $LET_d$  of 0.3 keV/ $\mu$ m (blue), by photons with a  $LET_d$  of 1.0 keV/ $\mu$ m (cyan) Right: The progression in  $NTCP_{all}$  when substituting fractions of the clinical proton plan by a proton plan including 3 half-transmission bundles (red), or by a proton plan including 2 half-transmission bundles (magenta, green, yellow).

#### 3.6.3. Comparison of combined radiotherapy modalities

However, an improvement in NTCP is at the cost of the mean brain dose ( $D_{mean}$ (brain-CTV)) (figure 3.12) and mean dose to surrounding organs. When all fractions of the IMPT plan are substituted by fractions with photons, the average absorbed brain dose increases from 10.4 Gy<sub>RBE</sub> to 17.9 Gy. By comparison, the IMPT-pTB plans deliver less mean dose to the brain (15.1 Gy<sub>RBE</sub> (red), 14.4 Gy<sub>RBE</sub> (magenta), 12.7 Gy<sub>RBE</sub> (green), 12.9 Gy<sub>RBE</sub> (yellow)).

The trade-off between  $NTCP_{all}$  and mean brain dose changes with the same rate for two of the IMPT-pTB plan (red and magenta) and for the IMPT-VMAT <sub>$LET_d = 0.3$  keV/ $\mu$ m</sub> plan, only for an  $NTCP > 26\%$  and a mean brain dose  $< 12.7$  Gy<sub>RBE</sub>. This corresponds to a substitution of 8, 14 or 16 fractions, respectively.

The remaining IMPT-pTB plans (green and yellow) provide a steeper slope in the  $NTCP_{all}-D_{mean}$  (brain-CTV) trade-off. In other words, a similar  $NTCP_{all}$  can be achieved while delivering a lower mean dose to the brain.

Similar results are obtained using data from patient 2 (appendix figure 6.11). In contrast, the IMPT-pTB plans of patient 3 are competitive with the IMPT-VMAT plan for an  $NTCP_{all}$  above 51% (magenta and orange), or less advantageous (red and green) (figure 6.13).

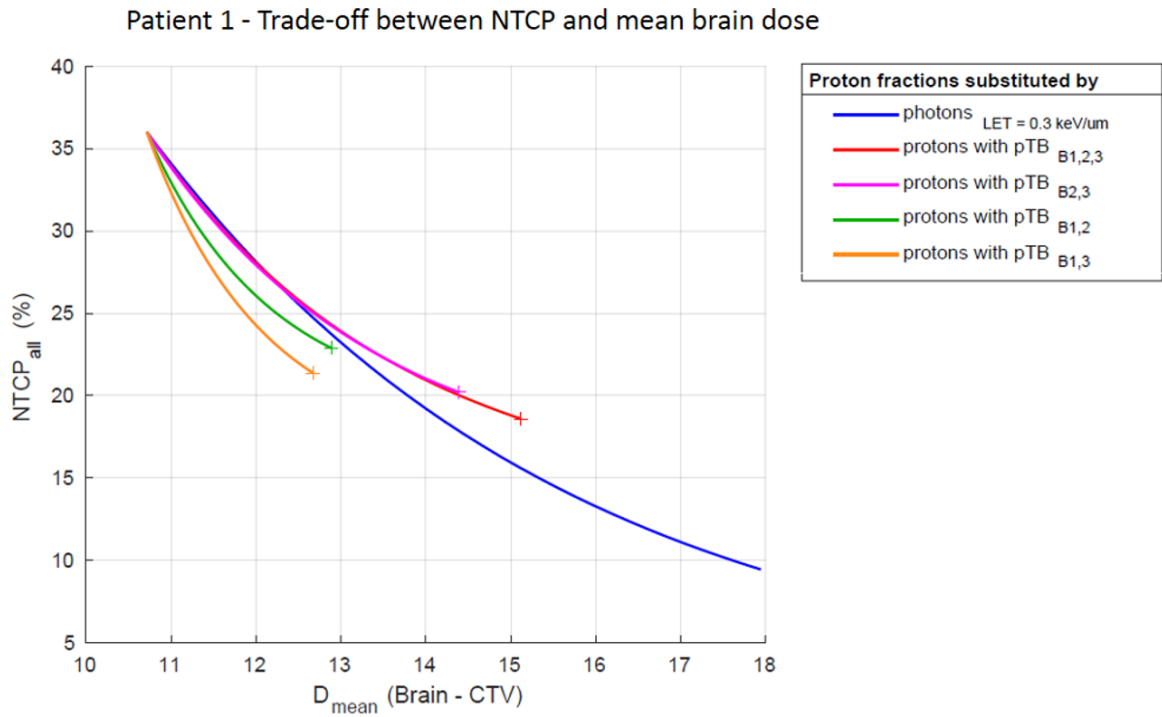


Figure 3.12: The trade-off in  $NTCP_{all}$  and overall brain dose using data from patient 1. An improvement in  $NTCP_{all}$  obtained by combining different treatment modalities results in an increase in the mean dose given to the brain minus CTV. The trade-off is given for the clinical proton plan combined with photons $_{LET=0.3keV/\mu m}$  (blue), and for various combination with proton transmission beams (red, magenta, green, yellow). For clarity, the endpoint of the proton transmission beams is indicated by a '+'-sign.

A more quantitative presentation of dose distribution is given by the dose-volume histogram (DHV) (figure 3.13, top). The VMAT plan (blue), IMPT-pTB plans (red and magenta) and the clinical IMPT plan re-optimized with a minimal objective list (green) deliver a comparable dose to the CTV (dashed lines). In contrast to the VMAT plan that irradiates the entire brain (solid lines), the clinical proton plan spares a part of the healthy tissue as only 40% of the brain is irradiated. In comparison, the IMPT-pTB plans irradiate at most 75% of the brain. Furthermore, the linear energy transfer-volume histogram (LHV) (figure 3.13, bottom) shows that the  $LET_d$  distribution becomes indeed more uniform by eliminating the Bragg peaks compared to the clinical proton plan.

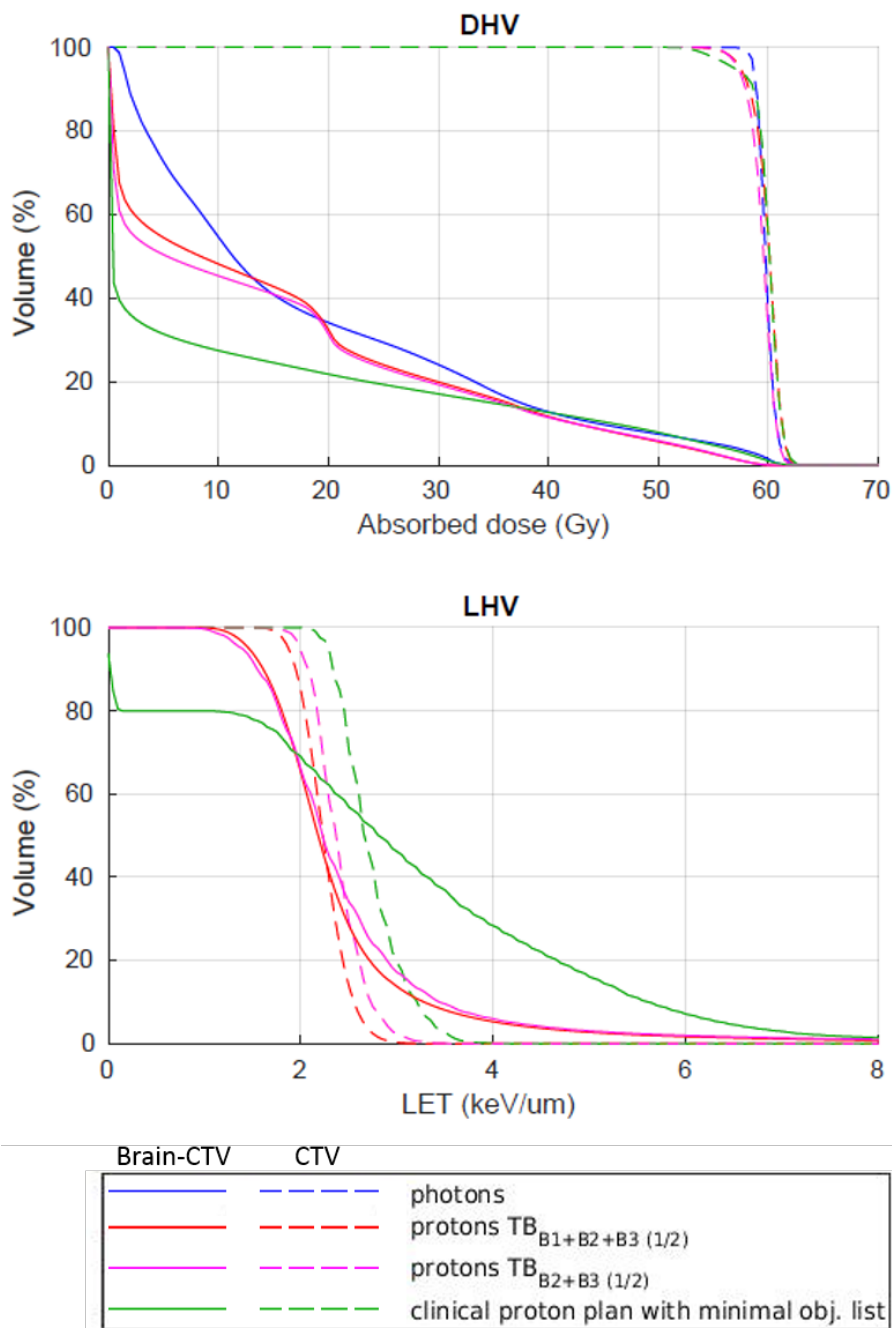


Figure 3.13: Dose- and  $LET_d$ -volume histogram for the CTV and the brain minus CTV using data from patient 1. The dose-volume histogram (top) and dose-weighted linear energy transfer ( $LET_d$ ) volume histogram for the brain (solid lines) and CTV (dashed lines) are given for the VMAT plan (blue), for the proton plans including partial transmission beams (red and magenta), and for the clinical proton plan optimized with a minimal objective list (green). The photon  $LET_d$  is not visualized since the  $LET_d$  is a constant.

A visual representation of the dose distribution is given by figure 3.14 at different depths. The IMPT-pTB plans (left and middle column) have the potential to spare a part of the frontal lobe compared to the VMAT plan (right column).

However, using of transmission beams, the dose exceeds the dose limit set as a clinical goal for several organs (appendix 6.2, table 6.3). Nevertheless, different combinations of partial transmission beams have the potential to spare several critical organs, or to limit the increase in dose. For example, an IMPT plan with two transmission beams can spare the lens entirely. When using a different combination of paired transmission beams, it is possible to spare the pituitary, while sacrificing the right lens. Furthermore, all plans exceed the limit set for the brainstem core.

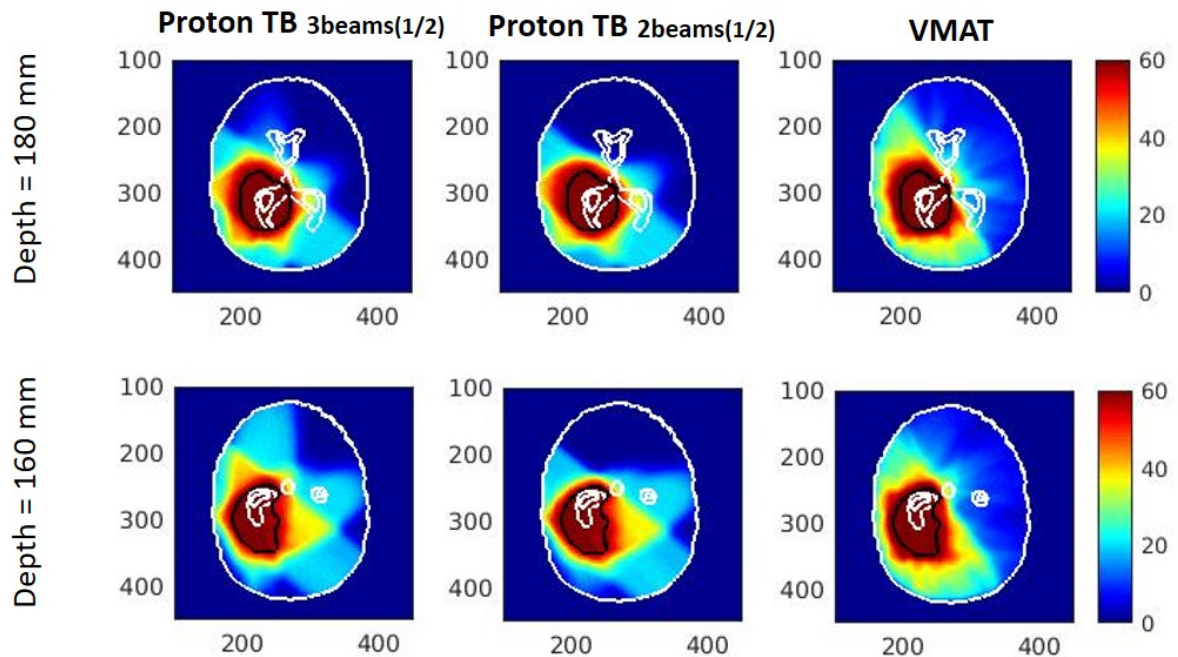


Figure 3.14: Visualization of the absorbed dose distribution using data from patient 1. The absorbed dose distribution at two depths are given for the proton plan with half-transmission beams for all three beams (left column), the proton plan with two half-transmission beams (middle column), and for the VMAT plan (right column). For reference, the area between the inner white structures represent the periventricular region (PVR), the outer white boundary shows the body surface, and the black structure depicts the CTV.

### 3.7. Comparison of different planning strategies

A comparison of the different strategies is given in figure 3.15. Data from this figure can be compared with the data in figure 6.14 and 6.12, which give an overview of the results obtained with the data from patient 2 and patient 3, respectively. Interestingly, the results of the different strategies differs for all patients. Considering the results obtain with the dataset of patient 2, the application of transmission beams is better in terms of the  $NTCP_{all}$ - $D_{mean}$ (brain-CTV) trade-off than the beam angle re-arrangement. However, one of the beam angle arrangements is comparable to the IMPT-pTB plans. The opposite is observed using the data of patient 3. For patient 1, non of the beam angle arrangements had a positive response on the  $NTCP_{all}$ . However, the IMPT-pTB plans provide an intermediate result in terms of  $NTCP_{all}$  and mean brain dose, compared to the clinical IMPT and VMAT plan.

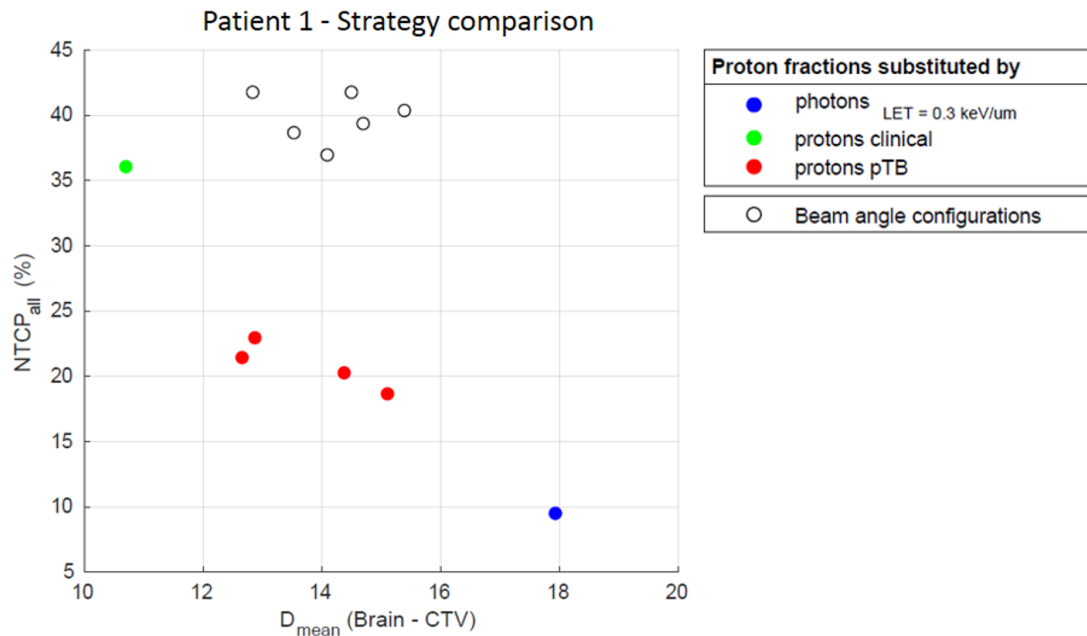
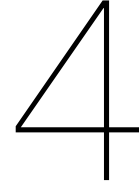


Figure 3.15: Comparison of all three treatment strategies in terms of  $NTCP$  and mean brain dose for patient 1. The results are given for all beam angle arrangements (open black circles), the clinical IMPT plan (green), the VMAT plan (blue), and the proton transmission beams extended by the tipping-fraction (red). The results are plotted in terms of  $NTCP_{all}$  against the mean brain dose.





# Discussion

Based on the POLO model, we evaluated the impact of the RBE/LET effect in current IMPT plans and we investigated the impact of (i) the beam angle selection, (ii) the use of transmission beams, (iii) the robustness, and (iv) the combination of two modalities in terms of the mean brain dose and the RBE model-based NTCP [1]. We compared the results of the clinical used IMPT plan with the results obtained by the modified IMPT plans. In this chapter, the results will be discussed.

## 4.1. The impact of robustness on the NTCP

The strategy of making the proton plan less sensitive to variation in range had the potential to smear-out the LET affecting the  $NTCP_{all}$  as larger margins results in a less sharp dose fall-off. However, we found no significant difference in  $NTCP_{all}$  between IMPT optimized with a different robustness. The spread of Bragg-peaks over a few millimeters may be negligible because the Bragg-peaks at the edge of the radiation field still overlaps. Although a larger margin allows an increase in the radiation field, the increase in POLO values is limited. The latter might also be negligible since the margin does not exceed the voxel dimension in all directions ( $(0.6 \times 0.6 \times 3.0 \text{ mm}^3)$ ). Altogether, the robustness has an inconsequential impact on the  $NTCP_{all}$ .

## 4.2. The impact of field angle arrangement on the NTCP

### 4.2.1. Improvement with a 2-field arrangement

By choosing appropriate beam angles, we improved the NTCP with a limited degree. In general, the NTCP improved by modifying a treatment plan as such that the  $LET_d$  distribution becomes more uniform. High- $LET_d$  values occur at the end of the field range. These are even more pronounced when multiple fields stop within the same region. Therefore, overlapping of the end-of-the-beam range should be avoided, e.g., by applying larger angles between different beams. With a 2-field, we easily achieved a uniform  $LET_d$  distribution by using opposite beams. This resulted in an maximum improvement of 7% (19.4%) in  $NTCP_{all}$ . No improvement in NTCP is found by applying tilted fields. Probably the NTCP increased because the end-of-the-beam range is directed towards the PVR that is located in the inferior-anterior part of the CTV. Moreover, field arrangements with overlapping regions in the PVR worsen the NTCP (e.g. figure 6.4, 5<sup>th</sup> and 6<sup>th</sup> row). High- $LET_d$  values can be kept away from the PVR by choosing field angles that overlap outside the PVR, e.g., by using beams that are separated with a large angle (e.g. figure 6.3, 5<sup>th</sup> row).

### 4.2.2. Improvement with a 3-field arrangement

At HollandPTC, it is more common to use three beams. Therefore, we modified the used clinical IMPT plan considering the observations discussed above. The use of an additional beam has the potential to spread out the high  $LET_d$  portions and to lower the effect of a single beam [43].

Our results shows no improvement in  $NTCP_{all}$  for patient 1, a small improvement of 5.2%. (11.6%) for patient 2, and a significant improvement of 16.9%. (37.0%) for patient 3. The tumor in patient 2 and patient 3 is larger in size, more elongated in shape, and located more superficially. Therefore, it is

easier to avoid overlapping of the end-of-the-beam range, while sparing as much of the brain tissue. The clinical IMPT plan of patient 3 consists of two-out-of-three beams that were directly pointed towards the PVR. The additional modification of rotating beams towards the transversal plane potentially boost the improvement in  $\text{NTCP}_{\text{all}}$ . In contrast, patient 1 has a relatively small tumor compared to patient 2 and patient 3. Remarkably, the migration of high- $\text{LET}_d$  values resulted in a decrease in NTCP when only including voxels outside the CTV. The largest improvement in  $\text{NTCP}_{\text{CTV}}$  we found for patient 1 is 5.5%. (27.4%) (option 5). This implies that the modifications in field arrangement still improved the probability of complications outside the tumor volume. At the same time, the contribution of voxels that correspond to the CTV, and the PVR inside the CTV, must be the cause for the increase in  $\text{NTCP}_{\text{all}}$ . A potential cause for this observation is that the lateral end-of-the beam still overlaps and causes no spread in  $\text{LET}_d$  within the CTV.

#### 4.2.3. The underlying POLO distribution to determine the NTCP

Not only the NTCP, but also the underlying probability distribution provides information about the patient-level risk. In general, voxels that contribute substantially to the NTCP are found in the part of the PVR that is located inside the CTV, at the edge of CTV, or within the region with overlapping beams.

Furthermore, critical organs like the brainstem are of concern. One way to take critical organs into account during treatment planning is by lowering the POLO within those regions, e.g., by lowering the  $\text{LET}_d$ . For example, a lower  $\text{LET}_d$  in the brainstem can be realized by applying oblique angles passing the brainstem laterally (e.g. figure 6.3, 5<sup>th</sup> row). Similar observations were made by Giantsoudi et al. [38]. Although  $\text{LET}_d$  optimization (e.g. [35, 36]) does not guarantee a reduction in NTCP, it redistributes the POLO.

#### 4.2.4. Towards the optimum beam angle selection

In this thesis, we analyzed the impact of the beam angle arrangement on the NTCP for a limited number arrangements. Potentially, there are more appropriate beam angle configurations. Ideally, a full beam angle configuration analysis should be done using a 4-pi beam angle simulation while considering the NTCP and the dose objectives. However, this task is too computational expensive due to (i) the direct optimization of the dose and  $\text{LET}_d$  in relation with the (ii) biological endpoint optimization. Therefore, a full beam angle analysis is not feasible. Besides, the improvement in NTCP due to beam angle optimization potentially remains limited.

### 4.3. Impact of transmission beams on the NTCP

Removing high- $\text{LET}_d$  values by transmission layers has the largest impact on the NTCP when only including protons. The  $\text{NTCP}_{\text{all}}$  improved by 31-50% relative to the clinical IMPT plan with exclusively transmission beams. The influence of a single transmission beam is limited by an improvement in  $\text{NTCP}_{\text{all}}$  of 7%. using the data from patient 1. The first few transmission layers boost the integral dose of the brain by the increase in number of voxels that contribute to the  $\text{NTCP}_{\text{all}}$  calculation. Besides, the removal of the high- $\text{LET}_d$  from the first layers is ineffective as the first layers consist of only 3 to 9 pencil beams. Together, the increase in dose dominates the removal of the high- $\text{LET}_d$  values in the first few layers (figure 3.7, top). This explains the increase in NTCP before decreasing. The increase in dose outweighs the  $\text{LET}_d$  a second time when the  $\text{LET}_d$  stabilizes, resulting in a minimum in NTCP.

In the next paragraphs focus on the impact of the inclusion of at least two (partial) transmission beams. The results are separately discussed for the brain, PVR, organs at risk, and the CTV.

#### Brain

The  $\text{NTCP}_{\text{all}}$  decreases almost to its minimum when only half of the layers (patient 1) or one-third of the layers are transmitted (patients 2 and 3). With each additional transmission layer, the  $\text{LET}_d$  barely improves, while the dose delivered to the healthy brain tissue still increases. Consequently, the  $\text{NTCP}_{\text{CTV}}$  increases after the tipping-fraction. In other words, the chance that a brain lesion originates in healthy brain tissue increases. So, the optimal impact of transmission beams on the NTCP is met when the  $\text{LET}_d$  stabilizes.

#### PVR

A part of the PVR outside the CTV is potentially located within the region of  $\text{LET}_d$  hot-spots. The removal of the high- $\text{LET}_d$  values causes the initial decrease in the the radiation effectiveness and allows

for a rapid decrease in NTCP. The following increase in radiation effectiveness is the result of the increase in dose with each additional transmission layer. However, the  $NTCP_{all}$  does not increase with the increasing radiobiological effectiveness in the PVR. Therefore, together with the observations in the brain, we assume that the NTCP is mostly the trade-off between dose and  $LET_d$ .

### Organs at risk

With the increase in mean dose to the brain, a group of critical organs like the brainstem, hippocampus, pituitary, optical nerves, optic chiasm, lenses, and cochleas receive additional dose. Unfortunately, the use of transmission beams unavoidably exceeds the dose limits that were set as a clinical goal. Nevertheless, different combinations of partial transmission beams have the potential to spare several critical organs or to stay below the dose limit. Especially overdosing the brainstem core leads to critical brainstem toxicities. Further research should be done to optimize transmission beams. The first step is to optimize and extend the objective list. Second, other beam angles could be more favorable for organ sparing. In this study, we investigated the impact of partial transmission beams by extending an equal fraction for two or three beams at once. A third approach is to investigate different combinations of beam fractions. Potentially, fewer layers are needed for a beam to obtain a similar NTCP. Consequently, less dose could be delivered to the surrounding tissue. In general, the goal is to get an almost uniform  $LET_d$  distribution. Last, instead of shooting through a whole beam layer, single pencil beams or half a layer or layers could be applied.

### CTV

In contrast, the physical dose delivered to the CTV remains almost constant, while the  $d$  decreases to a value of 2.0 to 2.5 keV/ $\mu$ m. Consequently, the radiation effectiveness decreases with increase transmission fractions. Altogether, the mean absorbed dose decreases. Potentially, we lose tumor control with the use of partial transmission beams.

The currently used RBE of 1.1 is based on the presence of Bragg peaks within the tumor region. However, a transmission beam lacks the Bragg peak, and thus the pronounced increase in  $LET_d$ . Therefore, the physical characteristics a transmission beam can be compared to that of the protons entrance region. Still, protons have an average  $LET_d$  of 2 keV/ $\mu$ m within the entrance region, which is higher than a photon  $LET_d$  of 0.3 keV/ $\mu$ m. Therefore, proton transmission layers will remain more effective than photons, but potentially less effective than a characteristic proton beam. A potential solution to compensate for the decrease in absorbed dose is to apply a lower RBE for the transmission beams or for specific beam layers. However, an increase in physical dose causes an increase in NTCP. For example, when using the clinical IMPT plan of patient 1, three transmission beams results in an  $NTCP_{all}$  of 29.4% when applying an RBE of 1.05, instead of an  $NTCP_{all}$  of 17.46% when applying an RBE of 1.1. Nonetheless, biological studies found that an RBE in the entrance region does not significantly differ from the RBE found within the tumor region [17]. In addition, Sethi et al. [?] found no indication that the RBE was overestimated for a medulloblastoma. As this type of brain tumor has a high  $\alpha/\beta$  (28Gy) [15], we could assume that the decline in radiation effectiveness also might not significantly affect gliomas. Furthermore, the RBE model provided by Wedenberg et al. [21] (appendix 6.1) assumes that a decrease in  $LET_d$  from 2.7 keV/ $\mu$ m to 2.2 keV/ $\mu$ m does not affect the RBE when applying an  $(\alpha/\beta)_{photon}$  of 10 Gy - a  $\alpha/\beta$  generally used for tumors. Consequently, the decrease in  $LET_d$  appears not to be of concern when considering the tumor control.

## 4.4. The impact of combined treatment modalities

### 4.4.1. The opportunity to combine different treatment modalities

In our analysis, we evaluated both photons having a  $LET_d$  of 0.3 keV/ $\mu$ m and of 1.0 keV/ $\mu$ m. The difference in  $LET_d$  could significantly affect the outcome in NTCP. Purely on the basis of the NTCP, photons $_{LET=0.3 \text{ keV}/\mu\text{m}}$  always win over protons, while photons $_{LET=1.0 \text{ keV}/\mu\text{m}}$  are similar compared to proton transmission beams. Since, the Erasmus Medical Center uses a 6 MV linac to produce photons, photons $_{LET=0.3 \text{ keV}/\mu\text{m}}$  are more relevant to compare with. On the other hand, protons are advantageous when considering only the dose delivered to the brain. A combination of both modalities has the opportunity to profit from the proton and photon characteristics. Compared to the clinical IMPT plan and VMAT plan, proton transmission beams provide an intermediate result in terms of NTCP and mean brain dose.

#### 4.4.2. Trade-off between NTCP and brain dose

In principle, the ideal treatment plan covers the target without giving a significant dose to surrounding healthy tissue, i.e., deliver as low as possible dose to the brain. For this purpose, the  $NTCP_{all}$  should decrease rapidly without an increase in mean brain dose. However, a decrease in  $NTCP_{CEBL}$  always pairs with an increase in dose delivery to a specific organ. In-between the two extremities, multiple fraction ratios could be made with two modalities. Unfortunately, no clear tipping-point in the  $NTCP_{CEBL}-D_{mean}(\text{brain-CTV})$  trade-off has been observed. The question rises whether it is preferable to spare part of the healthy tissue entirely and potentially having hot-spots in the POLO distribution resulting in a higher NTCP, or to have a lower POLO for all irradiated tissue due to a more uniform  $LET_d$ , while a larger portion of the brain is irradiated.

Within the range of  $NTCP_{all}$  we observed by using proton transmission beams, the IMPT-pTB plans are competitive with the IMPT-VMAT plan in terms of  $NTCP-D_{mean}(\text{brain-CTV})$ , or are more beneficial. The trade-off is even more beneficial when including only two partial transmission beams instead of all three. To choose between the IMPT-pTB<sub>2</sub> plans, the selection should mainly be based on the mean brain dose. The  $NTCP_{all}$  deviates only with a maximum of 14% relative to the  $NTCP_{all}$  of the clinical IMPT plan, while the mean brain dose increases relatively with a maximum of 29%. Besides, the most favorable trade-off in  $NTCP-D_{mean}(\text{brain-CTV})$  is realized when combining the clinical IMPT plan with the IMPT-pTB<sub>2</sub> that delivers the least mean brain dose. However, several deviations are observed using the data from patient 3. No IMPT-pTB plan results in a better  $NTCP-D_{mean}(\text{brain-CTV})$  trade-off than the VMAT-IMPT plan. Still, the IMPT-pTB plan that deliver the lowest mean dose to the brain of all transmission beam plans is competitive with the IMPT-VMAT plan within the range of  $NTCP_{all}$  we achieved with protons.

At this moment, it is impossible to make a statement about the trade-off between the  $NTCP_{CEBL}$  and mean brain dose since there is no clear cut-off point, and the clinical significance of both parameters are still not fully understood.

#### 4.4.3. Sequence of fractionation for a multi-modality radiation treatment

Combining different treatment modalities brings practical issues and considerations. A main practical issue is that not all radiotreatment institutes have access to both modalities. Potentially, proton transmission beams could be used as a replacement for photons. Furthermore, the order of treatment should be considered. For example, the first half of the fractions can be given by one modality and the last half with the other modality. Another option is to alternate between the two modalities. An alternative option could be to deliver both modalities during each fraction. However, these options, especially the last two, are paired with additional practical issues, like treatment scheduling and communication to agree with the proton center and medical institute.

The initiation of the RBE in proton therapy corrects for differences in biological effectiveness. Therefore, the outcome after one proton fraction or photon fraction is assumed to be equal, no matter which order is applied. On the other hand, protons and photons activates different repair ways and cell processes [44]. Consequently, both modalities potentially result in a different biological endpoint after a fraction. This speculation indicates a dependence between the order and the biological outcome.

#### 4.4.4. Optimization of combined radiotherapy modalities

To optimally benefit from both protons and photon treatment, the two modalities should be fully integrated, i.e., the treatment plans should be designed and optimized for protons and photons together, and it should be ensured that both treatments modalities could be delivered at once. Despite all practical and technical issues, it might be interesting to elaborate about the idea to combine protons with photons.

In addition, the optimization of proton plans including currently planned plans and transmission beams could be further explored. An optimization of both IMPT and IMPT-pTB has the potential to prevent high  $LET_d$  from critical organs, while maintaining dose delivery at the edge of the CTV. However, this approach requires LET optimization. Otherwise, the end results are similar as the IMPT plans optimized with current optimization.

## 4.5. Comparison of different planning strategies

With the re-arrangement of beam angles, we found the lowest  $NTCP_{all}$  when two beams are positioned (almost) in opposite direction (e.g. beam angle configuration option 5 and option 6 with patient 1, or option 3 and option 4 using the data of patient 2). The opposed beams can be compared with a single transmission beam, except that high- $LET_d$  values are still present when using opposing fields. In other words, the use of transmission beams can lead to a similar, or potentially better NTCP than opposing beams. For example, when considering the data from patient 1, beam angle arrangement option 2 is comparable to the clinical IMPT plan with a single transmission beam - beam 3. The latter improves the  $NTCP_{all}$ , while the former worsens the  $NTCP_{all}$  with respect to the clinical IMPT plan.

Like mentioned before, improvements in  $NTCP_{all}$  were achieved by a field angle re-arrangement for patient 2 and patient 3. The beam angle re-arrangement strategy has also a more favorable impact on patient 3 than inclusion of transmission beams. The  $NTCP_{all}$  improved by 37.0% relative to the clinical IMPT plan, while only increasing in mean dose relatively with a maximum of 11%. In contrast, the impact of transmission beams is more beneficial in case of patient 2. The clinical data of patient 2 and patient 3 mainly differ in the location of the tumor. Only the lateral part of the tumor in patient 2 is located along the skull, while both the lateral and anterior side of the tumor is located at the surface of the brain. Therefore, the change in mean brain dose could be more limited when re-arranging the beam angle configuration.

Taking all results together, we found that a re-arrangement in beam angle configuration potentially decreases the NTCP only if a significant part of the tumor is located superficially. In other cases, transmission beams affect the  $NTCP_{all}$  to a larger extent. These results suggest that the geometry and location of the tumor may play a role in the effectiveness of beam angle arrangement on the NTCP. Still, the inclusion of photon fractions has the largest degree of freedom in terms of  $NTCP-D_{mean}$  (brain-CTV) trade-off in all cases. Furthermore, it is hard to further optimize treatment planning strategies in terms of  $NTCP_{all}$  with current planning methodology. Accordingly, HollandPTC generates IMPT plans with sufficient NTCP values.

## 4.6. Interpretation and relevance of the NTCP model

### 4.6.1. Inter-patient comparison

Since tumors differ in size, the  $NTCP_{all}$  values we found for the three clinical IMPT plans are hard to compare. In definition, the NTCP is a multiplication of voxel values. Additional voxels contribute to a higher NTCP. Our results suggest a correlation between the  $NTCP_{all}$  and the tumor volume. Therefore, the  $NTCP_{CTV}$  seems like a valid definition to compare NTCP values inter-patiently as it neglects the target volume.

### 4.6.2. Relation with symptomatic development

Like mentioned before, the clinical significance of the RBE model-based NTCP it is fully known. In general, the POLO model predicts the occurrence and localization of contrast-enhancing brain lesions on MRI. However, an change on MRI does not necessarily imply that the patient will develop toxicities. For example, the study of Gunther et al. [45] evaluated 37 ependymoma patients treated with protons. Sixteen (43%) had changes on MRI. However, only four patients with image changes were symptomatic. None of the patients without image changes showed post-treatment symptoms. Giantsoudi et al. [46] observed similar results. A group of 111 pediatric medulloblastoma patients underwent proton irradiation. Only ten patients were identified with changes on MRI, of whom four had symptomatic development. Patients without images change were all asymptomatic. Furthermore, we evaluated the treatment plans for three patients. Patient 1 had the lowest  $NTCP_{all}$  of all three patients, but a similar  $NTCP_{CTV}$  compared to patient 2. The highest  $NTCP_{all}$  and  $_{CTV}$  were obtained for patient 3. However, only patient 1 developed serious toxicities. Patient 2 and patient 3 are asymptomatic.

Altogether, it is not yet known to what extent visual changes on MRI are predictive for clinically symptomatic toxicity. Therefore, the relevance of the POLO model is questionable. On the other hand, all symptomatic patients had changes on MRI. An improvement in NTCP potentially lowers the risk to observe image changes, and thereby, the risk to develop symptoms also potentially decreases.

## 4.7. Delineation uncertainties

The tissue surrounding the ventricular system, PVR, has an increased risk to develop brain lesions. Therefore, the PVR is incorporated in the POLO model. However, deviations in the defined PVR potentially lead to deviations in the POLO, and therefore in the NTCP. Bahn et al [1] mentioned that the model predictions are robust against varying the threshold distance for the binary risk factor PVR. However, the identification and contouring of the ventricular system were hard to carry out, because the complex structured ventricles are not clearly seen within the target volume and the lower parts are difficult to deviate from other brain structures. Therefore, the contoured ventricles and its extension are likely to deviate from the true structure, especially when the PVR is located within a high-LET<sub>d</sub> region. The deviation in the PVR definition has a minor effect on the NTCP. Assuming that the contour deviates with a maximum of 1 mm, the NTCP is impaired with an uncertainty of 2%. But a systematic deviation of 1 mm of the PVR is already a large margin, and therefore it might not occur with this extend. Besides, a deviation of 2% at NTCP<sub>all</sub> levels we found in IMPT plans is relatively small. Therefore, deviation in PVR definition has a minor effect on the NTCP. However, if the contoured structure does not include the whole PVR or is not-intentionally extended by structures that do not belong to the PVR, then the NTCP is paired with a larger uncertainty. Besides, it is hard to define the structure after resection performed around the PVR. Independent verification of different clinicians is necessary to limit the uncertainty in PVR contouring. Still, uncertainties in NTCP will remain due to contouring uncertainties.

## 4.8. Future perspectives

Ideally, both physical objectives, i.e. dose and LET<sub>d</sub>, and NTCP objectives are integrated into treatment planning optimization to generate a treatment plan with the lowest risk of developing side effects. The next step to identify organs that are more sensitive for an elevated RBE/LET<sub>d</sub> or to specify thresholds in the radiation effectiveness (dose × LET<sub>d</sub>) is by reporting the RBE and a continuous assessment of LET<sub>d</sub> of prospective clinical datasets. These observations can be used as objectives for LET<sub>d</sub> optimization or could be included in the assessment during treatment planning. Additionally, the LET<sub>d</sub> evaluation step during treatment planning can be implemented to avoid LET<sub>d</sub> hot-spots.

In general, more validation and clinical data are necessary to integrate radiation response models in the clinic. For further improvement of the RBE models, a better understanding of the relation between image changes and side effects is desired. Second, the development of better predictive bio-markers on MRI could be of interest to prevent unusual proton therapy-associated toxicity. Third, additional model predictors affecting the RBE could lead to a more accurate risk prediction, and should therefore be investigated. Potentially there are organs like the PVR that are more sensitive to radiation than other organs. Moreover, it is also likely that the impact of RBE will vary between subgroups. For example, the combination of proton therapy with systemic treatments, a resection of the tumor, or the use of steroids may lead to variation in toxicity (see appendix, section 7.6). Differences could also be based on clinical characteristics, biomaterials or diagnostic imaging [23]. All in all, a continuous assessment of clinical outcomes and RBE models is required.

In addition to the RBE migrating strategies we evaluated in this study, it could be of interest to increase the number of beams. Although we found no improvement in NTCP when going from a treatment plan with two beams to a plan with three beams, additional beam angles allow a further smearing-out of the elevated LET<sub>d</sub> without increasing the integral dose. One approach is to increase the number of fixed beam angles that delivers radiation by switching off between gantry movements. Another approach is to deliver radiation continuously as the gantry rotates around the patient, which is called proton modulated arc therapy (PMAT). Besides the benefits in shaping dose around irregular and concave target volumes and the reduction in isodose volumes for most dose levels [47], coplanar or non-coplanar PMAT plans reduces volume exposed to intermediate LET<sub>d</sub> levels.

# 5

## Conclusion

We evaluated the RBE/LET effect in IMPT plans for three glioma patients planned and treated to 59.4 Gy<sub>RBE</sub> at HollandPTC. Second, we analyzed the impact of planning strategies considering the RBE model-based NTCP to develop radiation-induced brain lesions (CEBL). We found that the smearing-out or the removal of LET<sub>d</sub> hot-spots is a promising approach to lower the NTCP<sub>CEBL</sub>. However, an improvement in NTCP<sub>CEBL</sub> is always at the cost of an increase in dose to surrounding organs.

When considering the current treatment planning methodology applied at HollandPTC, the clinical IMPT plans have an appropriate NTCP<sub>CEBL</sub>. A different robustness would have a negligible effect on the NTCP<sub>CEBL</sub>. But choosing more appropriate beam angles that result in a spread-out LET<sub>d</sub> distribution could improve the NTCP moderately, especially for relatively large tumors. Though, a more promising approach to lower the NTCP is by turning several beams into partial proton transmission beams (IMPT-pTB). The number of transmission layers at which the mean LET<sub>d</sub> stabilizes results in the optimum NTCP. Still, a VMAT plan is always better in terms of NTCP<sub>CEBL</sub> than protons, while a IMPT plan is advantageous in terms of mean brain dose. To benefit from both photon and proton therapy, an intermediate NTCP-D<sub>mean</sub>(brain - CTV) trade-off can be made with different ratios of two modalities: IMPT-VMAT or IMPT-pTB. Unfortunately, it is impossible to make a statement about the trade-off between the NTCP<sub>CEBL</sub> and mean brain at this moment. Nevertheless, this study supports the continued investigation to combine different modalities for high dose-fractionated glioma patients, like the optimization of radiotreatment plans including both protons and photons.

At present, a continuous assessment of LET<sub>d</sub> of prospective clinical datasets or during treatment planning is a good first step to integrate RBE effects into clinical practise. For further improvement of RBE models, more validation on clinical data and a better understanding of the relation between visual changes on MRI with the clinically symptomatic toxicity or better biomarkers on MRI are necessary to adopt the radiation response models in clinic.



# 6

## Appendix

### Overview of figures and tables

#### Impact of the beam angle

*Figure 6.1* - Dose, LET and POLO for the clinical IMPT and VMAT treatment plan for patient 2 and patient 3. (page 47).

*Figure 6.2* - Dose and LET distribution for various beam angle configurations for patient 2 and patient 3 (page 48).

*Figure 6.3* - Visualization of the dose, LET and POLO distribution for different beam angle configurations for patient 1. Beam 1 is fixed, while beam 2 is rotating in transverse axis (page 49).

*Figure 6.4* - Visualization of the dose, LET and POLO distribution for different beam angle configurations for patient 1. Beam 2 is fixed, while beam a is rotating in transverse axis (page 50).

#### Impact of transmission beams

*Figure 6.5* - NTCP progression by extending beam layers of multiple beams for patient 2 and 3 (page 51).

*Figure 6.6 to 6.9* - Dose,  $LET_d$  and  $Dose \times LET_d$  progression by extending beam layers of multiple beams using data of patient 2 and patient 3 (page 52 to 53).

*Figure 6.10* - The impact of combining different treatment plans on the NTCP using data from patient 2 and patient 3 (page 54).

*Figure 6.11 and 6.13* -The trade-off in NTCP and mean brain dose using the data of patient 2 and patient 3, respectively (page 55 and 56).

*Figure 6.12 and 6.14* - Comparison of all investigated strategies discussed in this study for using the data of patient 2 and patient 3, respectively (page 55 and 56).

*Table 6.1* - Objective list used to optimize the beam settings for the clinically used treatment plan and different beam angle configurations (page 57).

*Table 6.2* - Minimal objective list used for the (re-)optimization of the protons transmission beams plans (page 57).

*Table 6.3 to 6.5* - Evaluation of the clinical goals for patient 1 to patient 3, respectively, when applying different configurations of proton transmission beams (page 58 to 60).

## 6.1. Models for the Relative Biological Effectiveness

Different approaches have been derived from the Carabe-Fernandez et al. model [48], equation 1.4, based on different assumptions. In this section, three models will be presented.

### Model 1

The Carabe et al. model [49] gives a relationship between RBE and  $LET_d$  for an average  $\alpha/\beta_x$  of 2.686 Gy. The average of  $\alpha/\beta$  was taken from data of V79 cell line experiments. By a linear regression analysis on these datasets, the following relationship was established:

$$RBE_{\max} \left( \left[ \frac{\alpha}{\beta} \right]_x, LET_d \right) = 0.843 + 0.154 \frac{2.686}{\left[ \frac{\alpha}{\beta} \right]_x} LET_d$$

$$RBE_{\min} \left( \left[ \frac{\alpha}{\beta} \right]_x, LET_d \right) = 1.09 + 0.006 \frac{2.686}{\left[ \frac{\alpha}{\beta} \right]_x} LET_d$$

with the parameters 0.843 and 1.09 as intersection and 0.154 and 0.006 as the slope.

### Model 2

The same approach had been determined by the McNamara et al. model [50]. It has been assumed that both  $RBE_{\min}$  and  $RBE_{\max}$  depends on  $(\alpha/\beta)_x$ . In contrast to the previous model, the parameters  $p_{0-3}$  must fit the clinical experimental data. Additionally, a non-linear relationship is assumed for  $RBE_{\min}$  on  $(\alpha/\beta)_x$ . This results in the following relationship:

$$RBE_{\max} \left( \left[ \frac{\alpha}{\beta} \right]_x, LET_d \right) = p_0 + \frac{p_1}{\left[ \frac{\alpha}{\beta} \right]_x} LET_d$$

$$RBE_{\min} \left( \left[ \frac{\alpha}{\beta} \right]_x, LET_d \right) = p_2 + p_3 \sqrt{\left[ \frac{\alpha}{\beta} \right]_x} LET_d$$

### Model 3

The Wedenberg et al. model [21] assumes that the  $\alpha$  over  $\alpha_x$  linearly varies with LET. In other words, when a lower LET is observed, the  $\alpha$  approaches towards  $\alpha_x$ . Thereby, it is known that  $\alpha/\alpha_x$  decreases for  $LET < 30 \text{ keV}/\mu\text{m}$ , which is within the range of clinical expected LET values. Further, it is assumed that the slope  $k$  has an inverse relationship with tissue response  $(\alpha/\beta)_x$ :

$$\frac{\alpha}{\alpha_x} = 1 + k \cdot LET = 1 + \frac{q}{\left[ \frac{\alpha}{\beta} \right]_x} \cdot LET$$

with  $q$  as a free parameter independent of the physical parameters. It has been determined by experimental parameter fitting that  $q$  has a value of  $0.434 \text{ Gy} \cdot \mu\text{m}/\text{keV}$ . At last, this approach assumes that  $\beta$  is independent of LET ( $\beta = \beta_x$ ). Applying the same formalism as for the other models, the following is found:

$$RBE_{\max} \left( \left[ \frac{\alpha}{\beta} \right]_x, LET_d \right) = 1.00 + \frac{0.434}{\left[ \frac{\alpha}{\beta} \right]_x} \cdot LET_d$$

$$RBE_{\min} = 1.0$$

In general, all RBE models derived from the LQ model state that the RBE depends on the dose per fraction, tissue type, and the secondary particles' energy deposition. All models show that there is an inverse relationship of the photon  $\alpha/\beta$  with the LET, which indicates that the LET effects are more significant in cells with low  $\alpha/\beta$  ratios.

## 6.2. Figures and Tables

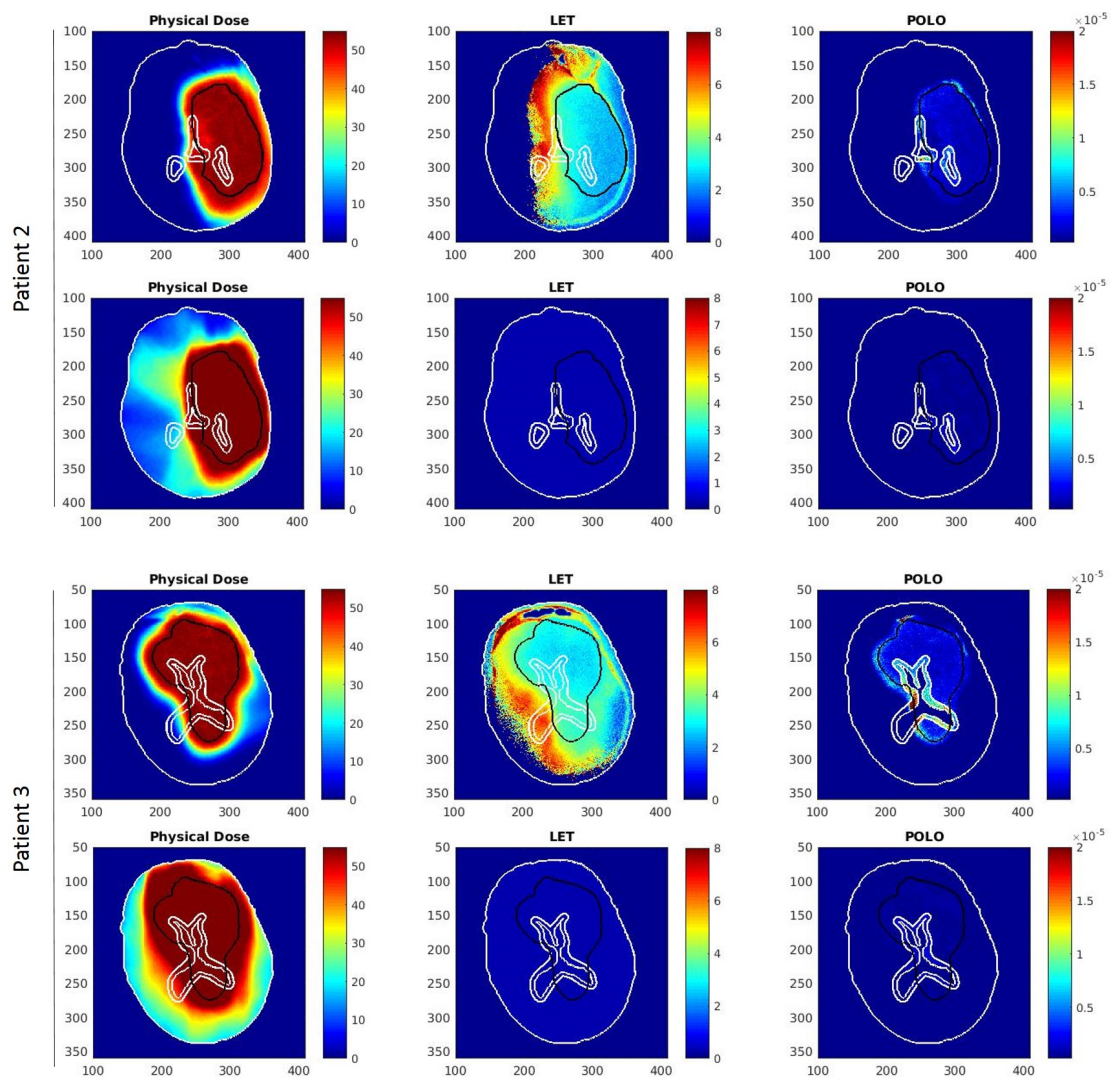


Figure 6.1: Dose, LET and POLO for the clinical IMPT and VMAT treatment plan. The first two rows represent data from patient 2. The second two rows represent data from patient 3. Left column: The physical dose is weighted in the IMPT plan (top row) by the biological effectiveness (RBE) of 1.1. No weighting is applied for the VMAT plan (bottom row). Middle column: The dose-averaged linear energy transfer ( $LET_d$ ) is only shown for doses above 0.2 Gy. A uniform  $LET_d$  of  $0.3 \text{ keV}/\mu\text{m}$  is assumed for the VMAT plan. Right column: The per voxel probability of lesion origin (POLO). The area between the inner white structures represents the periventricular region (PVR), the outer white boundary shows the body surface, and the black structure depicts the CTV.

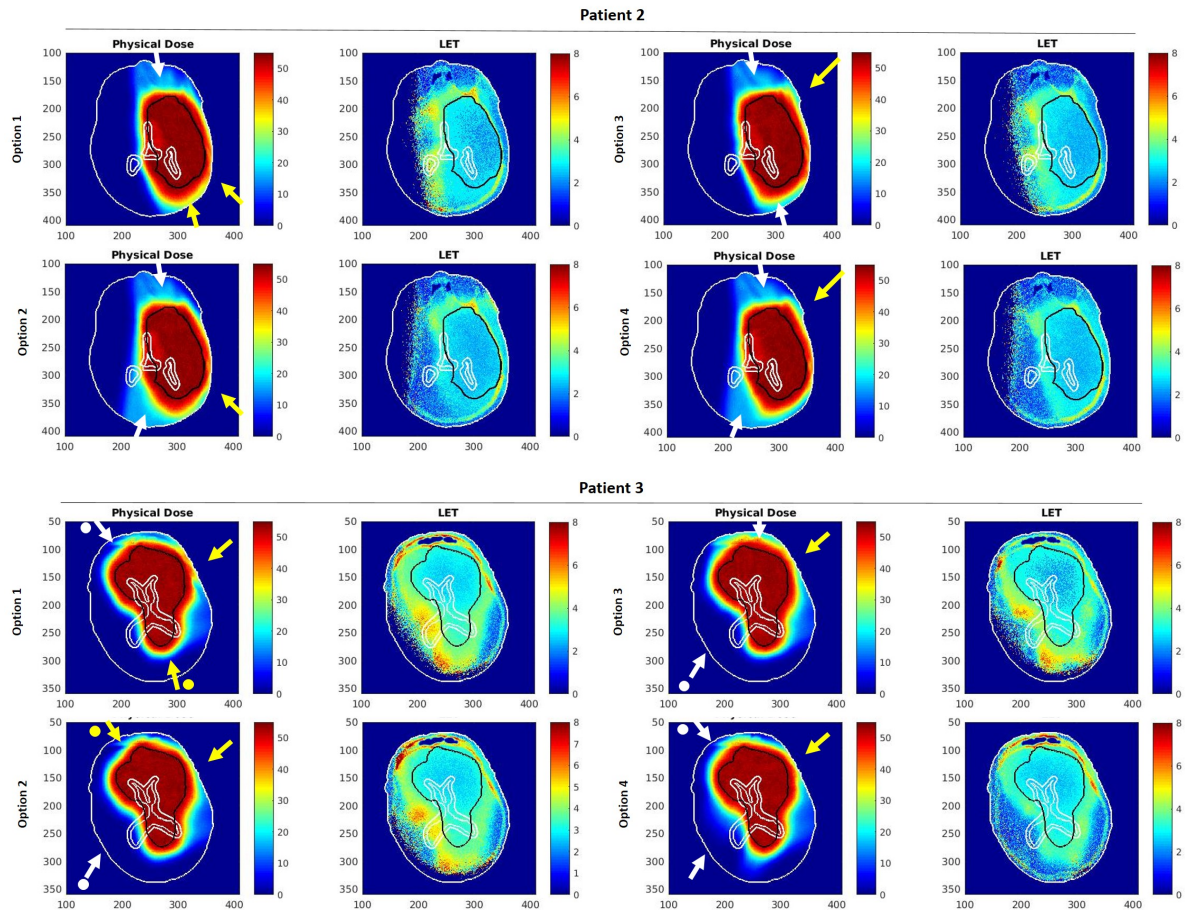


Figure 6.2: Dose and LET distribution for various field angle arrangements for patient 2 and 3. Various options of beam angle arrangements are applied to patient 2 (first two rows) and patient 3 (second two rows). For each option, the physical dose weighted by the biological effectiveness (RBE) of 1.1 (right figure) is given. The dose-averaged linear energy transfer ( $LET_d$ ) is only shown for doses above 0.2 Gy. The arrows represent the directions of the beam. When the arrow is yellow, the angle of the clinical plan is used. When the arrow is white, the angle has been modified. When a dot is added to the yellow arrow, the beam enters the patient superior. When a dot is added to the white arrow, the beam enters the patients lateral-superior. All other beams are close the the transversal plane. For reference, the area between the inner white structures represents the periventricular region (PVR), the outer white boundary shows the body surface, and the black structure depicts the CTV.

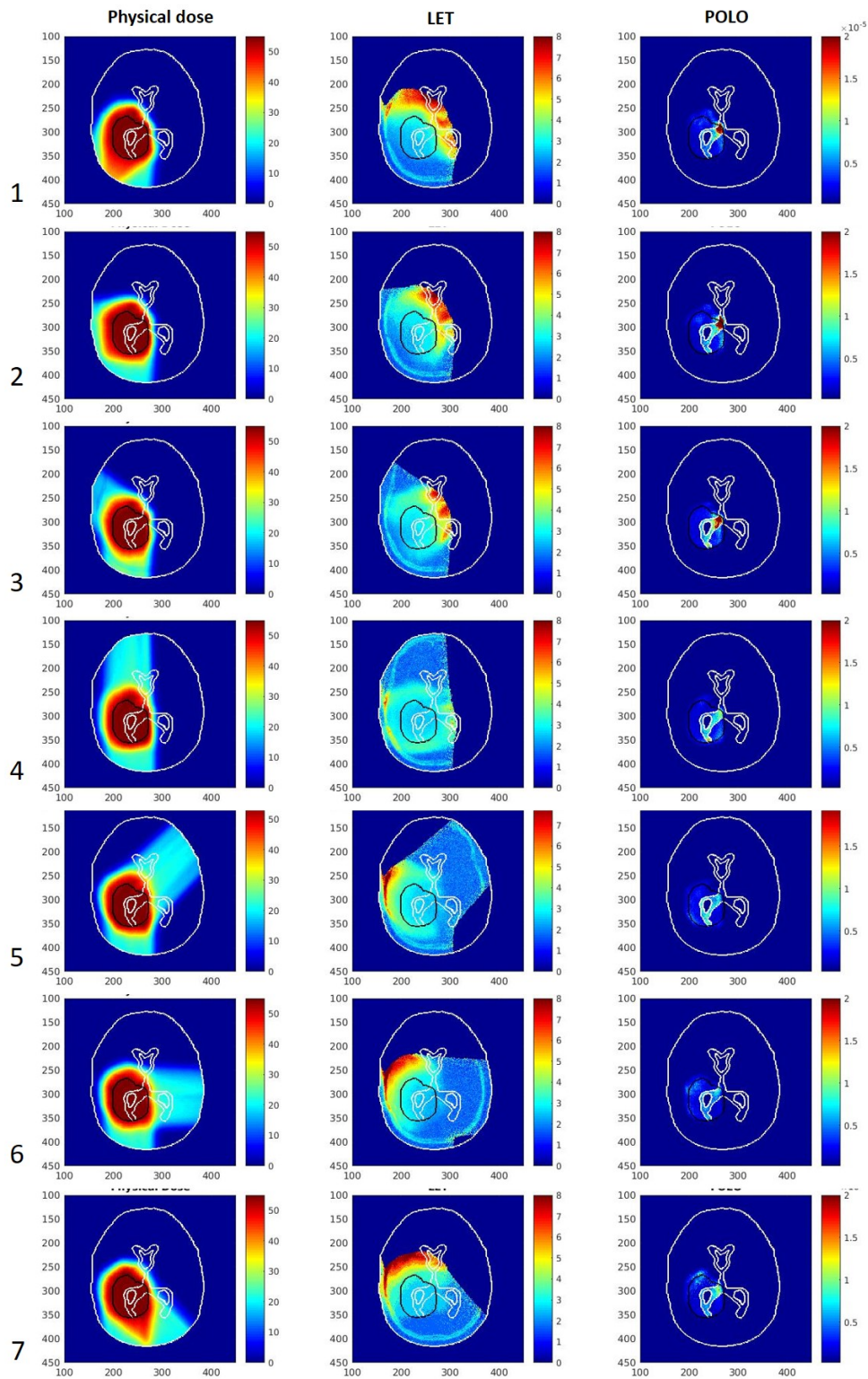


Figure 6.3: Visualization of the dose, LET and POLO distribution when fixing beam 1 and rotating beam 2 in transverse axis for patient 1. Left: The physical dose weighted by the used biological effectiveness ( $RBE = 1.1$ ). Middle: Dose-averaged linear energy transfer ( $LET_d$ ), only showed for doses above 0.2 Gy. Right: The per voxel probability of lesion origin (POLO). The area between the inner white structures represents the periventricular region (PVR), the outer white boundary shows the body surface, and the black structure depicts the CTV.

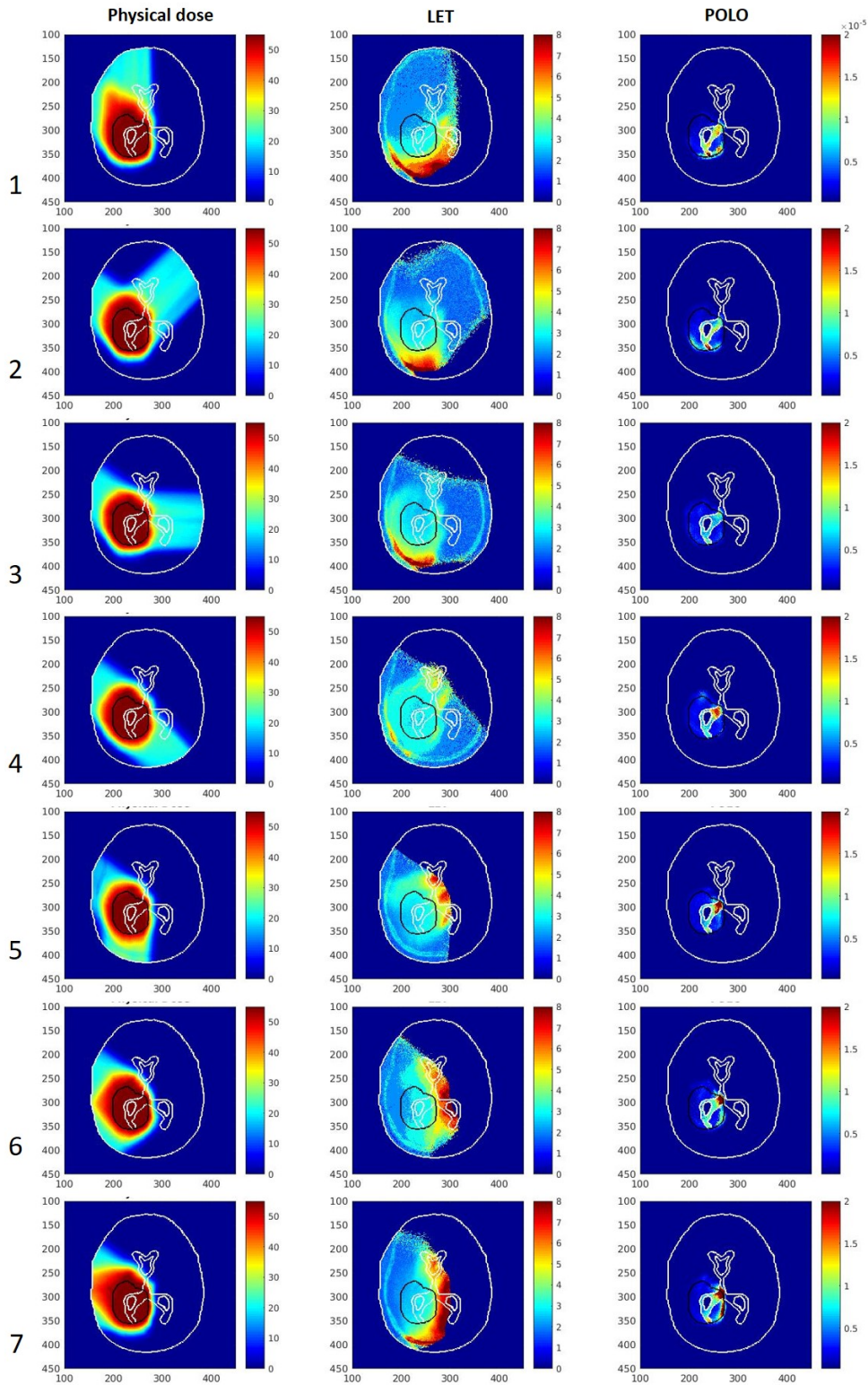


Figure 6.4: Visualization of the dose, LET and POLO distribution when fixing beam 2 and rotating beam 1 in transverse axis for patient 1. Left: The physical dose weighted by the used biological effectiveness (RBE) = 1.1. Middle: Dose-averaged linear energy transfer ( $LET_d$ ), only showed for doses above 0.2 Gy. Right: The per voxel probability of lesion origin (POLO). The area between the inner white structures represents the periventricular region (PVR), the outer white boundary shows the body surface, and the black structure depicts the CTV.

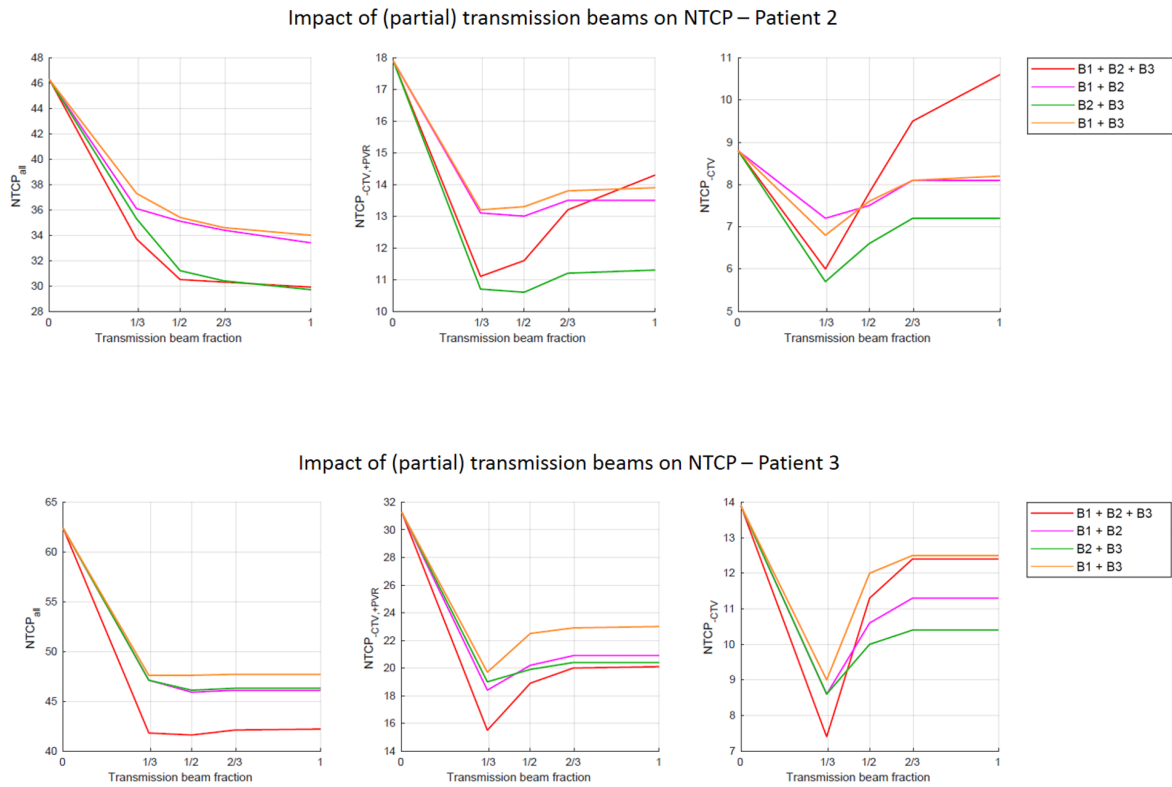


Figure 6.5: NTCP progression by extending beam layers of multiple beams for patient 2 and 3. A fraction of beam layers is increased for all beams together (blue line) or in dual (red, yellow and purple line). This impacts the  $NTCP_{all}$  (left),  $NTCP_{CTV,+PVR}$  (middle),  $NTCP_{CTV}$  (right).

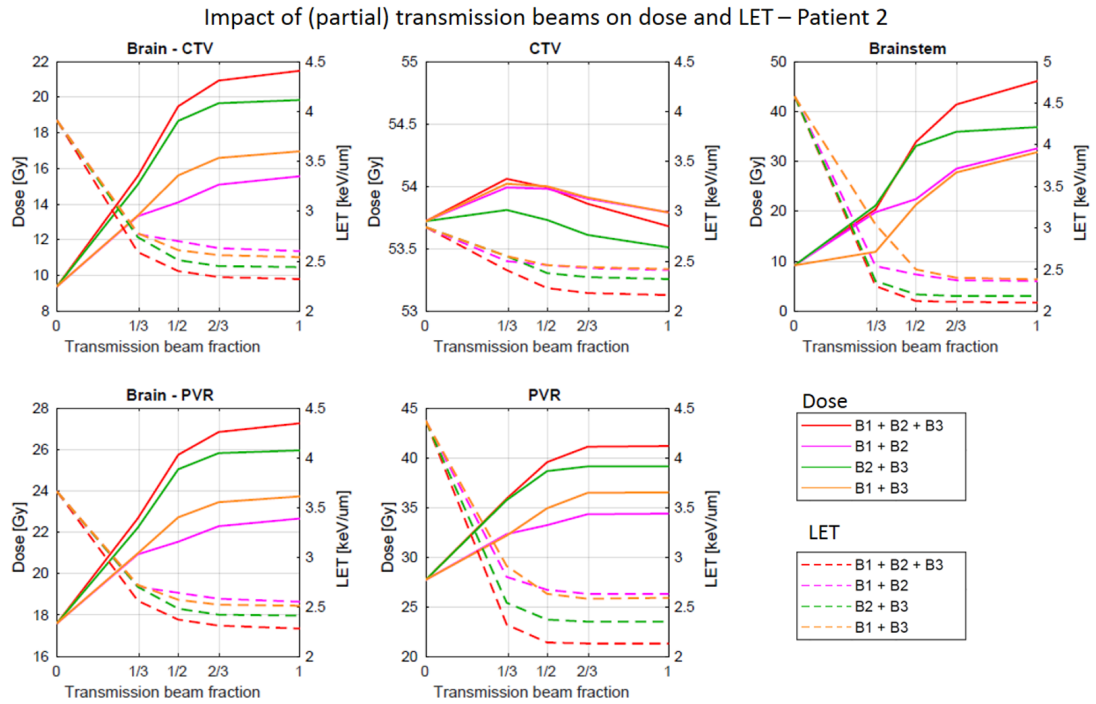


Figure 6.6: Dose and  $LET_d$  progression by extending beam layers of multiple beams using data of patient 2. A fraction of beam layers is increased for all beams together (blue line) or in dual (red, yellow and purple line). This affects the mean physical dose (solid line) and mean  $LET_d$  (dashed lines) in the brain minus CTV (top left), CTV (top center), brainstem (top, right), brain minus periventricular region (bottom left), and periventricular region (bottom center).

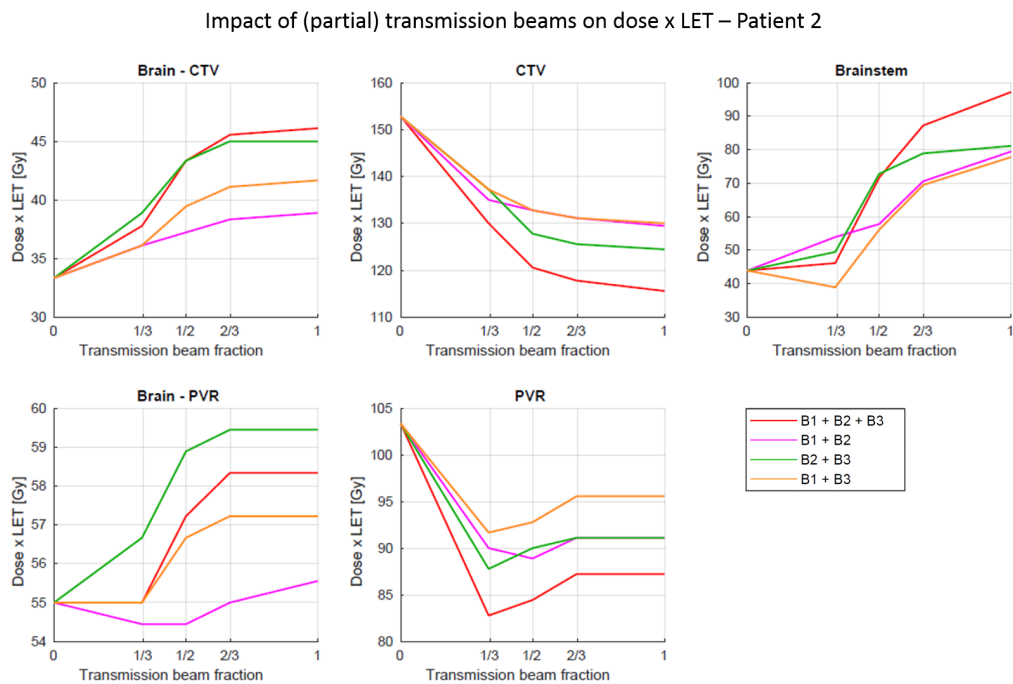


Figure 6.7: Radiation effectiveness progression by extending beam layers of multiple beams using data of patient 2. A fraction of beam layers is increased for all beams together (blue line) or in dual (red, yellow and purple line). This affects the mean radiation effectiveness in the brain minus CTV (top left), CTV (top center), brainstem (top, right), brain minus periventricular region (bottom left), and periventricular region (bottom center).

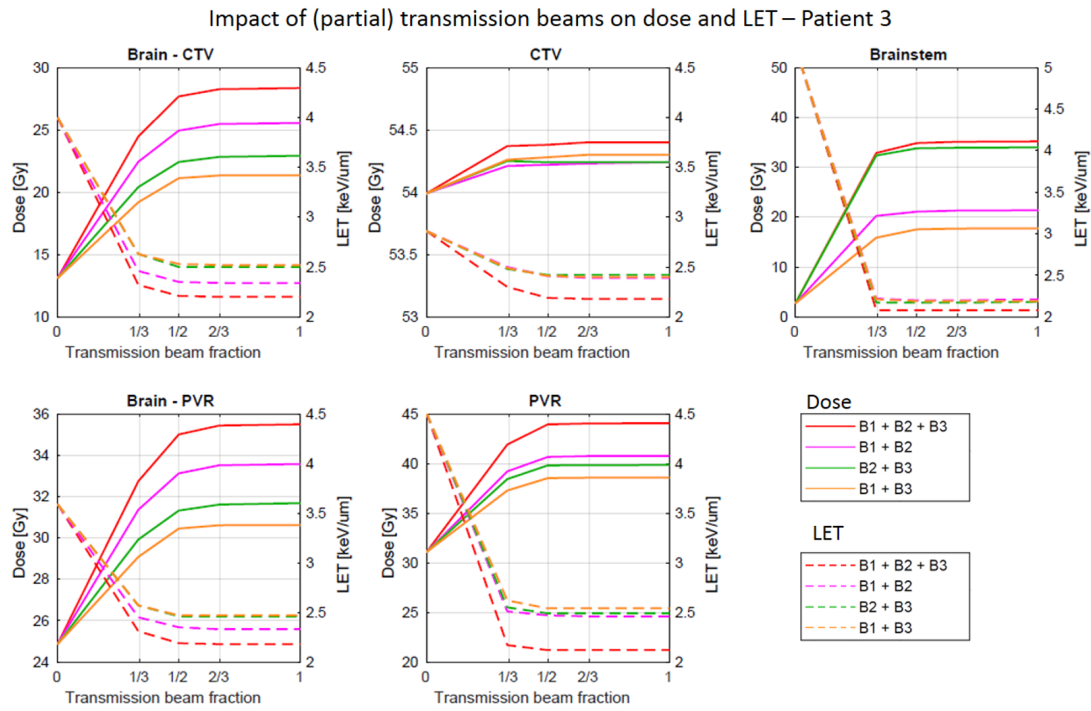


Figure 6.8: Dose and LET<sub>d</sub> progression by extending beam layers of multiple beams using data of patient 3. A fraction of beam layers is increased for all beams together (blue line) or in dual (red, yellow and purple line). This affects the mean physical dose (solid line) and mean LET<sub>d</sub> (dashed lines) in the brain minus CTV (top left), CTV (top center), brainstem (top, right), brain minus periventricular region (bottom left), and periventricular region (bottom center).

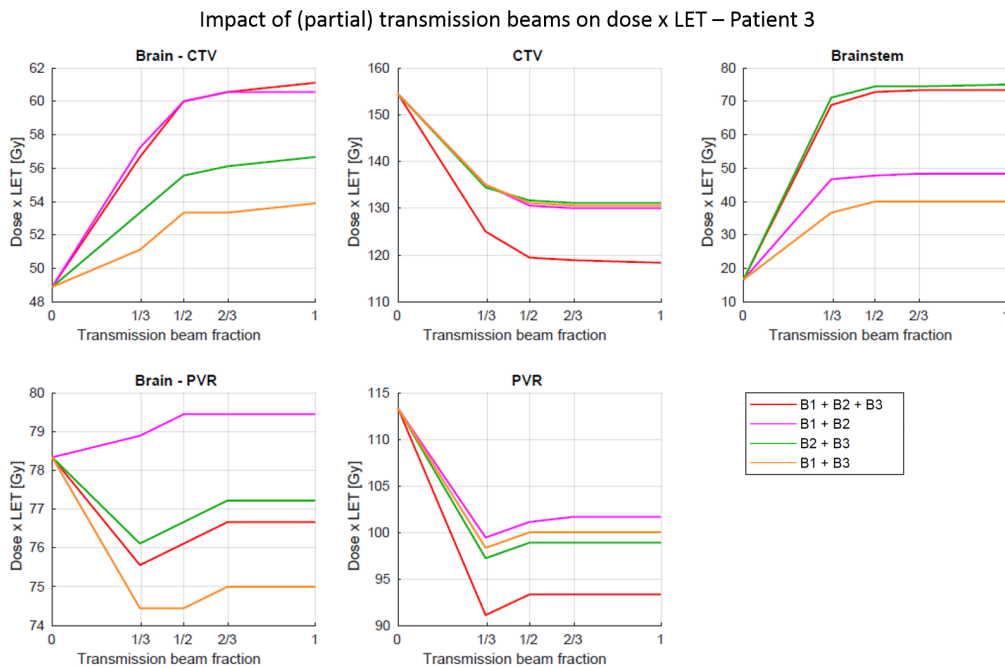


Figure 6.9: Radiation effectiveness progression by extending beam layers of multiple beams using data of patient 3. A fraction of beam layers is increased for all beams together (blue line) or in dual (red, yellow and purple line). This affects the mean radiation effectiveness in the brain minus CTV (top left), CTV (top center), brainstem (top, right), brain minus periventricular region (bottom left), and periventricular region (bottom center).

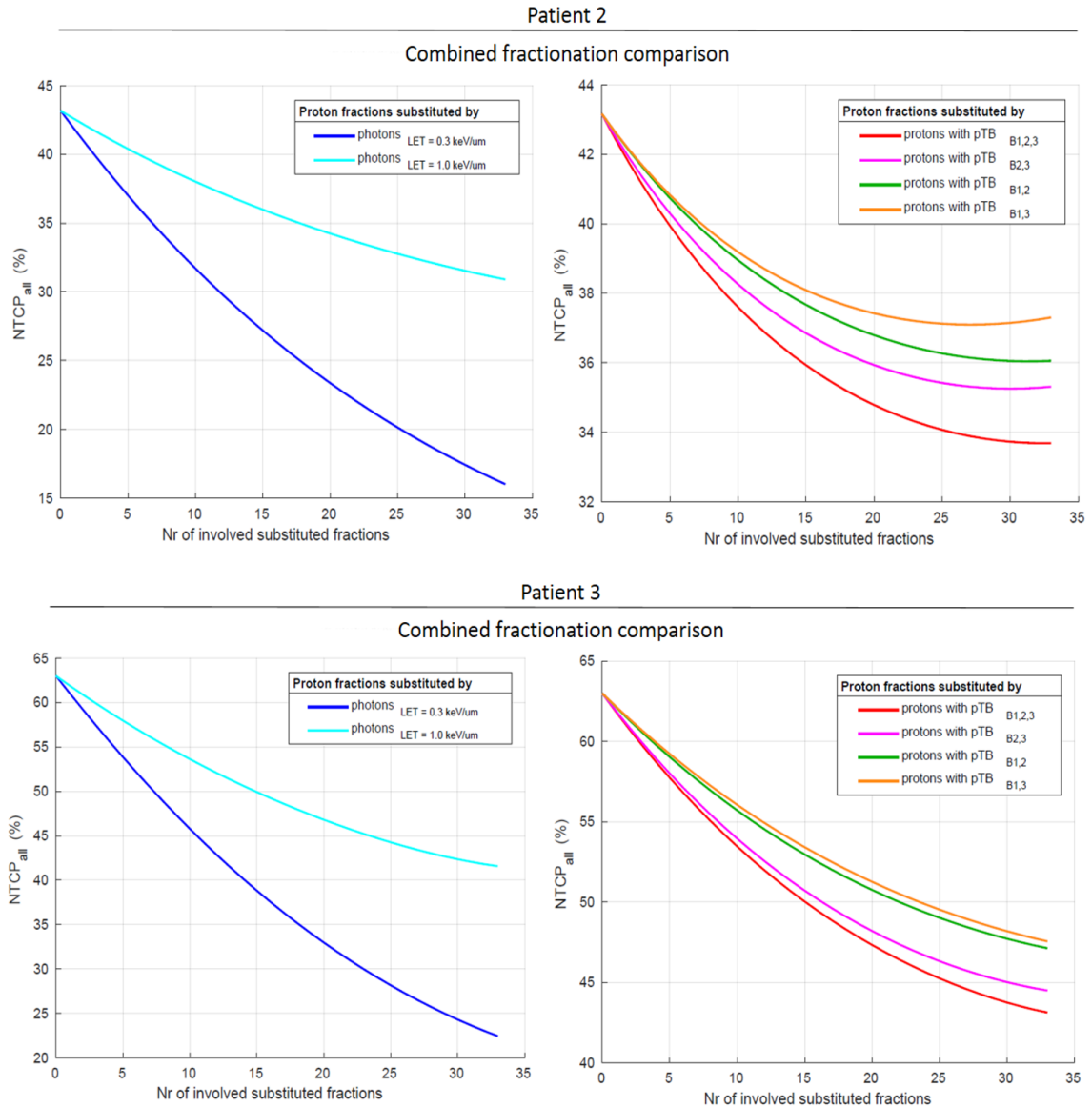


Figure 6.10: The impact of combining different treatment plans on the NTCP using data from patient 2 and patient 3. Left: The progression in  $NTCP_{all}$  when substituting fractions of the clinical proton plan by photons with a  $LET_d$  of  $0.3 \text{ keV}/\mu\text{m}$  (blue), by photons with a  $LET_d$  of  $1.0 \text{ keV}/\mu\text{m}$  (cyan). Right: The progression in  $NTCP_{all}$  when substituting fractions of the clinical proton plan by a proton plan including 3 partial transmission beams (red), or by a proton plan including 2 partial transmission beams (magenta green, yellow).

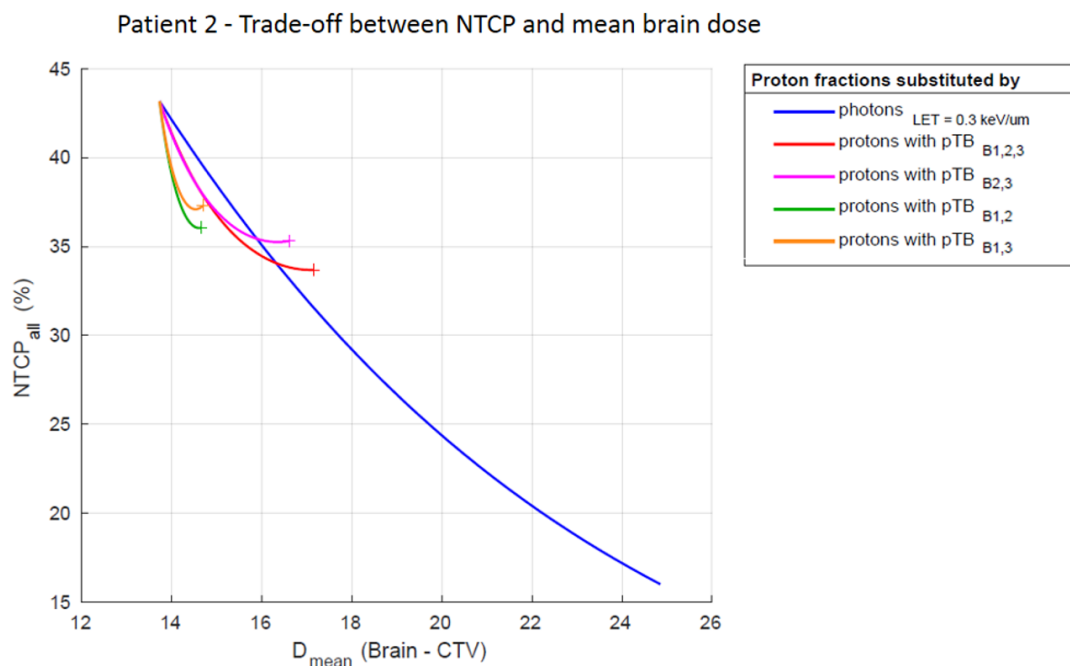


Figure 6.11: The trade-off between  $NTCP_{all}$  and overall brain dose using data from patient 2. The trade-off is given for the clinical proton plan combined with  $photons_{LET=0.3keV/\mu m}$  (blue), as well as for various combination with proton transmission beams (red, magenta, green, yellow). For clarity, the endpoint of the proton transmission beams are indicated by a '+'-sign.

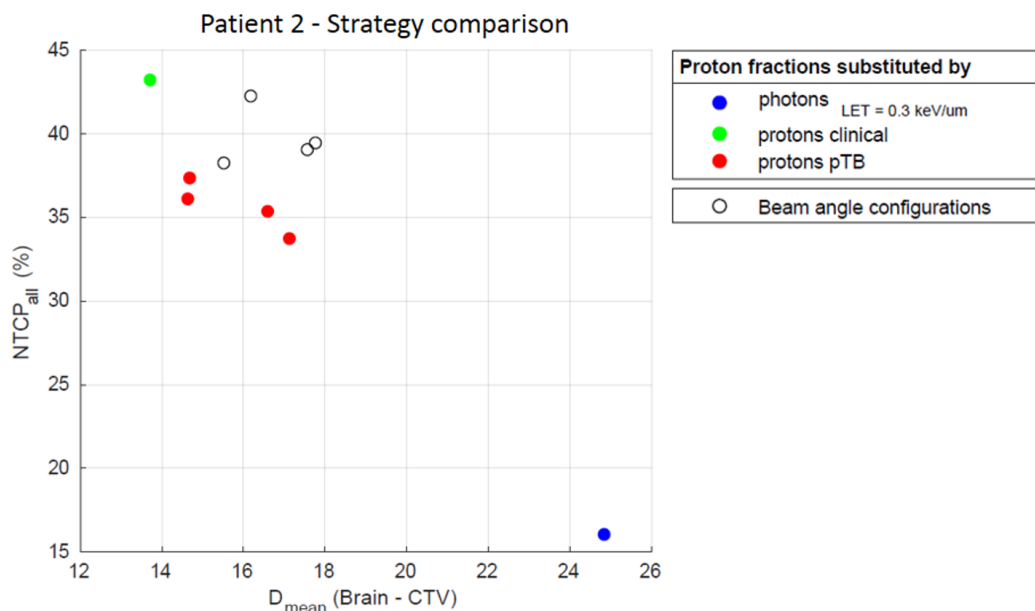


Figure 6.12: Comparison of all three treatment strategies in terms of NTCP and mean brain dose for patient 2. The results are given for all beam angle arrangements (open black circles), the clinical IMPT plan (green), the VMAT plan (blue), and the proton transmission beams extended till the tipping-fraction (red) and plotted in terms of  $NTCP_{all}$  against the mean brain dose.

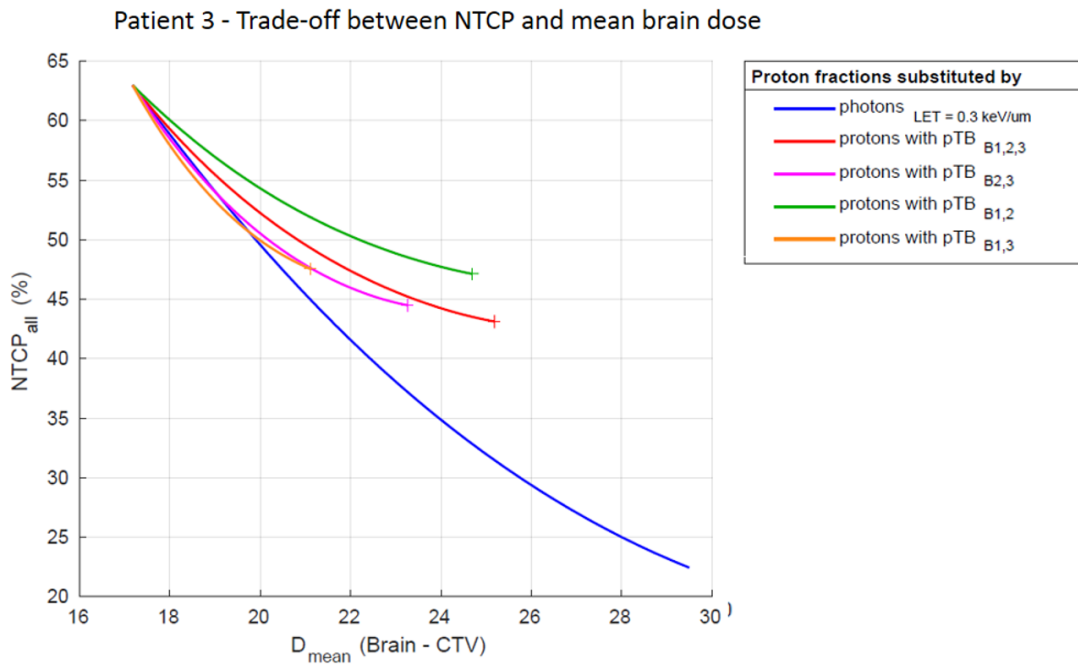


Figure 6.13: The trade-off between  $NTCP_{all}$  and overall brain dose using data from patient 3. The trade-off is given for the clinical proton plan combined with photons $_{LET=0.3\text{keV}/\mu\text{m}}$  (blue), as well as for various combination with proton transmission beams (red, magenta, green, yellow). For clarity, the endpoint of the proton transmission beams are indicated by a '+'-sign.

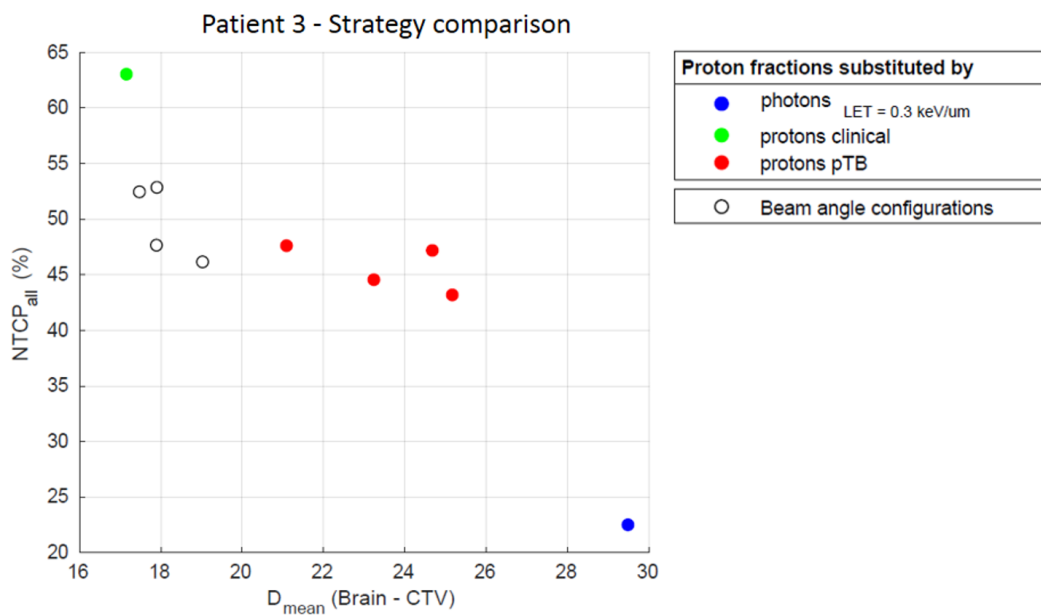


Figure 6.14: Comparison of all three treatment strategies in terms of NTCP and mean brain dose for patient 3. The results are given for all beam angle arrangements (open black circles), the clinical IMPT plan (green), the VMAT plan (blue), and the proton transmission beams extended till the tipping-fraction (red) and plotted in terms of  $NTCP_{all}$  against the mean brain dose.

Table 6.1: Objective list used for the optimization of the clinically used IMPT plan and different beam angle configurations. This objective list is only specified for patient 1.

Structure	Description	Beam	Weight	Robust	Constrain
CTV	Min dose 59.40 Gy	All	400	*	
	Max dose 59.40 Gy	All	150	*	
Brainstem core	Max dose 54.60 Gy			*	
	Max dose 53.70 Gy	All	500	*	
	Max dose 18.40 Gy	Beam 1	100		
	Max dose 18.20 Gy	Beam 2	100		
	Max dose 54.00 Gy			*	*
Brainstem surface	Max dose 59.90 Gy	All	30	*	
External	Dose Fall-Off [H] 59.90 Gy [L] 0.00 Gy	All	1		
	Max dose 20.00 Gy	Beam 1	200		
	Max dose 20.00 Gy	Beam 2	20		
Optic chiasm	Max dose 55.70 Gy			*	
	Max dose 18.00 Gy	Beam 1	1		
	Max dose 16.00 Gy	Beam 2	1		
	Max dose 55.00 Gy			*	*
Cochlea (R)	Max EUD 39.00 Gy		1		
Pituitary	Max EUD 6.00 Gy		1		
Hippocampus (L)	Max dose 10.00 Gy		1		
Optic nerve (R)	Dose Fall-Off [H] 16.00 Gy [L]0.00 Gy		1		

Table 6.2: Minimal objective list used for the (re-)optimization of the proton transmission beam plans.

Structure	Description	Beam	Weight <sup>1</sup>		
			Patient 1	Patient 2	Patient 3
CTV	Min dose 19.80 Gy	Beam 1	400	100	120
	Max dose 19.80 Gy	Beam 1	150	100	100
	Min dose 19.80 Gy	Beam 2	250	100	120
	Max dose 19.80 Gy	Beam 2	250	100	100
	Min dose 19.80 Gy	Beam 3	150	100	120
	Max dose 19.80 Gy	Beam 3	150	100	100
Brainstem	Max dose 20.00 Gy	Beam 1	100	100	30
	Max dose 20.00 Gy	Beam 2	100	100	30
	Max dose 20.00 Gy	Beam 3	100	100	30
External	Max dose 18.40 Gy	Beam 1	20	20	5
	Max dose 18.40 Gy	Beam 2	200	20	5
	Max dose 18.40 Gy	Beam 3	20	20	5

<sup>1</sup> Weight given for different patients. The weights for the CTV are similar for the clinically used objective list. The weights for the brainstem and external are scaled w.r.t. the weights used for patient 1.

Table 6.3: Evaluation of the clinical goals for patient 1 when applying transmission beams. The amount of gray (Gy) represent the dose that exceeds the clinical goal. The plans including transmission beams are generated with a minimal objective list, only including the CTV, brainstem and external as objective. For reference, the clinical goals are also reviewed for the clinical IMPT plan with the original objective list and the clinical plan re-optimized with the minimal objective list.

TB (frac) <sup>1</sup>	Clinical goals					
	Hippocampus (L) (7.4 Gy, $V_{40\%}$ ) <sup>2</sup>	Pituitary (20.0 Gy, mean) <sup>3</sup>	Brainstem core (54.0 Gy, $V_{0.03cm^3}$ ) <sup>4</sup>	lens (R) (10 Gy, $V_{0.03cm^3}$ ) <sup>4</sup>	Optic Chiasm (55.0 Gy, $V_{0.03cm^3}$ ) <sup>4</sup>	
B <sub>Original obj.</sub> list	-	-	-	-	-	-
B <sub>Minimal obj.</sub> list	-	-	2 Gy	-	-	-
B <sub>1,2,3</sub> (1/3)	12 Gy	4 Gy	4 Gy	11 Gy	-	-
B <sub>1,2,3</sub> (1/2)	20 Gy	7 Gy	4 Gy	11 Gy	-	-
B <sub>1,2,3</sub> (2/3)	22 Gy	11 Gy	4 Gy	11 Gy	-	-
B <sub>1,2,3</sub> (1/1)	22 Gy	11 Gy	4 Gy	10 Gy	-	-
B <sub>1,2</sub> (1/3)	6 Gy	-	3 Gy	10 Gy	-	-
B <sub>1,2</sub> (1/2)	11 Gy	-	2 Gy	11 Gy	-	-
B <sub>1,2</sub> (2/3)	12 Gy	-	3 Gy	11 Gy	-	-
B <sub>1,2</sub> (1/1)	12 Gy	-	3 Gy	11 Gy	-	-
B <sub>2,3</sub> (1/3)	13 Gy	4 Gy	3 Gy	-	-	-
B <sub>2,3</sub> (1/2)	20 Gy	4 Gy	2 Gy	-	-	-
B <sub>2,3</sub> (2/3)	22 Gy	4 Gy	3 Gy	-	-	-
B <sub>2,3</sub> (1/1)	22 Gy	4 Gy	3 Gy	-	-	-
B <sub>1,3</sub> (1/3)	11 Gy	6 Gy	2 Gy	11 Gy	-	-
B <sub>1,3</sub> (1/2)	12 Gy	8 Gy	3 Gy	11 Gy	-	-
B <sub>1,3</sub> (2/3)	12 Gy	9 Gy	3 Gy	11 Gy	1 Gy	-
B <sub>1,3</sub> (1/1)	12 Gy	11 Gy	3 Gy	11 Gy	2 Gy	-

<sup>1</sup> TB = Transmission beam. The clinically used IMPT plan (minimal obj. list) is edited by extending the beam x (B<sub>x</sub>) by the given proportion noted in brackets, starting at the highest energy layers. For reference, the clinical goals for the clinically used IMPT plan (original obj. list) are added.

<sup>2</sup> At most x Gy dose at y % volume.

<sup>3</sup> At most x Gy average dose

<sup>4</sup> At most x Gy dose at y cm<sup>3</sup> volume

Table 6.4: Evaluation of the clinical goals for patient 2 when applying transmission beams. The amount of gray (Gy) represent the dose that exceeds the clinical goal. The plans including transmission beams are generated with a minimal objective list, only including the CTV, brainstem and external as objective. For reference, the clinical goals are also reviewed for the clinical IMPT plan with the original objective list and the clinical plan re-optimized with the minimal objective list.

TB (frac) <sup>1</sup>	Clinical goals									
	Hippocampus (R) 7.4 Gy, $V_{40\%}^2$	Pituitary 20.0 Gy, mean <sup>3</sup>	Brainstem core 54.0 Gy, $V^4_{0.03cm^3}$	lens (R) 10 Gy, $V^4_{0.03cm^3}$	lens (L) 10 Gy, $V^4_{0.03cm^3}$	Optic Chiasm 55.0 Gy, $V^4_{0.03cm^3}$	Optic Nerve (R)(L) 55.0 Gy, $V^4_{0.03cm^3}$	Cochlea (L) 45 Gy, mean <sup>3</sup>		
B <sub>Original obj. list</sub>	-	8 Gy	-	-	-	-	-	-	-	-
B <sub>Minimal obj. list</sub>	-	5 Gy	-	-	-	2 Gy	-	-	-	2 Gy
B <sub>1,2,3 (1/3)</sub>	27 Gy	17 Gy	-	-	11 Gy	1 Gy	3 Gy	1 Gy	-	1 Gy
B <sub>1,2,3 (1/2)</sub>	31 Gy	30 Gy	1 Gy	20 Gy	11 Gy	4 Gy	4 Gy	1 Gy	-	1 Gy
B <sub>1,2,3 (2/3)</sub>	31 Gy	37 Gy	2 Gy	26 Gy	11 Gy	4 Gy	4 Gy	2 Gy	-	2 Gy
B <sub>1,2,3 (1/1)</sub>	32 Gy	38 Gy	2 Gy	26 Gy	11 Gy	4 Gy	5 Gy	8 Gy	-	8 Gy
B <sub>1,2 (1/3)</sub>	12 Gy	19 Gy	3 Gy	4 Gy	11 Gy	3 Gy	2 Gy	-	-	-
B <sub>1,2 (1/2)</sub>	12 Gy	20 Gy	2 Gy	26 Gy	11 Gy	2 Gy	3 Gy	1 Gy	-	1 Gy
B <sub>1,2 (2/3)</sub>	13 Gy	27 Gy	3 Gy	26 Gy	11 Gy	3 Gy	4 Gy	4 Gy	-	4 Gy
B <sub>1,2 (1/1)</sub>	13 Gy	27 Gy	3 Gy	26 Gy	11 Gy	3 Gy	5 Gy	6 Gy	-	6 Gy
B <sub>2,3 (1/3)</sub>	27 Gy	25 Gy	-	-	11 Gy	-	-	1 Gy	-	1 Gy
B <sub>2,3 (1/2)</sub>	31 Gy	26 Gy	3 Gy	7 Gy	11 Gy	3 Gy	2 Gy	-	-	-
B <sub>2,3 (2/3)</sub>	31 Gy	28 Gy	4 Gy	10 Gy	11 Gy	4 Gy	5 Gy	2 Gy	-	2 Gy
B <sub>2,3 (1/1)</sub>	31 Gy	28 Gy	4 Gy	10 Gy	11 Gy	4 Gy	5 Gy	7 Gy	-	7 Gy
B <sub>1,3 (1/3)</sub>	9 Gy	6 Gy	-	-	11 Gy	3 Gy	1 Gy	1 Gy	-	1 Gy
B <sub>1,3 (1/2)</sub>	12 Gy	28 Gy	3 Gy	6 Gy	11 Gy	3 Gy	2 Gy	-	-	-
B <sub>1,3 (2/3)</sub>	12 Gy	25 Gy	2 Gy	7 Gy	11 Gy	2 Gy	2 Gy	1 Gy	-	1 Gy
B <sub>1,3 (1/1)</sub>	13 Gy	26 Gy	3 Gy	7 Gy	11 Gy	3 Gy	3 Gy	3 Gy	-	3 Gy

<sup>1</sup> TB = Transmission beam. The clinically used IMPT plan (minimal obj. list) is edited by extending the beam x ( $B_x$ ) by the given proportion noted in brackets, starting at the highest energy layers. For reference, the clinical goals for the clinically used IMPT plan (original obj. list) are added.

<sup>2</sup> At most x Gy dose at y % volume.

<sup>3</sup> At most x Gy average dose

<sup>4</sup> At most x Gy dose at y cm<sup>3</sup> volume

Table 6.5: Evaluation of the clinical goals for patient 3 when applying transmission beams. The amount of gray (Gy) represent the dose that exceeds the clinical goal. The plans including transmission beams are generated with a minimal objective list, only including the CTV, brainstem and external as objective. For reference, the clinical goals are also reviewed for the clinical IMPT plan with the original objective list and the clinical plan re-optimized with the minimal objective list.

TB (frac) <sup>1</sup>	Clinical goals									
	Hippocampus (R) 7.4 Gy, $V_{40\%}^2$	Hippocampus (L) 7.4 Gy, $V_{40\%}^2$	Pituitary 20.0 Gy, mean <sup>3</sup>	lens (L) 10 Gy, $V^4$ <sub>0.03cm<sup>3</sup></sub>	Optic Chiasm 55.0 Gy, $V^4$ <sub>0.03cm<sup>3</sup></sub>	Optic Nerve (L) 55.0 Gy, $V^4$ <sub>0.03cm<sup>3</sup></sub>	Retina (L) 45.0 Gy, $V^4$ <sub>0.03cm<sup>3</sup></sub>	GlnD lacrimal 30 Gy, mean <sup>3</sup>		
B <sup>Original obj. list</sup>	5 Gy	-	-	-	-	-	-	-	-	-
B <sup>Minimal obj. list</sup>	5 Gy	-	-	-	2 Gy	-	-	-	-	-
B <sub>1,2,3</sub> (1/3)	2 Gy	20 Gy	-	10 Gy	-	1 Gy	2 Gy	6 Gy	-	-
B <sub>1,2,3</sub> (1/2)	11 Gy	22 Gy	-	11 Gy	-	-	4 Gy	5 Gy	-	-
B <sub>1,2,3</sub> (2/3)	14 Gy	31 Gy	-	11 Gy	-	-	4 Gy	5 Gy	-	-
B <sub>1,2,3</sub> (1/1)	13 Gy	31 Gy	-	11 Gy	-	-	4 Gy	4 Gy	-	-
B <sub>1,2</sub> (1/3)	2 Gy	9 Gy	2 Gy	-	-	2 Gy	-	-	-	-
B <sub>1,2</sub> (1/2)	11 Gy	17 Gy	2 Gy	-	-	-	-	-	-	-
B <sub>1,2</sub> (2/3)	15 Gy	17 Gy	-	-	-	-	-	-	-	-
B <sub>1,2</sub> (1/1)	14 Gy	17 Gy	-	-	1 Gy	-	-	-	-	-
B <sub>2,3</sub> (1/3)	2 Gy	19 Gy	-	10 Gy	-	1 Gy	2 Gy	6 Gy	-	-
B <sub>2,3</sub> (1/2)	4 Gy	33 Gy	-	11 Gy	-	1 Gy	6 Gy	7 Gy	-	-
B <sub>2,3</sub> (2/3)	8 Gy	34 Gy	-	11 Gy	-	2 Gy	6 Gy	7 Gy	-	-
B <sub>2,3</sub> (1/1)	37 Gy	34 Gy	-	11 Gy	-	2 Gy	6 Gy	7 Gy	-	-
B <sub>1,3</sub> (1/3)	2 Gy	19 Gy	-	10 Gy	-	1 Gy	2 Gy	5 Gy	-	-
B <sub>1,3</sub> (1/2)	3 Gy	19 Gy	-	12 Gy	1 Gy	1 Gy	2 Gy	5 Gy	-	-
B <sub>1,3</sub> (2/3)	2 Gy	19 Gy	-	12 Gy	-	2 Gy	2 Gy	5 Gy	-	-
B <sub>1,3</sub> (1/1)	3 Gy	19 Gy	-	12 Gy	-	1 Gy	2 Gy	4 Gy	-	-

<sup>1</sup> TB = Transmission beam. The clinically used IMPT plan (minimal obj. list) is edited by extending the beam x (B<sub>x</sub>) by the given proportion noted in brackets, starting at the highest energy layers. For reference, the clinical goals for the clinically used IMPT plan (original obj. list) are added.

<sup>2</sup> At most x Gy dose at y % volume.

<sup>3</sup> At most x Gy average dose

<sup>4</sup> At most x Gy dose at y cm<sup>3</sup> volume

# 7

## Literature study

This literature study has been part of my master with the aim to provide a context for my master thesis project. This review provides an overview of the current status of knowledge of RBE from available biological experiments and clinical cohort studies to investigate if there are "*Rationales for a variable RBE*" presented in recent literature. Special attention is given to identify the extent to which the LET impacts the RBE and causes an increased rate of toxicities. Besides, current examined strategies on how to minimize potential variations in RBE by treatment planning are presented.

### 7.1. Literature search

For this literature study, the studies which provides clinical evidence were used as a starting point. The literature search was primarily limited to references from these primary publications about photon and proton toxicity incidence numbers, reviews of in vitro studies correlating RBE to biological outcomes, and strategies migrating the RBE effect during treatment planning. Besides, references within these secondary publications were also included. Additional publications were obtained were searched on PubMed and Google Scholar.

### 7.2. Biological studies

An easy approach to access the intrinsic radiosensitivity of cells is to study the cell survival rate [51]. To this end, most in vitro studies use clonogenic cell survival as an endpoint for assessing the clinical RBE on tissue response. In an extensive review by Paganetti [17], ~90% of the available clonogenic cell survival data points published between 1970-2014 were collected from 76 experimental reports. Restrictions were applied to come up with a more clinically relevant subset of data. Datapoints with dose  $>30$  Gy and LET  $> 20$  keV/ $\mu$ m were removed from the initial set [52]. Data were extracted from various cancer cells or cell lines of Chinese hamsters, rats, mice, and humans. Since the commonly used RBE model is derived from the linear-quadratic function of cell survival by assuming the same survival fraction after photon and proton therapy (Appendix 6.1), the RBE model of Carabe-Fernandez et al. [48] is also applied in this cell survival study. The goal was to establish the relation between RBE with dose, LET, and the tissues radiosensitivity parameter  $\alpha/\beta$ . As the dose-averaged LET is more appropriate in describing the biological effect than the track-averaged LET, LET<sub>d</sub> is used to describe RBE.

The next sections present the relationship of RBE as a function of LET<sub>d</sub>, dose, and  $\alpha/\beta$ . Note that the results are averages over all cell lines, whose radiosensitivity is given for different energies of the reference photon radiation.

#### RBE as function of LET<sub>d</sub>

As protons slow down with depth, the LET initially increases slowly towards the distal end of the Bragg peak, followed by a rapid increase at the end of the range. The maximum is reached after the Bragg peak, where protons lose their energy fastest [53]. With the increasing LET, the cellular response in terms of cell death increases along mono-energetic proton beams, indicating an increasing RBE with

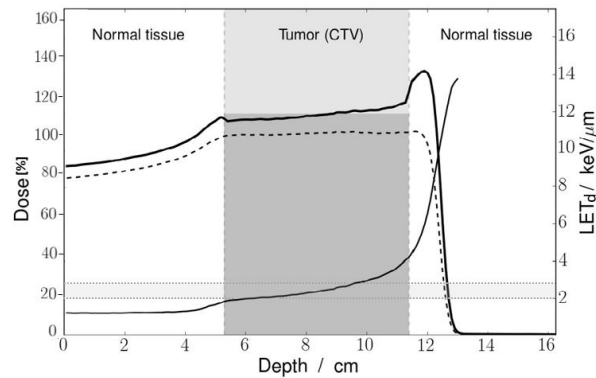


Figure 7.1: Depth-dose and depth-LET distribution for a modulated proton beam. The relative physical dose distribution for a modulated beam (dashed line) and the respective dose-averaged linear energy transfer ( $LET_d$ ) (solid line) are visualized. The Spread-Out Bragg Peak covers the tumor region (vertical gray area). The product of physical dose times the RBE gives the effective biological dose (bold line). Typical  $LET_d$  values within the center region of the SOBP are 2-3 keV/ $\mu\text{m}$  (horizontal gray area). The figure is taken from [23]. Some adaptations are made, which are inspired by [17].

increasing LET [22]. A similar pattern is observed for a modulated beam (fig.7.1). Although the relative dose (dashed line) in the entrance region is higher for the modulated beam than for a mono-energetic beam, the LET (solid line) remains unaffected. Based on the average value of the extended clonogenic cell survival assay [17], the  $LET_d$  turns out to be 0-2 keV/ $\mu\text{m}$ . Then, the  $LET_d$  slowly increases within the SOBP to 3 keV/ $\mu\text{m}$  at the center of the SOBP, to 6 keV/ $\mu\text{m}$  towards the end of the SOBP, and further to 9 keV/ $\mu\text{m}$  at the distal edge of the region. Finally, the LET progressively increases to a maximum of 15 keV/ $\mu\text{m}$  just after the SOBP.

By correlating the observed LET values with the survival rate, a relation between RBE and LET was established. Relative to 6 MV photons with a LET value of 0.3 keV/ $\mu\text{m}$  and a dose of 2 Gy per fraction, a similar pattern is observed in the biological effect as for LET. The RBE in the entrance region corresponded to a value of 1.1. Then, the RBE increases with the rise in  $LET_d$  to 1.21 in the second half of the SOBP, to 1.35 at the distal edge region of the SOBP, and up to a maximum of 1.72 just behind the Bragg peak. The RBE significantly increases above the currently used RBE of 1.1, especially after the distal end of the proton range. Thereby, a higher effective biological dose ( $D_{\text{physical}} \times \text{RBE}$ ) is given to the healthy tissue within the first few millimeters after the clinical target volume (CTV) (bold line).

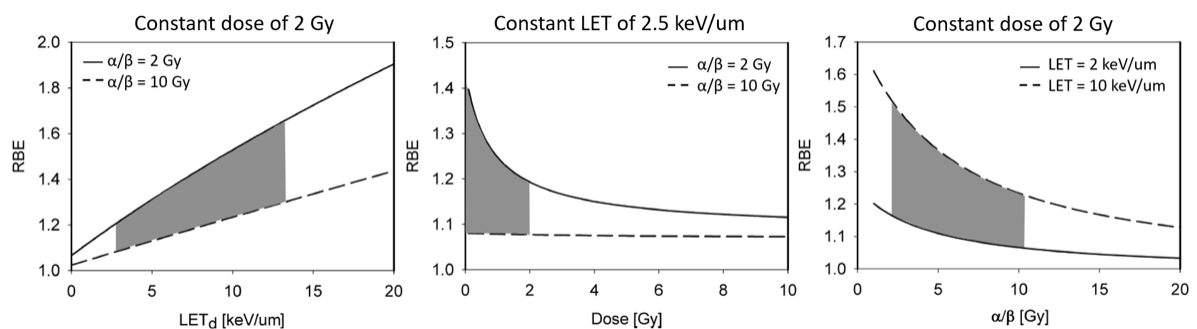


Figure 7.2: Proton RBE for clonogenic cell survival as a function of  $LET_d$ , dose, and  $(\alpha/\beta)$ . Left: The linear RBE-LET relationship is given for tissue with  $(\alpha/\beta)$  of 2 Gy (solid) and 10 Gy (dashed) at a dose of 2 Gy; Middle: The RBE-dose relationship for tissue with  $(\alpha/\beta)$  of 2 Gy (solid) and 10 Gy (dashed) with a constant LET of 2.5 keV/ $\mu\text{m}$ . Right: The RBE-radiosensitivity relation with a dose of 2 Gy per fraction and a LET of 2 keV/ $\mu\text{m}$  (solid) and 10 keV/ $\mu\text{m}$  (dashed). The grey area shows the clinically most relevant region as treatment planning considerations are typically based on  $LET_d$  between 2.5 and 13 keV/ $\mu\text{m}$ , dose  $<2\text{Gy}$ , and  $(\alpha/\beta)$  between 3 and 10 Gy. The figure is taken from [53] and edited.

The linear increase of RBE with  $LET_d$  marks the importance of LET affecting the RBE. However, the slope varied when discriminating the data points on cell sensitivity. Figure 7.2 (left) presents the RBE-LET relationship for late responding tissue (low  $\alpha/\beta$ , e.g., 2 Gy) and acute reacting tissue (high  $\alpha/\beta$ , e.g., 10 Gy). Still, a more or less linear behavior is observed. The response of cells that differ in radiosensitivity is further discussed in section 7.2.

The RBE of 1.1 was primarily chosen for the tumor. When we assume that  $LET_d$  values of 2-3 keV/ $\mu$ m are typically observed within the central region of the SOBP, as indicated by the vertical gray shaded area in figure 7.1, an RBE of  $\sim 1.15$  is found as average for the dose plateau. Although there is a slight increase relative to the current RBE value of 1.1, an RBE of 1.1 seems reasonable if an average for the midpoint of an SOBP is assigned in terms of tumor control. However, if the goal is to investigate the spatial variations in RBE among the treatment field, it is insufficient to consider only the center of the treatment volume.

There is a concern that the high-LET values at the distal end of the proton treatment field enter into the healthy tissue, especially with low  $\alpha/\beta$  (fig. 7.3b), and causes that the effect mostly appears within this region (fig. 7.3c) [54]. Figure 7.3d illustrates the additional biological effect. By this, high-LET regions should be avoided in the area of critical healthy tissues behind the target volume.

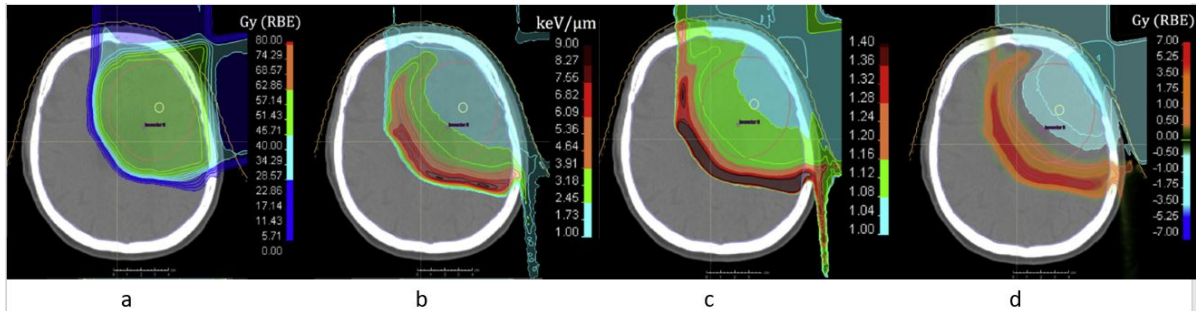


Figure 7.3: Proton dose, LET and RBE distribution for a primary brain tumor patient. The prescribed dose to the CTV is 60 Gy<sub>RBE</sub>. (a) Absorbed physical dose,  $D_{\text{physical}}$ , (b) LET distribution, (c) Spatial variation of a variable RBE based on experimental data from [22], (d) Difference in RBE-weighted dose ( $D_{\text{physical}} \cdot (RBE - 1.1)$ ). The figure is taken from [54].

### RBE as function of dose

When increasing the dose per fraction up to 6 Gy, the RBE values increase more moderately with the proton depth than with a dose of 2 Gy. The RBE appeared to be 1.1 in the entrance region, 1.13 in the center of the SOBP, 1.27 at the distal edge, and 1.6 in the distal fall-off region [17]. The in vitro experiments show that the RBE increases with decreasing dose per fraction, which is especially true for late responding tissue in the clinically relevant dose region (fig. 7.2, middle).

### RBE as function of $\alpha/\beta$

As already mentioned in previous paragraphs, in vitro studies found higher RBE values in cells with a smaller  $\alpha/\beta$  (fig. 7.2, right). However, variations in RBE might only be significant for tissue with an  $\alpha/\beta < 5$  Gy [55].

As healthy tissue has, in general, a low  $\alpha/\beta$  value, e.g., the central nervous system has a value  $< 3$  Gy [13, 14], the RBE will vary with dose. The increase in RBE will be even more pronounced for higher LET values. In contrast, most CNS tumors have a higher  $\alpha/\beta$  value, e.g., the brain tumor radiosensitivity ranges between 10-28 Gy [13, 15]. As these tumors are hardly fractionation-sensitive, the RBE could even fall below 1.1. However, Sethi et al. [?] found no indication that the RBE was overestimated.

Since  $\alpha$  values of protons tend to increase with LET with a larger extent than  $\beta$ , the  $\alpha/\beta$  value increases with depth [13, 56]. As in clinical the fractionation dose is generally 2.0 Gy or 1.8 Gy, the influence on RBE may be more significant for late responding tissue (low  $\alpha/\beta$ ), e.g., healthy tissue at the end of the SOBP, than for acute reacting tissues (high  $\alpha/\beta$ ), e.g., tumors that already have a high  $\alpha/\beta$  ratio (fig. 7.2, middle). In terms of healthy tissue toxicity, one might expect that healthy tissue with low  $\alpha/\beta$  positioned at the region behind the tumor that receives intermediate dose levels is of higher risk. For example, Carabe et al. [57] found elevated RBE values within the brainstem ( $\alpha/\beta = 2.1$  Gy) as it has to be (partially) irradiated during treatment of posterior fossa tumors to achieve sufficient tumor coverage [46].

When increasing the dose per fraction, the difference in RBE between late and acute responding tissue rapidly decreases for a dose  $< 4$  Gy per fraction, and then the curve gradually decreases [58]. Therefore, hypo-fractionated proton beams potentially reduce the impact of late tissue morbidity, as prospected by Jones, B. [13].

Despite a large amount of in vitro cell survival data relating variation in RBE to clinically relevant LET, doses, and tissues'  $\alpha/\beta$  values, the proton RBE still bears considerable uncertainties. Sources for the RBE uncertainties are related to the uncertainties in biological input parameters when estimating the RBE [57] and experimental uncertainties [17]. Therefore, the data only support the idea of how the RBE responds to LET<sub>d</sub>, fractionation dose, and tissue radiosensitivity.

### Other endpoints

However, experiments are not only performed by using clonogenic cells. Paganetti et al. [17] also reviewed experiments investigating the tumor response in mice. The amount of surviving cells was used as an endpoint. In general, the RBE value did not significantly differ from the current 1.1. However, most of these studies used large doses between 10-20 Gy, in which the RBE effect may be expected to be small.

Besides cell survival, other in vitro endpoints, including the chromosome aberrations, mutations, induction of reactive oxygen species leading to oxidative stress leading to DNA pathway responses, foci formation, single and double-strand DNA breaks (DSB), were evaluated. Most studies agreed with the clinical RBE of 1.1. However, some selected endpoints found considerable deviation.

Even though most in vitro studies using other endpoints than clonogenic cell survival did not reveal deviations from the currently used RBE, the concern remains of underestimating the RBE in healthy tissue in vivo [23]. Moreover, cell survival studies might be more relevant for tumor control probability (TCP), while other biological endpoints are potentially more relevant for healthy tissue complication probability (NTCP). With this, an RBE derived from cell survival studies might not be an appropriate measurement for RBE values in healthy tissue [17].

## 7.3. From pre-clinical to clinical

When going from cells to a living organism, the cell processes after radiation become more complicated due to the impact of the tumors' environment, the immune responses, and vasculature [43].

More clinically relevant endpoints in case of brain tumors are local tumor control or recurrence (local failure), early and late healthy tissue toxicity effects such as pseudo-progression (PsP) [1, 45, 59], brainstem injury and brain necrosis [46] or cognitive tests [60].

Comparing the incidence rate of pseudo-progression (PsP) between photon and proton treatment plans, Bronk et al. [59] found a similar incidence rate of PsP between photon- and proton treatment for 67 oligodendroglioma patients (14.3% and 16%, respectively), and 32 astrocytoma patients (13% and 11.1%, respectively). Other photon-studies found a PsP incidence rate of 20% with a median dose of 50.4 Gy [61, 62]. In contrast, patients treated with protons were significantly more likely to develop PsP compared to patients treated photons (45% vs. 25%, respectively) reviewing 143 glioma patients [63]. Further, Gunther et al. [45] found a higher likelihood of observing image changes in ependymoma patients treated with protons than photons (43% vs. 27%, respectively). Moreover, both Bronk et al. [59] and Gunther et al. [45] found a similar or shorter time to develop PsP or observe image changes after proton treatment than after photon treatment. The task group by Paganetti [64] reviewed, i.a., the incidence of brainstem injury and found a more extensive range after proton therapy (0% to 16%) than after photon treatment (2.2% to 8.6%). All these studies used photon doses between 50.4 Gy and 57.0 Gy or physical proton doses of 50.4 Gy<sub>RBE</sub> and 59.0 Gy<sub>RBE</sub>.

These reports on toxicity suggest that, in general, there are currently no apparent differences in unwanted side effects. However, it might be that the outcomes between protons and photons are hardly comparable because of differences in physical properties and biological responses, e.g., angiogenesis and cell migration and patterns of gene expression [65], DNA methylation [66], and production of ROS [67]. Further, the particle ionization track structure affects the type of damage and the involved repair-ways. As the energy deposition is more heterogeneous with proton than photons, protons might cause more clustered DNA breaks leading to increased complexity in DNA damage [44]. Therefore, non-homologous recombination is predominantly involved after photon irradiation, while proton irradiation stimulates homologous repair mechanisms. Their response can also differ between tumors. For example, tumors with homologous-deficient tumor cells are more sensitive to protons than photons [18].

However, the relation of these biological responses after proton irradiation with the underlying RBE variations is not well understood. Therefore, their relevance for RBE variations in clinical patient treat-

ment is limited. Nevertheless, the undesirable effects in clinical outcomes are better understood concerning the dose distribution and achieved dose constraints for critical organs. Nonetheless, with the introduction of proton beams into clinical practice, it was assumed that increased conformality and absence of exit-dose might overcome toxicity up to a certain level.

In the early days of proton therapy, there was already the awareness that the RBE may deviate. With the currently available data, the awareness of potential RBE deviations leading to these unforeseen toxicities is growing. Hence, a re-assessment of the justification of the commonly used RBE of 1.1 in the clinic is warranted. As the dose distribution for proton is more heterogeneous than with photons and as organ effects depend on the dose distribution instead of mean dose, the spatial variations in RBE should be identified, ideally voxelwise [17, 43, 53]. This approach is a step toward a clinical RBE.

## 7.4. Clinical data

Although the number of publications is still limited, clinical evidence for a variable RBE is growing. A few papers have correlated CNS injury with LET or RBE in patients for brain tumors, like medulloblastoma [46], ependymoma [24], and glioma [1, 25, 26]. Their main focus was to identify a (voxel-wise) correlation between the observed changes in magnetic resonance imaging. As contrast-enhancement on MRI images characterize increased evidence of radiation-dependent brain tissue damage, it indicates a potential variation in biological effectiveness.

### Methods

All studies calculated the dose and LET distribution using a Monte Carlo (MC) (dose) engine, which is also used to determine a voxel-by-voxel LET. Except for Giantsoudi et al. [46], the clinical evidence studies used a voxel-wise correlation to predict the observation for image changes. The generalized model to calculate the probability to observe image changes,

$$P_{IC} = \frac{1}{1 + e^{-c}}, \quad (7.1)$$

was fitted to the experimental data to derive the weighting factors  $b_n$  for the model predictors  $X_n$  in the linear combination,

$$c = b_0 + \bar{b}_n \cdot \bar{X}_n. \quad (7.2)$$

The weighting factors for the corresponding parameter were obtained by univariate and multivariate logistic regression analyses (table 7.1). To validate their model and test its robustness a multi-fold cross-validation was performed, including patients without image changes [1, 24], or only based on left-out patients with image change [1, 25]. As Bahn et al. [1] only included the smallest 30% of the lesions during analysis, they performed an extended validation on the remaining 70%. For evaluating the model's accuracy, the area under the curve (AUC) was calculated. Based on the established model, the toxicity of healthy tissue can be predicted by the  $TD_x$  (the tolerance dose at which x% of healthy tissue shows toxicity) [24–26] or normal tissue complication probability (NTCP) [1].

All studies used passive scattering proton therapy, except the group of Bahn et al. [1], who used 3-dimensional spot scanning or intensity-modulated proton therapy.

### Relating RBE with radiographic change among brain patients

Giantsoudi et al. [46] treated 111 pediatric medulloblastoma patients by proton craniospinal irradiation. They identified post-radiation image changes for 10 patients, of whom 4 had symptomatic development. In contrast to the other studies, no clear correlation was found between the sites of image changes, LET and RBE. However, by comparing the areas showing image changes with the whole irradiated target volume in patients having symptomatic injury (not showing only radiation necrosis), the image changed area had a significantly higher mean LET (2.7 vs. 2.4 keV/ $\mu$ m, respectively,  $p < 0.5$ ). Using the Carabe model [49], a higher mean RBE was found in the area of observed image changes. However, these findings were not significant ( $p > 0.05$ ). In the asymptomatic group, the areas showing image changes had a lower mean LET (2.2 vs. 2.5 keV/ $\mu$ m, respectively). Further, the LET distribution in the brainstem did not differ between different groups.

A distinction was made between patients in whom the brainstem was entirely or partially irradiated. Patients who received a full boost had a higher risk of developing symptoms than those who got partial brainstem irradiation (7.7% and 1.4%, respectively,  $P = .094$ ). Asymptomatic patients who received a

Table 7.1: Univariable and multivariable RBE model coefficients and accuracy

Group of		Coefficients (Predictors)					Accuracy
		$b_0$ (intercept)	$b_1$ ( $\text{Gy}^{-1}$ ) (Dose)	$b_2$ ( $(\text{keV}/\mu\text{m})^{-1}$ ) (LET)	$b_3$ ( $(\text{Gy}\cdot\text{keV}/\mu\text{m})^{-1}$ ) (Dose·LET)	$b_4$ (PRV <sup>1</sup> )	AUC
Peeler et al. [24]	$M_1$	-11.2	0.14	1.2			0.91
Eulitz et al. (1) [26]	$M_2$	-17.7	0.18	2.15			0.88
Eulitz et al. (2) [25]	$M_3$	-6.17	0.03	-			0.65
	$M_4$	-5.23	-	0.19			0.64
	$M_5$	-5.59	-	-		3.03	0.75
	$M_6$	-15.99	0.15	1.75			0.88
	$M_7$	-13.91	0.11	1.37		2.43	0.91
	$M_8$	-8.26	0.003	-	0.03	2.35	0.91
Bahn et al. [1]	$M_9$	-26.3	0.19	-	0.0018	1.19	0.94

<sup>1</sup> Periventricular region (PVR) is binary: 1 (voxel inside PVR) or 0 (voxel outside PVR)

whole brainstem boost showed no image change in the brainstem. All patients showing image changes having a whole brainstem boost had a median dose  $>52.4 \text{ Gy}_{\text{RBE}}$  and a maximum dose of  $56 \text{ Gy}_{\text{RBE}}$ .

Peeler et al. [24] was the first who showed clinical evidence of a correlation between healthy tissue radiation damage and an increase in biological effectiveness due to increased dose and LET. The study was performed with a subset of 37 ependymoma patients from Gunther et al. [45] of whom 16 (43%) had changes in the image. Of the 16 patients, 13 patients were irradiated in the infratentorial region, and 11 of them had image changes in the brainstem. Patients with image change had a higher median dose (59.4 vs. 54 Gy). Specific changes in the brainstem were more frequently found when patients were treated with a mean dose  $>44.2 \text{ Gy}$  ( $p=0.016$ ), a higher  $D_{50}$  ( $p=0.045$ ) of  $>54 \text{ Gy}$  ( $p=0.024$ ).

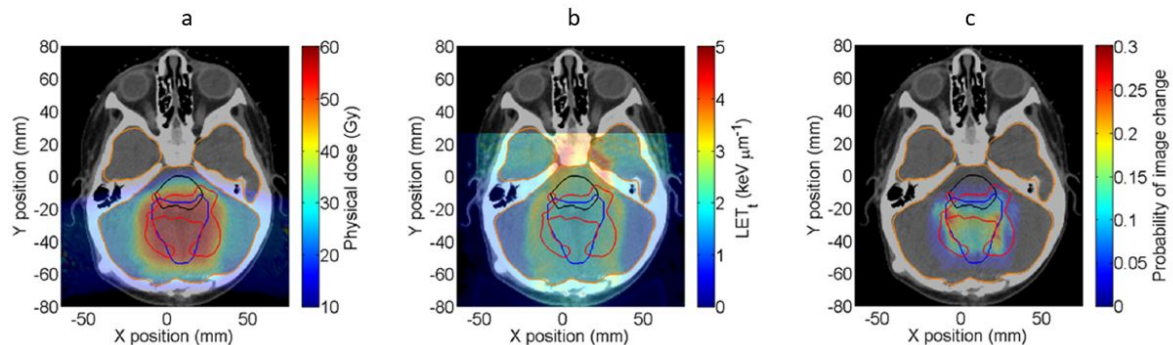


Figure 7.4: Probability of image change correlating with dose and LET. A voxelwise correlation of the physical dose (a) and  $\text{LET}_t$  distribution (b) with changes observed in the image (red contour). (c) illustrates the probability of image change for each voxel. Additional structure contours include the CTV (blue line) and the brainstem (black line). The figure is taken from [24].

In this study, the track-averaged LET ( $\text{LET}_t$ ) was used as a predictor, although RBE models usually use the dose-averaged LET ( $\text{LET}_d$ ). In a previous study, they found that  $\text{LET}_t$  is proportional to  $\text{LET}_d$  for low LET values (clinical treatment plans mostly encounter such ranges) [?]. Thereby, Peeler et al. [24] validated the use of  $\text{LET}_t$  as an acceptable approximation. Besides  $\text{LET}_t$ , the dose was also incorporated in the model,  $M_1$  (table 7.1), as a predictor for image changes. The model had an AUC of 0.91. An increase in the probability of image change was found mainly at the edge of the CTV (fig. 7.4). This could be explained by the relation of dose with LET. Within the CTV, the dose is highest with low to intermediate LET levels. The region outside the CTV receives a lower physical dose, but the LET is higher (up to  $3 \text{ keV}/\mu\text{m}$ ).

To compare these results, Eulitz et al. (1) [26] presented the same type of radiation response model based on dose and  $\text{LET}_t$ . Although the small number of patients (4 patients with glioma grade III), the

dose and  $LET_t$  strongly correlated with the necrotic lesions. In contrast to Peeler et al. [24] who investigated early radiation response (the image changes were observed at three months after treatment), the model of Eulitz et al. (1),  $M_2$  is based on late effects (the image changes were observed after two years). This could explain the different obtained slope ( $AUC = 0.88$ ).

To validate the model, Eulitz et al. (2) performed a follow-up study with a cohort of 6 new glioma grade II and III patients [25]. Different univariate and multivariate models were investigated based on dose,  $LET_t$ , and the area around the ventricle system ( $M_{3-8}$ ). The latter is incorporated in the model to evaluate the healthy tissue response around the periventricular region (PVR), where lesions are frequently observed. Earlier studies (e.g., [28]) found that the dose-response in the tissue of the CNS shows a correlation within the 4 mm area around the ventricular system. Therefore, Eulitz et al. (2) [25] adopted the distance of 4 mm extension of the ventricular system to their model. The inner liquid cavities were excluded from analysis as no image changes related to radio-necrosis were expected in these regions.

Univariate models based on dose,  $M_3$  ( $AUC = 0.65$ ), or  $LET$ ,  $M_4$  ( $AUC = 0.64$ ), provide a weak correlation of RBE with the observed images changes. The multivariate models that incorporate both dose and  $LET$ ,  $M_6$  ( $AUC = 0.88$ ), offer a better prediction of image change, emphasizing the importance of the  $LET$  in proton treatment planning. Notice that  $M_6$  and  $M_2$  are similar models as they are based on the same predictors. Although these models do have the same response rate, a difference in coefficients is observed.

By extending the multivariable model by the third variable PVR,  $M_7$  ( $AUC = 0.91$ ), the probability of predicting the change image in a specific voxel becomes even more accurate. The same accuracy was obtained by  $M_8$  using dose· $LET_t$  instead of using  $LET_t$ . Considering the univariable models, the PVR,  $M_5$  ( $AUC = 0.75$ ), is most accurate in predicting image changes. Together with the fact that the weighting factor for PVR remained almost unaffected in all models, Eulitz et al. (2) [25] suggested that the PVR has an increased radio-sensitivity with a high risk of developing late brain injury.

The most recent clinical evidence is given by the group of Bahn et al. [1]. Their aim was not to generalize a model to predict image changes, as the previous studies described. Instead, they created a model to predict the origin of contrast-enhancing brain lesion (CEBLs), called the probability of lesion origin (POLO). The POLO model was based on the physical parameters dose and dose· $LET_d$ , and the binary risk factor PVR, just like model  $M_8$  from Eulitz et al. (2) [25]. The PVR was included for the same goal and under the same conditions mentioned above. As commonly used in RBE models, the dose-averaged  $LET$ ,  $LET_d$ , was applied. Figure 7.5 illustrates an example of applying a voxel-wise prediction. A high POLO (c) was particularly found at the edge of the CTV (yellow line) with high physical dose (a) and a high  $LET_d$  (b), which correlates to the area of the observed CEBL (white line) within the PVR (delineated by light and dark blue line). The POLO model,  $M_9$ , had the highest response rate of all presented models ( $AUC = 0.94$ ).

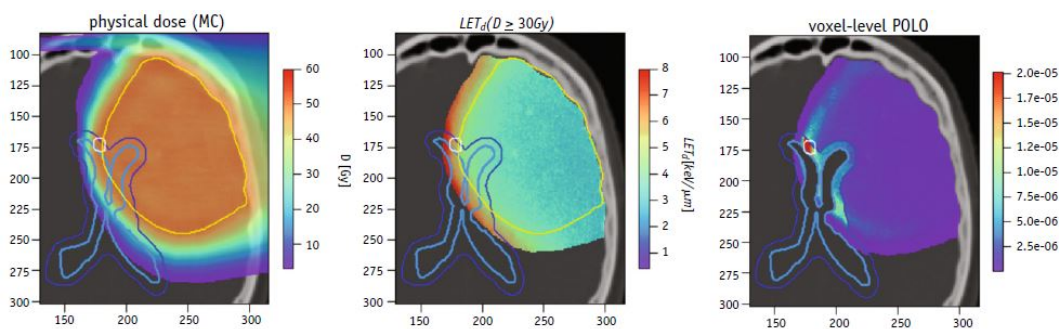


Figure 7.5: Voxel-wise prediction model based on dose and  $LET_d$ . (a) Physical dose ( $RBE = 1.1$ ). (b) The dose-averaged  $LET$  ( $LET_d$ ) distribution only shown in combination with doses above 30 Gy ( $RBE = 1.1$ ). (c) The predicted voxel-level probability of lesion origin (POLO) distribution. The light and dark blue lines depict the ventricular system and the 4-mm region around, respectively. The PTV is depicted by the yellow line, whereas the observed CEBLs contour is presented in white. The figure is taken from [1].

Voxels encountered as CEBLs indeed predicted high POLO, in regions of high dose (mean: 53.5  $Gy_{RBE=1.1}$  (median), max. 55.4  $Gy_{RBE=1.1}$  and high  $LET_d$  (range: 3.56 to 8.18  $\mu m/keV$ ). Most CEBLs were

located close to the ventricular system: 79% of the CEBLs were situated within 4 mm and 92% within 10mm distance from the ventricular system. Further, 90% of the CEBLs were found at the distal edge of at least 1 beam. Altogether, the model predicted a 3-fold increased risk in the 4 mm region around the ventricular system. As studies treating glioma and glioblastoma patients with photons observed similar results, Bahn et al. [1] believed that this behavior is independent of the radiation modality.

Based on the POLO model, a linear RBE-LET<sub>d</sub> relationship was derived:  $RBE = \frac{D_\gamma}{D_p} = 1 + k \cdot LET_d$ , with a slope  $k = 0.11 \text{ keV}/\mu\text{m}$ . As expected, the RBE increases linearly with LET<sub>d</sub>, with an RBE of 1.2 for LET<sub>d</sub>=2 keV/μm to 1.50 for LET<sub>d</sub>=5 keV/μm.

## Prediction of toxicity

To get a better understanding of dose-LET relation based on these models, Gunter et al. [24], Eulitz et al. (1) [26], Eulitz et al. (2) [25], derived the tolerance dose, TD<sub>50</sub>, at which a voxel has a 50% probability of showing toxicity from the clinical image response data. Figure 7.6 visualizes the relationship between the TD<sub>50</sub> and LET for model M<sub>1</sub>, M<sub>2</sub>, M<sub>6</sub>, and M<sub>7</sub>. The data suggest that the TD<sub>50</sub> decreases linearly with increasing LET. In other words, the biological effectiveness might increase as a combination of proton dose and LET.

Indelicato et al. [68] found that the mean dose for the brainstem >52.4 Gy<sub>RBE</sub> is associated as a risk factor for brainstem injury. Therefore, a dose of 52.4 Gy<sub>RBE</sub> is used as a reference to compare the TD<sub>50</sub> as a function of LET for the given models. By this, the models M<sub>1</sub>, M<sub>2</sub>, and M<sub>6</sub> expect a probability of >50% observing image change in a voxel of the brainstem with a LET<sub>t</sub>>3.3 keV/μm, >3.9 keV/μm and >4.6 keV/μm, respectively. Model M<sub>7</sub> predicts to observe a similar result with a LET<sub>t</sub>>4.2 keV/μm inside the PVR and a LET<sub>t</sub>>6 keV/μm outside the PVR.

The latter model investigated the corresponding RBE with the TD<sub>15</sub>. Translating the probability to observe a 15% image change of a voxel inside (LET = 2.9 keV/μm) or outside (LET = 4.6 keV/μm) the PVR relative to a photon LET of 1 keV/μm, Eulitz et al. (2) [25] found an RBE of 1.5 and 1.8, respectively.

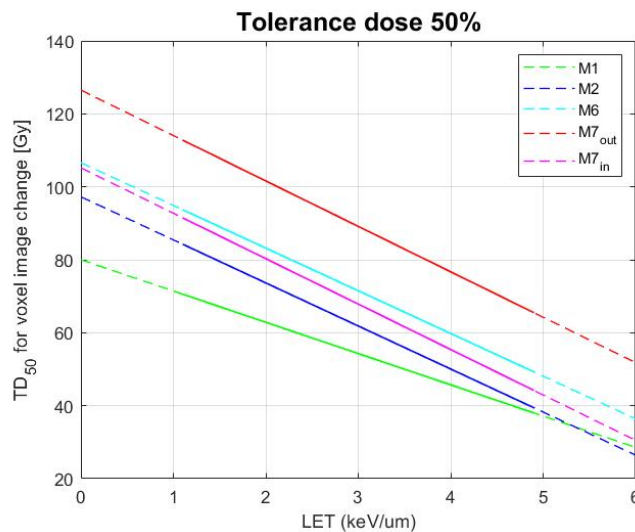


Figure 7.6: The tolerance dose as a function of LET. The physical doses that produce 50% probability of image change in voxels as a function of LET are shown for M<sub>1</sub>, M<sub>2</sub>, M<sub>6</sub>, and M<sub>7</sub>. The solid line represents the data within the range of available data, while the dashed line is extrapolated from the model. The data is extracted from [24–26].

Bahn et al. [1] published a different toxicity model, which predicts the patient-level risk to develop a CEBL. They used the patient's POLO distribution to derive the individual normal tissue complication probability (NTCP<sub>CEBL</sub>). In contrast to RBE models, Bahn et al. [1] tested the feasibility of the prediction model and found that the NTCP<sub>CEBL</sub> had a good characterization ability (AUC = 0.78). In general, the model assumes a lower NTCP<sub>CEBL</sub> when considering a lower dose, dose times LET, or avoiding sensitive tissue like the region around the ventricular system.

## Radiographic changes among chest-wall patients

Besides, the effect of RBE is not only studied in brain patients. A comparable analysis is performed by Tracy et al [27], who investigated RBE effects in chest-wall patients by analyzing late-phase lung density changes using computed tomography (CT). An increase in lung density can be characterized by an increase in Hounsfield Unit (HU), which indicates for asymptomatic fibrosis. Therefore, changes in HU point towards a potential increase in biological effectiveness. Asymptomatic fibrosis can be the result after irradiation of the breast as a small portion of the ipsilateral lung falls within the radiation field. When these patients are treated with protons, the distal edge of the beam falls in the anterior area of the lung. Therefore, the ipsilateral lung receives high LET values potential resulting in an increased RBE. For comparison, all 10 patient treated with protons were matched with a patient treated with photons. A total absorbed dose of 50.4 Gy was prescribed for all patients.

By Tracy et al [27], a quantitative analysis was performed by correlating the median HU of the post-treatment CT scans with dose (HU/Gy) (endpoint 1), and the median change in HU values between pre- and post-treatment CT scans with dose ( $\Delta$ HU/Gy) (endpoint 2). Both measurements showed a significant difference between patients treated with photons or protons ( $p_1=0.049$  and  $p_2=0.0002$ ). In conclusion, chest-wall patients treated with protons have a higher change to show late-phase image changes compared to patients treated with photons. Thereby, the radiographic changes were associated an increase in RBE.

## 7.5. RBE models

This section will describe the currently investigated strategies to minimize potential variations in RBE by treatment planning. Considering the RBE complexity, the strategies mainly focus on migrating potential RBE uncertainties by limiting high LET regions.

### Predictive toxicity models

The RBE models described in the previous section have shown that RBE depends on dose, LET, and the difference in radiosensitivity correlated to early radiation toxicity as the endpoint. Although evidence is growing that RBE plays a role in proton therapy, they all proposed to validate RBE models on more massive data sets. More clinical data is needed to allow recommendations for RBE values that differ from 1.1 for specific clinical situations [23] and for what level of RBE precision is clinically acceptable [43]. Clinical data with long-term toxicity should probably be used as they are more related to proton irradiation. However, high-quality clinical data on the long-term effectiveness and toxicity associated with the use of proton beam therapy is still lacking [69].

As long as RBE is associated with a lot of uncertainty, toxicity prediction models, like  $TD_{50}$  and  $NTCP_{POLO}$ , have the potential to design safe and more effective proton therapy treatments.

### LET- vs. RBE-based planning

Currently, RBE is associated with a broad range of uncertainty [57]. Although  $LET_d$  alone cannot determine the actual proton RBE, it is an indicator for local increase or decrease in RBE for a given  $\alpha/\beta$ . This allows biological optimization without knowing the dose accurately and even despite uncertainties in RBE values [37]. Besides, the advantage of  $LET_d$  over RBE is that it is a pure physical quantity that can be calculated quite accurately. Therefore, the optimization of LET may be a good surrogate for RBE in proton therapy, as internationally argued [23]. It has been shown for heavy ion therapy that the optimization of LET may improve TCP and lower NTCP [70]. Many studies have already investigated the impact of LET optimization in the research setting for proton therapy, e.g. [35–37].

### LET optimization strategies

Potential RBE mitigation strategies can be categorized into (a) pure LET optimization, (b) LET optimization based on metrics, (c) beam angle selection, (d) beam energy selection or even (e) robust optimization and (f) reduction of dose at the end of the SOBP, which will be discussed.

#### (a) LET optimization

During LET optimization, high-LET regions are minimized and kept away from regions near critical structures, for example, from tissue with low  $\alpha/\beta$ , resulting in a favorable plan for healthy tissue [35].

IMPT can achieve LET optimization by migrating individual pencil beams with higher biological effectiveness into the tumor [36]; reducing the weight of the pencil beam that stops in the brainstem; or increasing the fluence of pencil beams, which traverse the brainstem [35]. LET optimization can reduce LET hot-spots from critical organs like the brainstem (fig. 7.7, e and f), while simultaneously preserving the prescribed dose and dose constraints for the organs at risk, i.e., a dosimetric equal proton plan is generalized (c and d). As a consequence of migrating LET hot spots away from the brainstem, the therapeutic window might increase [37]. Figure 7.7b shows the difference between the physical dose distributions. The LET optimization results in a re-optimization of the beam weights.

In current clinical practice, a LET-based optimization step could be added to the treatment planning systems without altering current planning dose strategies, dose constraints, and clinical plan assessment [35]. Although LET optimization affects the physical prescribed dose, still almost identical dose distributions can be achieved.

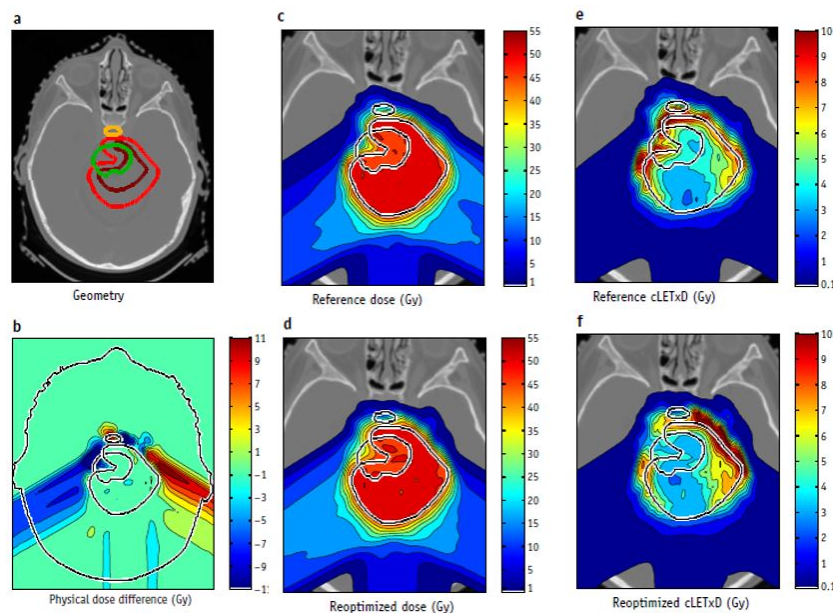


Figure 7.7: Comparison of a treatment plan after  $LET_d$  optimization. (a) The anatomical structures presented are the clinical target volume (red), gross target volume (brown), the brainstem (green), and optic structures, and the pituitary gland (yellow). Physical dose and  $cD \times LET$  for the reference plan (c and e) and the re-optimized plan (d and f). The empirical constant  $c$  is given in  $\mu\text{m}/\text{keV}$ . (b) The difference in physical dose between the reference plan and re-optimized plan. The figure is taken from [35].

However, proton modalities other than IMPT, like passive scatter are unable to optimize LET while preserving the dose constraints, as beams are invariably placed in healthy tissues just distal to the target volume [71, 72].

### (b) LET optimization based on metrics

Reducing the biological variability without explicitly calculating the RBE for optimization could be achieved by using simplified radiation response metrics based on a voxelwise dose and LET map. In general, LET optimization models are based on a simple product of dose and LET (dose- $LET_d$ ) or on a by adding a dose-LET weighted average to the physical dose. McMahon et al. [73] evaluated both models. The first approach commonly underestimates the RBE at low LET levels and significantly overestimates the impact of LET in high-LET regions. Further, a simple voxelwise product of dose and LET might be insufficient as a doubling of the dose usually leads to a more substantial effect in biological response as doubling the LET. In contrast, the second approach was more accurate in predicting variations in RBE, potentially because the weighted product of dose and LET represents the added biological dose given to tissue. Besides, they found that the LET-weighted dose model substantially reduces variability in the corresponding RBE. It even reduces effectively LET hot spots in OAR [35]. Note that these metrics are based on a similar approach as the models in the studies looking for clinical evidence, especially  $M_8$  by Eulitz et al. (2) [25] and  $M_9$  by Bahn et al. [1]. Furthermore, the advantage of this approach is

its linear behavior with the pencil beam fluence. Therefore, the same optimization algorithms used for dose optimization can be applied [53].

### **(c) Beam angle selection**

Even without LET or model-based optimization, e.g., choosing appropriate beam angles during treatment planning can avoid or reduce high-LET regions in OAR [38, 74]. An iso-effective dose plan with a favorable LET distribution can be generated by increasing the weight of one beam while reducing the other (fig. 7.7b). In general, it is advised to avoid proton beams directly towards the OAR by positioning the beam laterally to the OAR, for example, by using oblique beams with a large angle to spare LET into the brainstem during irradiation of posterior fossa tumors [38]. LET variations in lateral beam fall-off is not as sharp as at the distal edge of the proton range. Therefore, it might be neglected as the small variations in LET are not expected to affect the RBE significantly [36]. Further, it has been shown that changing the posterior field into a vertex field to the PTV, the mean  $LET_d$  in the brainstem can be reduced by 25% [74]. Another strategy investigated the effect of the number of proton beams being used. Additional proton beams potentially spread out the high RBE portions of the beam to different areas and minimize the effect of a single beam, possibly pointing toward a critical organ or tissue [43]. However, this approach does not guarantee a lower RBE [38]. Besides there is an increase in healthy tissue irradiation within the entrance region. Although one might reduce the high-LET regions by adapting beam angles, for example, if the brainstem overlaps with the tumor the physical dose to the tumor will be of more concern than the LET [74].

### **(d) Beam energy selection**

Alternatively, some centers apply whole boost beams [39], i.e., extending the proton beam range beyond a critical organ, or shoot-through beams [40], known as transmission beams. These approaches avoid placing the Bragg peak and the associated high LET within or close to the brainstem, or within the patient, respectively. Additionally to the latter, it is of benefit since transmission beams migrate range uncertainties. However, both approaches increase the dose delivered to healthy tissue and increase the brainstem dose volume. When applying whole boost beams, the end of the range is usually placed within structures, like the cochlea and neuroendocrine structures, leading to increased risk of organ injury [68, 75].

### **(e) Robust optimization**

During treatment planning, the uncertainty in proton dose delivery has been taken into account during robust optimization. The increasing capability to accurately deliver doses during treatment planning allows for applying smaller margins, resulting in a sharper dose-fall off. As a consequence, LET values might increase as well, resulting in elevated RBE values. Therefore, a strategy to diminish uncertainties of variance in RBE may be achieved by making the proton plan less sensitive to variation in range, e.g., by smearing out the dose gradients. In other words, one might consider implying less accurate robustness. However, this is in sharp contrast to the potential of high-precision proton delivery, which increases with a more careful and robust treatment planning [23, 54]. Though, it appears advisable to incorporate robustness up to a certain level during plan evaluation.

### **(f) Dose reduction**

At last, a scaling factor could be used to degrade the physical dose based within the last few millimeters of the proton SOBP to compensate for the extension of the biological effective range of the treatment field. The averaged in vitro sensitivity can be used as input [54]. Since the  $\alpha/\beta$ -ratio appears as a significant factor in RBE uncertainty [76], this strategy could lead to more robust plans towards RBE variability. For example, the RBE at the edge of the target volume could be increased to 1.2 or 1.3. Although it seems beneficial for healthy tissue with low  $\alpha/\beta$ , this approach is counter-intuitive to clinicians when realizing the potential of underdosing the tumor at the edge of the SOBP, leading to the potential of increased side effects [71]. Therefore, this strategy is not implemented in treatment planning optimization techniques for sure as long as strong clinical evidence on preserving tumor control is lacking.

## 7.6. Discussion

### Increased biological effectiveness outside the target volume

In vitro studies showed that RBE increases with depth in a therapeutic proton beam. Consequently, the biological effective range of the treatment field extends with 2-3 millimeters [77]. Because the clinically used RBE of 1.1 underestimates the physical equivalence of proton dose at the end of the beam. As a result, a higher biological dose than the photon equivalence tolerance dose is delivered, which potentially leads to unforeseen toxicities. The increased RBE behind the target volume, which is especially pronounced in healthy tissue with a low  $\alpha/\beta$ , may explain the appearance of the same incidence rate of side effects after proton treatment compared to photon therapy. In line with an increased RBE outside the target volume, the continued use of a fixed RBE may lead to increased toxicity and, thereby, to sub-optimal plans that do not fully exploit the potential benefit of proton therapy.

### RBE predictors

Amongst published in vitro cell survival studies, there is a consensus that proton RBE increases with LET within the clinically relevant range ( $LET_d < 15 \text{ keV}/\mu\text{m}$ ), and, hence, with depth in the proton beam. Further, RBE increases non-uniformly with lower fractionation dose, and tissue with a lower  $\alpha/\beta$  response rate, as shown by cell survival studies.

To better interpret the clinical outcome and improve radiation treatment design, tissue- and spatial variation of RBE might not be neglected. The first couple of patient cohort studies have confirmed clinical evidence on a variable RBE based on dose, LET, and tissue type. They mainly observed an increased risk of developing observable changes on images at the edge of CTV with a combination of high to intermediate-dose and  $LET > 3 \text{ keV}/\mu\text{m}$ . By this, they indicated the importance of LET and the potential of increased risk due to high LET.

Incorporating the periventricular region (PVR) within RBE models, as done by Eulitz et al. (2) [25] and Bahn et al. [1], has not been done before. Remarkably, integrating radiosensitive regions to a multivariable model of dose and LET results in the most accurate predictive toxicity RBE model. By this, Eulitz et al. (2) [25] suggest that the cells around the ventricular system react differently on proton irradiation as other healthy tissue. Several studies demonstrated that photon radiation preferentially activates pathways leading to apoptosis in undifferentiated multipotent precursors localized in, i.a., the ventricular zone (e.g., [? ]). This might be because stem cell niches exist along the entire ventricular system [? ]. Possibly more regions contain highly sensitive cells more prone to proton irradiation than others. Thereby, if we consider the difference in magnitudes in dose, LET, and PVR, then it turns out that these predictors all have approximately the same contribution.

### Effect of LET optimization on NTCP

The appearance of radiographic imaging changes does not always relate to clinical symptoms (e.g. [1, 24, 46]). However, as a subgroup of patients with CEBLs will develop symptoms, a good starting point is to reduce the incidence of CEBLs. Therefore, it might be more appropriate to translate these predictive models based on physical objectives into a clinical more relevant endpoint, like the patient-risk  $NTCP_{CEBL}$  [1].

By reviewing the LET optimization approach as an additional optimization step during treatment planning, the  $NTCP_{CEBL}$  is probably nearly unaffected. During LET optimization, high LET is relocated from a critical structure to another spot within the irradiated region. However, as no specific organs or tissue, except the PVR, are taken into account in the POLO model, the relocation of high LET to voxels that receive a similar dose will result in an almost similar  $NTCP_{CEBL}$ . Therefore, LET optimization might not be highly effective in terms of  $NTCP_{CEBL}$ .

Further, Bahn et al. [1] assumed that the  $NTCP_{CEBL}$  model is also valid for photons. If we compare the average proton LET of  $2.5 \text{ keV}/\mu\text{m}$  within the SOBPs with the general assumed photon LET of  $\sim 0.3 \text{ keV}/\mu\text{m}$  (e.g. [41]) or  $\sim 1.0 \text{ keV}/\mu\text{m}$  (e.g. [42]), it is questionable whether we can achieve the same  $NTCP_{CEBL}$  as with photons, or to which extent we can reach towards the photon biological outcome. Besides, when the high proton LET values are reduced from, e.g.,  $6 \text{ keV}/\mu\text{m}$  by a factor 2 or when we achieve a uniform  $LET_d$  distribution of  $2.5 \text{ keV}/\mu\text{m}$ , the question last of how much can we improve?

To investigate the impact of proton irradiation on the  $NTCP_{CEBL}$ , future studies can revise the described strategies or design alternative strategies using the model of Bahn et al. [1] as a clinical model.

The implementation of such strategies could predict and potentially prevent toxicity, resulting in improved radiation treatment designed and outcomes.

### **Uncertainties associated with RBE**

Despite evidence for an increased proton RBE at the distal fall-off the Bragg peak given by experimental studies, the biological effect is still less apparent in clinical cohorts. This may suggest that, otherwise, the increased RBE has caused more frequent side effects in past clinical trials [23]. However, planning uncertainties and uncertainties associated with RBE may cover a more prominent RBE effect.

### **Uncertainties during proton treatment**

The proton range is one of the main uncertainties in proton therapy, mainly due to the lack of accurate conversion of CT Hounsfield Units to the stopping power, and its strong dependence on tissue and tissue heterogeneity. Therefore, the RBE may vary within an organ or tissue, which should be considered. Other potential reasons for RBE uncertainty are introduced by range straggling, organ or patient motion, anatomy changes, inter-fractional position deviations, dose-volume effects, and tissue environment changes [23, 43? ]. Due to this, deviations between the actual delivered dose and the planned dose may occur. Thereby LET distributions might even be more inaccurate. With more precise capability to deliver Bragg peak to the location as planned, and reduced margins, the dose gradient becomes steeper, resulting in a smaller smear-out effect of RBE. Thereby, RBE may increase locally.

Due to the uncertainties in range and registration of the radiation field with the planning images, it is hard to obtain a perfect correlation between the images, dose, and LET on the voxel level. This remains a limitation for the models since they rely on the assignment to correlate toxicity voxel-wise to the radiation field. Nevertheless, the clinical evidence studies correlated observed toxicity on radiographic images with the prescribed dose and LET distribution with reasonable accuracy (AUC > 0.88).

### **Pre- and/or post-treatment effect**

In combination with radiotherapy, systemic treatments like immuno- or chemotherapy, or resection of the tumor are involved for cancer treatment. Besides, patients might use steroids to help with the side effects of the treatment. For example, the group from Houston [24, 45] treated most patients treated with steroids, and 20% of the patients received pre-treatment chemotherapy. All patients underwent surgery. However, little is known about the impact of systemic chemo- or immunotherapy in combination with radiotreatment on the biological effectiveness. Thereby, it is difficult to accurately predict causes for the appearance of image change that relate purely to irradiation.

Despite the limited number of comparative clinical studies on proton versus photon radiochemotherapy, proton radio-chemotherapy might lead to lower toxicity for lung- [78] and gastrointestinal tumors [79], but no firm conclusion was made. On contrary, an elevated risk of brainstem toxicity was suggested with chemotherapy or tumor resection. However, no clear relationship has been established so far [45, 68, 80].

### **Proton treatment modality**

Further, there might be potential differences in biological effectiveness between different treatment modalities [81]. By using IMPT, a higher LET<sub>d</sub> may be expected compared to passive beam scattering [72], likely due to the sharper dose gradient after the Bragg peak. So, as the use of IMPT increases, an elevated biological effect should be considered.

### **Reference Radiation**

Finally, variations in RBE might originate from the reference beam. To compare differences in biological effectiveness, all proton centers and studies should evaluate the outcome of all patients regarding the same photon source. Different photon sources are used in literature ranging from kilovoltage to megavoltage X-ray beams during cell studies (e.g. [17]). However, in the clinic, mostly the 6-10 MV photon beams generated by linear accelerators are used. Note that different photon energies also imply different LET values. Consequently, the use of various reference sources might not present a similar biological outcome.

## 7.7. Conclusion

Empirical cell studies and retrospective studies have shown spatial deviations of the current clinically used RBE of 1.1 potentially leading to increased risk of side effects. Physically, the increase in LET along the proton penetration path leads to an extension of the biological effective range. Biological speaking, increased biological effectiveness behind the target volume is especially pronounced in healthy tissue with a low  $\alpha/\beta$ . Clinical evidence of increased RBE was found by correlating sites of toxicity with dose and LET and the radiosensitive area around the ventricular system (PVR). Thereby, radiation response models indicate for a rationale towards a variable RBE.

Different strategies have already been identified on how to integrate current knowledge about RBE variations into clinical practice. A re-evaluation of these strategies using RBE models, which are translated into a biological endpoint, like NTCP, have the potential to come up with new insight about the impact of the variations in RBE and recommendations for current clinical practice.

For further improvement of the RBE models, additional predictors affecting the RBE should be reported and investigated. Besides, more validation and clinical data are necessary to adopt these radiation response models in the clinic. Further, a better understanding of the relation between image changes with side effects is desired. Besides, other biomarkers on MRI could be of interest. All with all, a continuous assessment of clinical outcomes and RBE models is necessary.

# Bibliography

- [1] E. Bahn, J. Bauer, S. Harrabi, K. Herfarth, J. Debus, and M. Alber. Late contrast enhancing brain lesions in proton-treated patients with low-grade glioma: Clinical evidence for increased periventricular sensitivity and variable rbe. *International Journal of Radiation Oncology\*Biophysics*, 9(3):571–578, July 2020. doi: 10.1016/j.ijro.2018.01.006.
- [2] Sofiya Choudhary. Deterministic and stochastic effects of radiation. *Cancer Therapy Oncology International Journal*, 12(2), 2018. doi: 10.19080/CTOIJ.2018.12.555834.
- [3] Cancer Research UK. Side effects of radiotherapy. URL <https://www.cancerresearchuk.org/about-cancer/brain-tumours/treatment/radiotherapy/side-effects>. Accessed on 2020-08-04.
- [4] W.P. Levin, H. Kooy, J.S. Loeffler, and T.F. DeLaney. Proton beam therapy. *British journal of cancer*, 93(8):849–854, Oct 2005. doi: 10.1038/sj.bjc.6602754.
- [5] A. Tran, J. Zhang, K. Woods, V. Yu, D. Nguyen, G. Gustafson, L. Rosen, and K. Sheng. Treatment planning comparison of impt, vmat and 4II radiotherapy for prostate cases. *Radiation Oncology*, 12(1), January 2017. doi: 10.1186/s13014-016-0761-0.
- [6] M. Chuong, S. Badiyan, M. Yam, Z. Li, K. Langen, W. Regine, C. Morris, J. III, M. Mehta, S. Huh, M. Rutenberg, and R. Nichols. Pencil beam scanning versus passively scattered proton therapy for unresectable pancreatic cancer. *Journal of Gastrointestinal Oncology*, 9(4):687–693, August 2018. doi: 10.21037/jgo.2018.03.14.
- [7] Segedin Barbara and Petric Primoz. Uncertainties in target volume delineation in radiotherapy - are they relevant and what can we do about them? *Radiology and Oncology*, 50(3):254–262, September 2016. doi: 10.1515/raon-2016-0023.
- [8] Robust radiotherapy planning. physics in medicine and biology. *Physics in medicine and biology*, 63(22), November 2018. doi: 10.1088/1361-6560/aae659.
- [9] Zorginstituut Nederland. Standpunt protontherapie bij neuro-oncologische tumoren, July 2019. URL <https://www.zorginstituutnederland.nl/publicaties/standpunten/2019/07/09/standpunt-protontherapie-bij-neuro-oncologische-tumoren>.
- [10] G. V. Dalrymple, I. R. Lindsay, J. D. Hall, J. C. Mitchell, Kundel H. L. Ghidoni, J. J., and I. L. Morgan. The relative biological effectiveness of 138-mev protons as compared to cobalt-60 gamma radiation. *Radiation research*, 28(2):489–506, June 1966. doi: 10.2307/3572211.
- [11] J. Tepper, L. Verhey, M. Goitein, and H. D. Suit. In vivo determinations of rbe in a high energy modulated proton beam using normal tissue reactions and fractionated dose schedules. *International journal of radiation oncology, biology, physics*, 2(11-12):1115–1122, November 1977. doi: 10.1016/0360-3016(77)90118-3.
- [12] McMahon S. J. The linear quadratic model: usage, interpretation and challenges. physics in medicine and biology. *Physics in Medicine Biology*, 64(1), Dec 2018. doi: doi.org/10.1088/1361-6560/aaf26a.
- [13] B. Jones. Clinical radiobiology of proton therapy: modeling of rbe. *Acta Oncologica*, 56(11):1–5, August 2017. doi: 10.1080/0284186X.2017.1343496.
- [14] J.F. Fowler. The radiobiology of prostate cancer including new aspects of fractionated radiotherapy. *Acta Oncologica*, 44(3):265–276, 2005. doi: 10.1080/02841860410002824.

- [15] R.V. Sethi, D. Giantsoudi, M. Raiford, I. Malhi, A. Niemierko, O. Rapalino, P. Caruso, T.I. Yock, N.J. Tarbell, H. Paganetti, and Shannon M. MacDonald. Patterns of failure after proton therapy in medulloblastoma; linear energy transfer distributions and relative biological effectiveness associations for relapses. *International Journal of Radiation Oncology, Biology and Physics*, 88(3): 655–663, March 2014. doi: 10.1016/J.IJROBP.2013.11.239.
- [16] O. Desouky and G. Zhou. Biophysical and radiobiological aspects of heavy charged particles. *Journal of Taibah University for Science*, 10(2):187–194, Apr 2016. doi: 10.1016/j.jtusci.2015.02.014.
- [17] H. Paganetti. Relative biological effectiveness (rbe) values for proton beam therapy. variations as a function of biological endpoint, dose, and linear energy transfer. *Physics in Medicine and Biology*, 59(22):R419, 10 2014. doi: 10.1088/0031-9155/59/22/R419.
- [18] H. Willers, A. Allen, D. Grosshans, S. McMahon, C. von Neubeck, C. Wiese, and B. Vikram. Toward a variable rbe for proton beam therapy. *Radiotherapy and Oncology*, 128(1):68–75, July 2018. doi: 10.1016/j.radonc.2018.05.019.
- [19] Radiation Effects Research Foundation. How radiation affects cells. URL [https://www.rerf.or.jp/en/programs/roadmap\\_e/health\\_effects-en/basicinfo-en/radcell-en/](https://www.rerf.or.jp/en/programs/roadmap_e/health_effects-en/basicinfo-en/radcell-en/). Accessed on 2020-07-30.
- [20] F Romano, Pablo Cirrone, Giacomo Cuttone, F. Rosa, Santi Mazzaglia, I Petrovic, Aleksandra Ristic-Fira, and A Varisano. A monte carlo study for the calculation of the average linear energy transfer (let) distributions for a clinical proton beam line and a radiobiological carbon ion beam line. *Physics in Medicine and Biology*, 59(12), 2014. doi: 10.1088/0031-9155/59/12/2863.
- [21] M. Wedenberg, B. Lind, and B. Hårdemark. A model for the relative biological effectiveness of protons: The tissue specific parameter  $\alpha / \beta$  of photons is a predictor for the sensitivity to let changes. *Acta oncologica (Stockholm, Sweden)*, 52(3):2–14, September 2012. doi: 10.3109/0284186X.2012.705892.
- [22] P. Chaudhary, T.I. Marshall, F.M. Perozziello, L. Manti, F.J. Currell, F. Hanton, S.J. McMahon, J.N. Kavanagh, P.G.A. Cirrone, F. Romano, K. Prise, and G.S. Schettino. Biological effectiveness variation along monoenergetic and modulated bragg peaks of a 62-mev therapeutic proton beam: A preclinical assessment. *International journal of radiation oncology, biology, physics*, 90(1): 27–35, june 2014. doi: 10.1016/j.ijrobp.2014.05.010.
- [23] A. Lühr, C. von Neubeck, J. Pawelke, A. Seidlitz, C. Peitzsch, S. M. Bentzen, Debus J. Bortfeld, T., E. Deutsch, J. A. Langendijk, J. S. Loeffler, R. Mohan, M. Scholz, B. S. Sørensen, D. C. Weber, M. Baumann, and M. Krause. Radiobiology of proton therapy”: Results of an international expert workshop. *Radiotherapy and Oncology*, 128(1):56–67, July 2018. doi: 10.1016/j.radonc.2018.05.018.
- [24] C. R. Peeler, D. Mirkovic, U. Titt, P. Blanchard, J. R. Gunther, A. Mahajan, R. Mohan, and D. R. Grosshans. Clinical evidence of variable proton biological effectiveness in pediatric patients treated for ependymoma. *Radiotherapy and oncology*, 121(3):395–401, December 2016. doi: 10.1016/j.radonc.2016.11.001.
- [25] J. Eulitz, Esther Troost, Felix Raschke, E. Schulz, B. Lutz, A. Dutz, Steffen Löck, P. Wohlfahrt, W. Enghardt, C. Karpowitz, Mechthild Krause, and Armin Lühr. Predicting late magnetic resonance image changes in glioma patients after proton therapy. *Acta Oncologica*, 58(10):1536–1539, October 2019. doi: 10.1080/0284186X.2019.1631477.
- [26] J. Eulitz, B. Lutz, P. Wohlfahrt, A. Dutz, W. Enghardt, C. Karpowitz, M. Krause, E. Troost, and A. Lühr. A monte carlo based radiation response modelling framework to assess variability of clinical rbe in proton therapy. *Physics in Medicine and Biology*, 64(22), November 2019. doi: 10.1088/1361-6560/ab3841.
- [27] T. Underwood, C. Grassberger, R. Bass, S. Macdonald, N. Meyersohn, B. Yeap, R. Jimenez, and H. Paganetti. Asymptomatic late-phase radiographic changes among chest-wall patients are associated with a proton rbe exceeding 1.1. *International Journal of Radiation Oncology\*Biology\*Physics*, 101, April 2018. doi: 10.1016/j.ijrobp.2018.03.037.

- [28] M. Alber and C. Belka. A normal tissue dose response model of dynamic repair processes. *Physics in Medicine and Biology*, 51(1), December 2005. doi: 10.1088/0031-9155/51/1/012.
- [29] K. Souris, J. Lee, and E. Sterpin. Fast multipurpose monte carlo simulation for proton therapy using multi- and many-core cpu architectures. *Medical Physics*, 43(4):1700–1712, April 2016. doi: 10.1118/1.4943377.
- [30] S. Agostinelli, J.R. Allison, K. Amako, J. Apostolakis, H.M. Araújo, P. Arce, M. Asai, D.A. Axen, S. Banerjee, G. Barrand, F. Behner, L. Bellagamba, J. Boudreau, L. Broglia, A. Brunengo, S. Chauvie, J. Chuma, R. Chytracsek, G. Cooperman, and D. Zschesche. Geant4-a simulation toolkit. *Nuclear Instruments and Methods in Physics Research Section A Accelerators Spectrometers Detectors and Associated Equipment*, 506(3):250–303, July 2003. doi: 10.1016/S0168-9002(03)01368-8.
- [31] G. Battistoni, F. Cerutti, A. Fasso, A. Ferrari, S. Muraro, J. Ranft, S. Roesler, and P. Sala. The fluka code: Description and benchmarking. *AIP Conference Proceedings*, 896:31–49, March 2007. doi: 10.1063/1.2720455.
- [32] B. Faddegon, J. Ramos, J. Schuemann, A. McNamara, S. Jungwook, J. Perl, and H. Paganetti. The topas tool for particle simulation, a monte carlo simulation tool for physics, biology and clinical research. *Physica Medica*, 72:114–121, April 2020. doi: 10.1016/j.ejmp.2020.03.019.
- [33] J. Sorriaux, M. Testa, H. Paganetti, J. Xivry, J. Lee, E. Traneus, K. Souris, S. Vynckier, and E. Sterpin. Experimental assessment of proton dose calculation accuracy in inhomogeneous media. *Physica Medica*, 38:10–15, June 2017. doi: 10.1016/j.ejmp.2017.04.020.
- [34] D. Wagenaar, L. Tran, A. Meijers, G. Marmitt, K. Souris, D. Bolst, B. James, G. Biasi, M. Povoli, A. Kok, E. Traneus, M.J. Goethem, J. Langendijk, A. Rosenfeld, and S. Both. Validation of linear energy transfer computed in a monte carlo dose engine of a commercial treatment planning system. *Physics in Medicine Biology*, 65(2), December 2019. doi: 10.1088/1361-6560/ab5e97.
- [35] J. Unkelbach, P. Botas, D. Giantsoudi, B. Gorissen, and H. Paganetti. Reoptimization of intensity modulated proton therapy plans based on linear energy transfer. *International Journal of Radiation Oncology\*Biography\*Physics*, 96(5):1097–1106, December 2016. doi: 10.1016/j.ijrobp.2016.08.038.
- [36] J. Wilkens and U. Oelfke. Three-dimensional let calculations for treatment planning of proton therapy. *Zeitschrift für medizinische Physik*, 14(1):41–46, February 2004. doi: 10.1078/0939-3889-00191.
- [37] D. Giantsoudi, C. Grassberger, D. Craft, A. Niemierko, A. Trofimov, and H. Paganetti. Linear energy transfer-guided optimization in intensity modulated proton therapy: Feasibility study and clinical potential. *International journal of radiation oncology, biology, physics*, 87(1):216–222, September 2013. doi: 10.1016/j.ijrobp.2013.05.013.
- [38] D. Giantsoudi, J. Adams, S. Macdonald, and H. Paganetti. Proton treatment techniques for posterior fossa tumors: Consequences for let and dose/volume parameters for the brainstem and organs at risk. *International Journal of Radiation Oncology\*Biography\*Physics*, 97(2):401–410, February 2016. doi: 10.1016/j.ijrobp.2016.09.042.
- [39] J. Buchsbaum, M. McDonald, P. Johnstone, T. Hoene, M. Mendonca, C. Cheng, I. Das, K. McMullen, and M. Wolanski. Range modulation in proton therapy planning: A simple method for mitigating effects of increased relative biological effectiveness at the end-of-range of clinical proton beams. *Radiation oncology (London, England)*, 9(1), January 2014. doi: 10.1186/1748-717X-9-2.
- [40] B. Mou, C. Beltran, S. Park, K. Olivier, and K. Furutani. Feasibility of proton transmission-beam stereotactic ablative radiotherapy versus photon stereotactic ablative radiotherapy for lung tumors: A dosimetric and feasibility study. *PloS one*, 9(6):e98621, June 2014. doi: 10.1371/journal.pone.0098621.

- [41] ICRU. Report 16. *Journal of the International Commission on Radiation Units and Measurements*, os9(1), June 1970. ISSN 1473-6691. doi: 10.1093/jicru/os9.1.Report16.
- [42] J. Meesungnoen, M. Benrahmoune, A. Filali, S. Mankhetkorn, and J. Jay-Gerin. Monte carlo calculation of the primary radical and molecular yields of liquid water radiolysis in the linear energy transfer range 0.3–6.5 keV/ $\mu\text{m}$ : Application to 137 cs gamma rays 1. *Radiation Research - RADIAT RES*, 155(2):269–278, February 2001. doi: 10.1667/0033-7587(2001)155[0269:MCCOTP]2.0.CO;2.
- [43] H. Paganetti, E. Blakely, A. Carabe, D. Carlson, I. Das, L. Dong, D. Grosshans, K. Held, R. Mohan, V. Moiseenko, A. Niemierko, R. Stewart, and H. Willers. Report of the aapm tg-256 on the relative biological effectiveness of proton beams in radiation therapy. *Medical Physics*, 46(3), January 2019. doi: 10.1002/mp.13390.
- [44] D.T. Goodhead, J. Thacker, and R. Cox. Effects of radiations of different qualities on cells: molecular mechanisms of damage and repair. *International Journal of Radiation Biology*, 63(5):543–556, May 1993. doi: 10.1080/09553009314450721.
- [45] J. Gunther, M. Sato, M. Chintagumpala, L. Ketonen, J. Jones, P. Allen, A. Paulino, M. Okcu, J. Su, J.y Weinberg, N. Boehling, S. Khatua, A. Adesina, R. Dauser, W. Whitehead, and A. Mahajan. Imaging changes in pediatric intracranial ependymoma patients treated with proton beam radiation therapy compared to intensity modulated radiation therapy. *International Journal of Radiation Oncology\*Biophysics*, 93(1):54–63, September 2015. doi: 10.1016/j.ijrobp.2015.05.018.
- [46] D. Giantsoudi, R. Sethi, B. Yeap, B. Eaton, D. Ebb, P. Caruso, O. Rapalino, Y. Chen, J. Adams, T. Yock, N. Tarbell, H. Paganetti, and S. Macdonald. Incidence of cns injury for a cohort of 111 patients treated with proton therapy for medulloblastoma: Let and rbe associations for areas of injury. *International Journal of Radiation Oncology\*Biophysics*, 95(1):287–296, May 2015. doi: 10.1016/j.ijrobp.2015.09.015.
- [47] L. Toussaint, D.J. Indelicato, K.S. Holgersen, J.B.B. Petersen, C.H. Stokkevåg, Y. Lassen-Ramshad, O. Casares-Magaz, A. Vestergaard, and L.P. Muren. Towards proton arc therapy: physical and biologically equivalent doses with increasing number of beams in pediatric brain irradiation. *Acta Oncologica*, 58(10):1451–1456, Oct 2019. doi: 10.1080/0284186X.2019.1639823.
- [48] A. Carabe, R. Dale, and B. Jones. The incorporation of the concept of minimum rbe (rbemin) into the linear-quadratic model and the potential for improved radiobiological analysis of high-let treatments. *International journal of radiation biology*, 83(1):27–39, January 2007. doi: 10.1080/09553000601087176.
- [49] A. Carabe, M. Moteabbed, N. Depauw, J. Schuemann, and H. Paganetti. Range uncertainty in proton therapy due to variable biological effectiveness. *Physics in medicine and biology*, 57(5):1159–1172, February 2012. doi: 10.1088/0031-9155/57/5/1159.
- [50] A. McNamara, J. Schuemann, and H. Paganetti. A phenomenological relative biological effectiveness (rbe) model for proton therapy based on all published in vitro cell survival data. *Physics in Medicine and Biology*, 60(21):8399–8416, November 2015. doi: 10.1088/0031-9155/60/21/8399.
- [51] T. Matsui, E. Nuryadi, S. Komatsu, Y. Hirota, A. Shibata, T. Oike, and T. Nakano. Robustness of clonogenic assays as a biomarker for cancer cell radiosensitivity. *international journal of molecular sciences*. 20(17):4148, August 2019. doi: 10.3390/ijms20174148.
- [52] A. McNamara, J. Schuemann, and H. Paganetti. A phenomenological relative biological effectiveness (rbe) model for proton therapy based on all published in vitro cell survival data. *Physics in Medicine and Biology*, 60(21):8399–8416, November 2015. doi: 10.1088/0031-9155/60/21/8399.
- [53] H. Paganetti. Proton relative biological effectiveness – uncertainties and opportunities. *International Journal of Particle Therapy*, 5(1):2–14, September 2018. doi: 10.14338/IJPT-18-00011.1.
- [54] A. Lühr, C. von Neubeck, M. Krause, and E.G.C. Troost. Relative biological effectiveness in proton beam therapy – current knowledge and future challenges. *Clinical and Translational Radiation Oncology*, 9:35–41, February 2018. doi: 10.1016/j.ctro.2018.01.006.

- [55] L.E. Gerweck and S.V. Kozin. Relative biological effectiveness of proton beams in clinical therapy. *Radiotherapy and oncology : journal of the European Society for Therapeutic Radiology and Oncology*, 50(2):135–142, February 1999. doi: 10.1016/s0167-8140(98)00092-9.
- [56] K. Maeda, H. Yasui, T. Matsuura, T. Yamamori, M. Suzuki, M. Nagane, J. Nam, O. Inanami, and H. Shirato. Evaluation of the relative biological effectiveness of spot-scanning proton irradiation in vitro. *Journal of radiation research*, 57(3), February 2016. doi: 10.1093/jrr/rrv101.
- [57] A. Carabe, S. España, C. Grassberger, and H. Paganetti. Clinical consequences of relative biological effectiveness variations in proton radiotherapy of the prostate, brain and liver. *Physics in medicine and biology*, 58(7), March 2013. doi: 10.1088/0031-9155/58/7/2103.
- [58] B. Jones. Towards achieving the full clinical potential of proton therapy by inclusion of let and rbe models. *Cancers*, 7(1):460–480, March 2015. doi: 10.3390/cancers7010460.
- [59] J. Bronk, N. Guha-Thakurta, P. Allen, A. Mahajan, D. Grosshans, and S. MCGovern. Analysis of pseudoprogression after proton or photon therapy of 99 patients with low grade and anaplastic glioma. *Clinical and Translational Radiation Oncology*, 9:30–34, February 2018. doi: 10.1016/j.ctro.2018.01.002.
- [60] M.B. Pulsifer, R.V. Sethi, K.A. Kuhlthau, S.M. MacDonald, N.J. Tarbell, and T.I. Yock. Early cognitive outcomes following proton radiation in pediatric patients with brain and central nervous system tumors. *International journal of radiation oncology, biology, physics*, 93(2):400–407, June 2015.
- [61] S. West, H. Bruin, Bart L., A. Swaak-Kragten, M. Bent, and W. Taal. Incidence of pseudoprogression in low-grade gliomas treated with radiotherapy. *Neuro-Oncology*, 19(5):719–725, May 2016. doi: 10.1093/neuonc/now194.
- [62] A. Lin, M. White, M. Miller-Thomas, R. Fulton, C. Tsien, K. Rich, R. Schmidt, D. Tran, and S. Dahiya. Molecular and histologic characteristics of pseudoprogression in diffuse gliomas. *Journal of Neuro-Oncology*, 130(3):529–533, December 2016. doi: 10.1007/s11060-016-2247-1.
- [63] E. Ludmir, A. Mahajan, A. Paulino, J. Jones, L. Ketonen, J. Su, D. Grosshans, M. F.s Mcaleer, S. MCGovern, Y. Lassen, A. Adesina, R. Dauser, J. Weinberg, and M. Chintagumpala. Increased risk of pseudoprogression among pediatric low-grade glioma patients treated with proton versus photon radiotherapy. *Neuro-oncology*, 21:686–695, May 2019. doi: 10.1093/neuonc/noz042.
- [64] M. S. Gentile, B. Y. Yeap, H. Paganetti, C. P. Goebel, D. E. Gaudet, S. L. Gallotto, E. A. Weyman, M. L. Morgan, S. M. MacDonald, D. Giantsoudi, J. Adams, N. J. Tarbell, H. Kooy, and T. I. Yock. Brainstem injury in pediatric patients with posterior fossa tumors treated with proton beam therapy and associated dosimetric factors. *International journal of radiation oncology, biology, physics*, 100(3):719–729, March 2018. doi: 10.1016/j.ijrobp.2017.11.026.
- [65] S. Girdhani, C. Lamont, P. Hahnfeldt, A. Abdollahi, and L. Hlatky. Proton irradiation suppresses angiogenic genes and impairs cell invasion and tumor growth. *Radiation research*, 178(1):33–45, July 2012. doi: 10.2307/23261975.
- [66] W. Goetz, M. Morgan, and J. Baulch. The effect of radiation quality on genomic dna methylation profiles in irradiated human cell lines. *Radiation research*, 175(5):575–587, March 2011. doi: 10.1667/RR2390.1.
- [67] E. Giedzinski, R. Rola, J. Fike, and C. Limoli. Efficient production of reactive oxygen species in neural precursor cells after exposure to 250 mev protons. *Radiation research*, 164(4):540–544, October 2005. doi: 10.1667/RR3369.1.
- [68] D.J. Indelicato, S. Flampouri, R.L. Rotondo, J.A. Bradley, C.G. Morris, P.R. Aldana, E. Sandler, and N.P. Mendenhall. Incidence and dosimetric parameters of pediatric brainstem toxicity following proton therapy. *Acta Oncologica*, 53(10):1298–1304, October 2014. doi: 10.3109/0284186X.2014.957414.

- [69] R. Leroy, N. Benahmed, F. Hulstaert, N. Damme, and D. Ruyscher. Proton therapy in children – a systematic review of clinical effectiveness in 15 pediatric cancers. *International Journal of Radiation Oncology\*Biography\*Physics*, 95(1):267–278, May 2015. doi: 10.1016/j.ijrobp.2015.10.025.
- [70] N. Bassler, O. Jäkel, C. Søndergaard, and J. Petersen. Dose- and let-painting with particle therapy. *Acta oncologica (Stockholm, Sweden)*, 49(7):1170–1176, October 2010. doi: 10.3109/0284186X.2010.510640.
- [71] R. Mohan, C. Peeler, F. Guan, L. Bronk, W. Cao, and D. Grosshans. Radiobiological issues in proton therapy. *Acta Oncologica*, 56(11):1367–1373, November 2017. doi: 10.1080/0284186X.2017.1348621.
- [72] C. Grassberger, A. Trofimov, A. Lomax, and H. Paganetti. Variations in linear energy transfer within clinical proton therapy fields and the potential for biological treatment planning. *International journal of radiation oncology, biology, physics*, 80(5):1559–1566, August 2010. doi: 10.1016/j.ijrobp.2010.10.027.
- [73] S. McMahon, H. Paganetti, and K. Prise. Let-weighted doses effectively reduce biological variability in proton radiotherapy planning. *Physics in Medicine and Biology*, 63(22), November 2018. doi: 10.1088/1361-6560/aae8a5.
- [74] L. Fjæra, zs Li, K. Ytre-Hauge, L. Muren, D. Indelicato, Y. Lassen, G.M. Engeseth, M. Brydøy, A. Mairani, S. Flampouri, O. Dahl, and C. Stokkevåg. Linear energy transfer distributions in the brainstem depending on tumour location in intensity-modulated proton therapy of paediatric cancer. *Acta oncologica (Stockholm, Sweden)*, 56(6):763–768, April 2017. doi: 10.1080/0284186X.2017.1314007.
- [75] E. S. Murphy, T. E. Merchant, Xiong X. Wu, S., R. Lukose, K. D. Wright, I. Qaddoumi, G. T. Armstrong, A. Broniscer, and A. Gajjar. Necrosis after craniospinal irradiation: results from a prospective series of children with central nervous system embryonal tumors. *International journal of radiation oncology, biology, physics*, 83(5):e655–e660, August 2012. doi: 10.1016/j.ijrobp.2012.01.061.
- [76] J. Ödén, Erikssonm K., and I. Toma-Dasu. Incorporation of relative biological effectiveness uncertainties into proton plan robustness evaluation. *Acta Oncologica*, 56(6):769–778, June 2017. doi: 10.1080/0284186X.2017.1290825.
- [77] J. J. Cuaron, C. Chang, M. Lovelock, D. S. Higginson, D. Mah, O. Cahlon, and S. Powell. Exponential increase in relative biological effectiveness along distal edge of a proton bragg peak as measured by deoxyribonucleic acid double-strand breaks. *International journal of radiation oncology, biology, physics*, 95(1):62–69, May 2016. doi: 10.1016/j.ijrobp.2016.02.018.
- [78] J. Chang, S. Jabbour, D. Ruyscher, S. Schild, C. Simone, R. Rengan, S. Feigenberg, A. Khan, N. Choi, J. Bradley, X. Zhu, A. Lomax, and B. Hoppe. Consensus statement on proton therapy in early-stage and locally advanced non-small cell lung cancer. *International Journal of Radiation Oncology\*Biography\*Physics*, 95(1):505–516, May 2016. doi: 10.1016/j.ijrobp.2016.01.036.
- [79] Lin S. H. Simone C. B. 2nd Mehta M. P. Verma, V. Clinical outcomes and toxicities of proton radiotherapy for gastrointestinal neoplasms: a systematic review. *Journal of gastrointestinal oncology*, 7(4):644–664, August 2016. doi: 10.21037/jgo.2016.05.06.
- [80] N. Sabin, T. Merchant, J. Harreld, Z. Patay, P. Klimo, I. Qaddoumi, G. Armstrong, K. Wright, J. Gray, D. Indelicato, and A. Gajjar. Imaging changes in very young children with brain tumors treated with proton therapy and chemotherapy. *AJNR. American journal of neuroradiology*, 34(2):446–450, February 2012. doi: 10.3174/ajnr.A3219.
- [81] Biological effects of passive versus active scanning proton beams on human lung epithelial cells. *Technology in cancer research treatment*, 14(1):81–98, February 2015. doi: 10.7785/tcrt.2012.500392.